AD_____

Award Number: W81XWH-06-1-0572

TITLE: Novel Breast Cancer Therapeutics Based on Bacterial Cupredoxin

PRINCIPAL INVESTIGATOR: Pernilla Wittung-Stafshede, Ph.D.

CONTRACTING ORGANIZATION: William Marsh Rice University
Houston, TX 77251

REPORT DATE: September 2008

TYPE OF REPORT: Final

PREPARED FOR: U.S. Army Medical Research and Materiel Command
Fort Detrick, Maryland 21702-5012

REPORT DOCUMENTATION PAGE

Form Approved
OMB No. 0704-0188

1. REPORT DATE	2. REPORT TYPE	3. DATES COVERED
14-09-2008	Final	15 AUG 2006 - 14 AUG 2008

4. TITLE AND SUBTITLE
Novel Breast Cancer Therapeutics Based on Bacterial Cupredoxin

5a. CONTRACT NUMBER

5b. GRANT NUMBER
W81XWH-06-1-0572

5c. PROGRAM ELEMENT NUMBER

6. AUTHOR(S)
Pernilla Wittung-Stafshede, Ph.D.

Email: pernilla@rice.edu

5d. PROJECT NUMBER

5e. TASK NUMBER

5f. WORK UNIT NUMBER

7. PERFORMING ORGANIZATION NAME(S) AND ADDRESS(ES)

Wiliam Marsh Rice University
Houston, TX 77251

8. PERFORMING ORGANIZATION REPORT NUMBER

9. SPONSORING / MONITORING AGENCY NAME(S) AND ADDRESS(ES)
U.S. Army Medical Research and Materiel Command
Fort Detrick, Maryland 21702-5012

10. SPONSOR/MONITOR'S ACRONYM(S)

11. SPONSOR/MONITOR'S REPORT NUMBER(S)

12. DISTRIBUTION / AVAILABILITY STATEMENT
Approved for Public Release; Distribution Unlimited

13. SUPPLEMENTARY NOTES

14. ABSTRACT
The tumor suppressor p53 is a major player in cell growth, genomic stability and cell death. Recent *in vivo* work suggested that bacterial *Pseudomonas aeruginosa* azurin can enter cancer cells and interact with p53 promoting cell death. Despite being a novel concept to target cancer, there are no thermodynamic details known for the proposed azurin-p53 complex. This project aims to fill this gap by employing biophysical methods in conjunction with purified proteins *in vitro* to address four aims. We will reveal (1.) which p53 domain interacts with azurin, (2.) the molecular mechanism by which azurin increases cellular levels of p53, (3.) the region on azurin that interacts with p53 and (4.) use the acquired information to propose smaller molecules that retain properties of azurin. We have found that azurin binds to the unstructured N-terminal domain of p53 and a small peptide is able to reproduce part of the azurin interaction. We have also assessed how Cu is metabolized inside cells as well has how the crowdedness of the cell milieu affects proteins. We have made several key discoveries that will aid in the development of azurin-based molecules that can be used as new treatments of cancer.

15. SUBJECT TERMS
p53, azurin, spectroscopy, calorimetry, peptide, copper, copperchaperones, crowding

16. SECURITY CLASSIFICATION OF:			17. LIMITATION OF ABSTRACT	18. NUMBER OF PAGES	19a. NAME OF RESPONSIBLE PERSON
a. REPORT	b. ABSTRACT	c. THIS PAGE			USAMRMC
U	U	U	UU	61	19b. TELEPHONE NUMBER *(include area code)*

Table of Contents

Introduction

The p53 tumor suppressor protein is involved in multiple central cellular processes, including transcription, DNA repair, genomic stability, cell cycle control and apoptosis; it is functionally inactivated by structural mutations, interaction with viral products and endogenous cellular mechanisms in many human cancers (1). *P. aeruginosa* azurin, a copper-containing redox protein (2), was recently discovered to enter mammalian cells and either induce apoptosis (wild-type) or inhibit cell-cycle progression (Met44LysMet64Glu azurin variant). Azurin specifically entered J774 cells, derived from murine reticulum cell sarcoma (3), and cancer cell lines such as melanoma UISO-Mel-2 cells and MCF-7 breast-cancer cells and caused cell death (4-7). In both instances, azurin formed a complex with the tumor suppressor protein p53, thereby somehow raising its intracellular level. High levels of p53 then triggered apoptosis in the cells through enhanced Bax formation and the release of mitochondrial cytochrome c to the cytosol. In addition, azurin was able to inhibit tumor growth in xeno-transplanted nude mice without toxicity symptoms. The support for the presence of a direct azurin-p53 complex was based on glycerol-gradient ultracentrifugation and pull-down experiments using GST-fusion constructs (7-9).

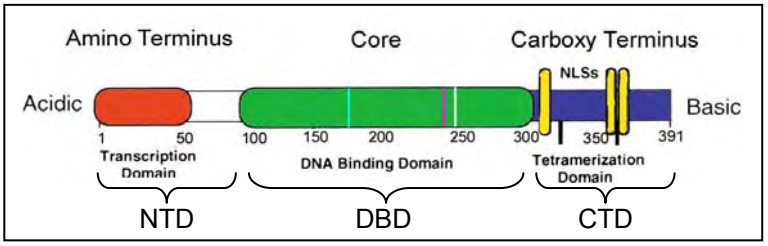

Figure 1. The diagram shows arrangements of domains in p53. Red, transcription domain which is part of NTD; green, DNA-binding domain DBD; blue, tetramerization domain which is part of CTD.

p53 is a 393-residue protein (1) that can be divided into three structural domains (Figure 1): (i) A transcription activation segment and a proline-rich segment form the N-terminal domain (NTD; residues 1-93). (ii) A DNA-binding domain which adopts a β-sheet structure and coordinates a zinc ion (DBD; residues 102-292). (iii) A helical tetramerization domain which together with a sequence-unspecific DNA-binding domain form the C-terminal domain (CTD; residues 293-393). Biophysical experiments have shown that NTD and CTD are mostly unstructured, whereas DBD is well folded, in solution (10-12). Under "latent" conditions, CTD interacts with DBD, preventing it from recognizing target DNA.

In addition, p53 can bind proteins through its NTD (*e.g.*, mouse double minute 2 homolog (MDM2) and jun-kinase (JNK)) which mediate the targeting of p53 to the proteasome for rapid degradation (*1, 13*). Thus, p53 is not only hindered from binding to DNA but it is also very unstable and rapidly disappears from the cell at non-stress conditions. Various stimuli are capable of releasing these interactions which result in a conformational change in p53 that exposes the DBD and allows for p53-mediated transcriptional activation (*1, 14, 15*).

Pseudomonas aeruginosa azurin is a 128-residue, blue-copper protein (also called cupredoxin) that is believed to facilitate electron transfer in denitrification/respiration chains (2). It was recently proposed that the physiological function of azurin in *P. aeruginosa* involves electron transfer directly related to the cellular response to oxidative stress (*16*). Azurin (Figure 2) has one α-helix and eight β-strands that fold into a rigid β-barrel structure arranged in a double-wound Greek-key topology (*2, 17*).

Figure 2. Ribbon structure of azurin (1AZU), with copper shown in blue space-filling and the five copper-ligands (Gly45, His46, Cys112, His117 and Met121) in stick representation.

In vivo, azurin coordinates a redox-active copper (Cu^{II}/Cu^{I}) *via* two histidine imidazoles, one cysteine thiolate, and two weaker axial ligands, sulfur of methionine and carbonyl of glycine in a trigonal bipyramidal geometry (Figure 2). The highly covalent nature of the copper-cysteine bond gives azurin an intense absorption at 630 nm (2). The copper in azurin can be eliminated, creating apo-azurin, or exchanged for other metals *in vitro* without change of the overall structure (*17, 18*). We have studied azurin extensively over the years as a model system to address the role of metals in protein folding (*19-27*).

In this project, we have employed a battery of biophysical tools and purified proteins to investigate molecular, structural and thermodynamic details of the azurin-p53 complex *in vitro*. We have also considered the *in vivo* environment where the p53-azurin interaction takes place by studies of Cu metabolism proteins (*28-32*) (that may steal Cu from azurin upon entry) and macromolecular crowding (as the volume occupancy of macromolecules in cells may be 40 % (*33, 34*), which may have large effects on protein

structures and binding reactions). Below follows a description of the progress we have made on the different tasks outlined in the original Statement of Work.

Task 1. ***Determine which p53 domain interacts with azurin and probe the affinity and stoichiometry of the complex in vitro***

Experiments have shown that the NTD domain is natively unfolded whereas full-length p53 (which is tetrameric at μM concentrations) exhibits high stability *in vitro* (*10, 11*). Also, p53's C-terminal domain appears to have unstructured regions (12). Earlier experiments, using fusion proteins and glycerol gradients, have suggested that *P. aeruginosa* azurin binds to the central or N-terminal portion of p53 (7-9). Therefore, we first prepared the NTD domain (i.e., residues 1-93 of p53). The protein was purified by standard methods as described in (11). Next, NTD was tested for azurin binding via isothermal titration calorimetry (ITC) to directly obtain stoichiometry and affinity of a potential azurin-NTD complex. From the data (Figure 3), it is clear that NTD does interact with azurin (pH 7.5, 25 ºC). The thermogram reveals a dissociation constant (K_D) of about 300 nM and a stoichiometry of 2 azurin molecules per NTD. From additional experiments, we found that the affinity remained the same also at 37 ºC, but decreased about 10-fold if the salt was removed from the buffer. The latter result suggests that hydrophobic interactions are important for azurin binding to p53/NTD.

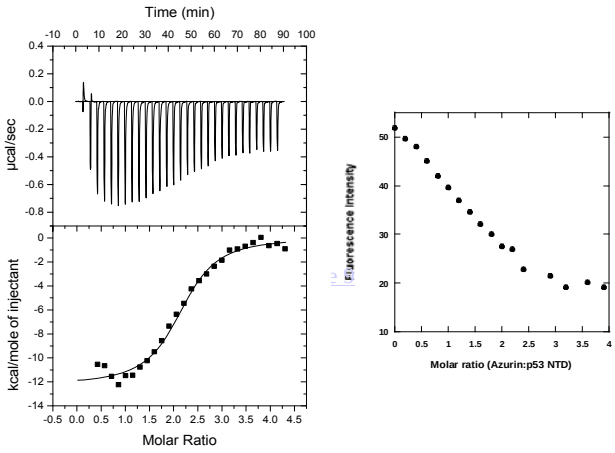

Figure 3. Left. ITC data showing the raw heat injections on top and, below, the thermogram with the integrated enthalpy as a function of azurin:NTD ratio. The solid curve is the best fit to the data. 5 μM NTD (in cell) was titrated with azurin (in syringe) in a buffer of 20 mM phosphate, 300 mM NaCl, pH 7.5, 20 °C. **Right.** Fluorescence at 350 nm of NTD (excitation at 295 nm; i.e. Trp) as a function of added Cu-azurin. The solvent conditions are the same as in the ITC experiments. Background emission from Cu-azurin was subtracted.

In earlier work (*35*), we used ITC to probe the complex between full-length p53 and azurin. We then revealed that the complex involved four azurin molecules per p53 monomer; the dissociation constant (K_D) for each site was 33±12 nM (pH 7.5, 25ºC). Thus,

the new data suggest that NTD is the site in p53 for azurin binding; nonetheless, the other p53 domains may also play a role (perhaps via long-range interactions/conformational changes) as the stoichiometry and affinity of azurin binding differs between the full-length and NTD p53 constructs.

Each p53 monomer contains four tryptophan residues: three in the NTD (Trp23, Trp53, Trp91) and one in the DBD (Trp146). The tryptophan in the DBD is highly quenched due to nearby charges; also the other tryptophans show weak emission, which has been explained by solvent exposure (*36*). Azurin has one tryptophan (Trp48) whose emission is highly quenched by the copper (*37*). Upon addition of the copper-form of azurin, we find NTD's tryptophan emission to decrease by ~ 70 % until a stoichiometry of 2:1 is reached (Figure 3). This result supports that when azurin molecules bind to NTD, the copper ions are positioned near the tryptophans so that metal-induced quenching can take place. We also tested if NTD's far-UV CD signal was affected by azurin binding. NTD is unstructured in the absence of azurin, however upon addition of 2-fold excess azurin, the negative CD signal around 210-220 nm from NTD grows larger indicating gain of structure (not shown). Infra-red (IR) spectroscopic studies of the NTD-azurin interactions suggest that β-sheet structure is formed. To reveal if some azurin molecules bind to the other p53 domains, future studies will include preparation and studies of the DBD and CTD domains of p53.

Task 2. ***Elucidate the molecular mechanism by which azurin may increase cellular levels of p53***

We propose that the increased cellular levels of p53 observed in the presence of azurin may be due to (*i*) increased intrinsic stability of p53, (*ii*) steric shielding of p53 from degradation enzymes or (*iii*) enhanced DNA-binding capacity. To reveal the molecular mechanism behind azurin's ability to promote p53-mediated cell death in cancer cells, we have investigated all three possibilities *in vitro* using full-length p53 and azurin.

Azurin's effect on p53's intrinsic thermodynamic stability was probed by equilibrium-unfolding experiments using GuHCl and temperature perturbations. Since there has been some conflicting reports on wild-type p53 stability (*11*, *12*), we first clarified this issue at our conditions. The observation on p53 in isolation was compared to unfolding data

when in complex with azurin. p53 was found to unfold before azurin (*i.e.*, at lower denaturant concentration and at lower temperature). This is reasonable since the copper-form of azurin has an usually high stability (52 kJ/mol, pH 7): its GuHCl-unfolding midpoint is ~4.5 M and it is thermally stable up to at least 75°C (*21, 38*). Unfolding of p53 was monitored by far-UV CD (*39*).

Our experiments showed that the thermal stability of full-length p53 as monitored by far-UV CD is not increased by azurin-complex formation (Figure 4). In agreement with published data on full-length p53 (*36*), the unfolding midpoint for p53 appeared at 65ºC and the unfolded state retains some secondary structure. In the presence of azurin, the midpoint shifts downwards by 5ºC; moreover, p53 unfolding becomes more complete (*i.e.* unfolded state appears more random-coil like). This implies (*i*) that azurin remains bound throughout p53's thermal transition, (*ii*) that the presence of bound azurin restricts long-range interactions that somewhat stabilize the native structure of p53 and, finally, (*iii*) that bound azurin limits retention of secondary-structure elements in the unfolded state. In analogy, the GuHCl-induced unfolding experiments at room-temperature revealed that also p53's thermodynamic stability towards chemical perturbation is not enhanced by the interaction with azurin. Based on these findings, the increased cellular levels of p53 in the presence of azurin are *not* due to increased wild-type p53 stability.

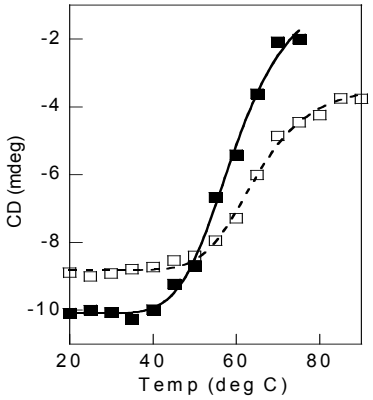

Figure 4. Thermal transitions monitored by CD at 218 nm for p53 alone (open symbols) and p53 in complex with azurin (filled symbols; azurin signals subtracted). Note that azurin (copper-form) does not unfold until above 75ºC.

Several inactivating enzymes bind to p53's NTD, thus masking the transcription activation segment. For example, the MDM2 protein is overactive in many tumors; its binding to the NTD results in p53 inactivation and degradation (13). If azurin binds to NTD, as suggested by the results in Task 1, its binding-site may overlap with those of inactivation and degradation proteins and, therefore, bound azurin molecules may sterically shield p53 from interacting with such proteins. Depending on the relative p53 affinities,

azurin may even displace degradation and inactivation proteins from p53. To address this hypothesis *in vitro*, we performed proteolysis experiments of full-length p53 in the presence and absence of azurin. Chymotrypsin, that hydrolyses peptide bonds involving tyrosines, phenylalanines and tryptophans, as well as trypsin, that is specific to lysines and arginines, was employed. p53 has four tryptophans, nine tyrosines, ten phenylalanines and forty-six residues that are either lysine or arginine. Extent of cleavage was monitored as a function of time and detected by standard gel-electrophoresis methods. Despite a large number of experiments in which we varied enzyme concentration, solvent conditions and temperature, we never detected any differences in the proteolytic pattern of p53 as a function of the presence/absence of azurin. Thus, at least with respect to chymotrypsin and trypsin, azurin binding does not protect p53 towards degradation.

To investigate the effect of azurin on p53's DNA-binding ability, we used a 20 base-pair DNA duplex (5'-AGGCATGTCTAGGCATGTCT-3' and 3'-TCCGTACAGATCCGTACAGA-5' oligonucleotides annealed) that contains the consensus sequence for p53 binding. We employed ITC to first reveal the affinity between p53 and the DNA target at our conditions. Next we tested p53's ability to bind DNA in the presence of azurin (Figure 5). Stronger DNA binding in the presence of azurin would provide a mechanistic explanation for how azurin mediates p53-induced apoptosis *in vivo*. However, we did not observe tighter binding in the presence of azurin; in fact, the presence of azurin did not affect the DNA binding of p53 to any degree (the dissociation constant for the p53-DNA complex was 50±20 nM both with and without azurin; pH 7.5, 20 ºC). This result provides further support that azurin binds to NTD, which is a domain that is not involved in DNA binding.

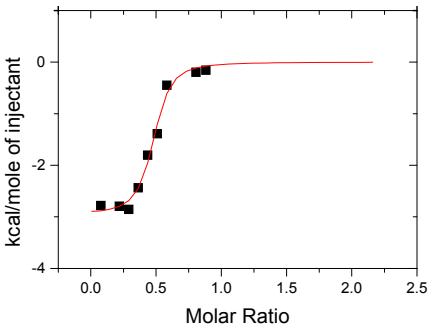

Figure 5. ITC data showing the integrated enthalpy as a function of DNA:p53 ratio. The solid curve is the best fit to the data. 5 μM p53 with 25 μM azurin (in cell) was titrated with pre-formed DNA duplex (in syringe) in a buffer of 350 mM phosphate, 150 mM NaCl, pH 7.5, 20 °C. The data analysis give a dissociation constant of about 50 nM and a stoichiometry of about 1 DNA duplex per two p53. The same parameters were found in the absence of azurin.

Task 3. ***Define the surface on azurin that interacts with p53 and reveal the role of azurin's metal cofactor in p53 binding***

We have made comparisons of the interactions between p53 and apo-, zinc- and copper-forms of azurin, respectively, by ITC. We find that the presence of a metal (Cu or Zn) is favorable for high affinity but that the apo-form of azurin can also bind to p53. It has earlier been shown that two residues in azurin (Met44 and Met64) are important for complex formation with p53. In contrast to wild-type azurin, the Met44LysMet64Glu double-mutant of azurin did not bind p53 (4-7). In the future (not possible within the time frame of this project), we will prepare a set of azurin surface mutants, focusing on residues in azurin's hydrophobic patch which include Met44 and Met64. This is the surface area of azurin known to be involved in interactions with other redox proteins *in vitro* (*40*). After preparation, the variants will be tested for p53 binding by ITC and gel-filtration experiments. We note that the peptide work described under task 4 below provides complementary information on what parts of azurin interacts with p53.

To explore the biological consequences of a possible need for the copper-form of azurin for tight binding to p53, we investigated the effects of copper on the structure and stability of two human proteins that participate in copper metabolism pathways. These proteins could be involved in interactions with azurin, which may result in azurin de-metallation or hinder azurin to reach p53, if azurin-based molecules are to be used as cancer drugs in the future. One of the proteins (*i.e.,* ceruloplasmin) has the same fold as azurin but contains 6 such domains and functions as a ferroxidase in the plasma. The other human protein (*i.e.,* copper-chaperone Atox1) has a different fold and is responsible for copper transport and delivery in the cytoplasm. Before assessing how these proteins may interact with azurin, it is required to elucidate their individual properties. The results of thermodynamic characterizations of these proteins are described in three manuscripts published in *Biochemisty, Biophys Journal* and *Biochem Biophys Acta* (*41-43*). From these studies we have learnt how Cu is inserted and how it affects protein structure and stability. In the case of ceruloplasmin, this is of high importance since mutations in this protein causes severe problems with Cu transport in patients. We note that in addition to their relevance to azurin and the purpose of targeting p53, these proteins appear to over-expressed in many cancers and it is proposed that copper accumulates in tumors.

We also characterized the novel bacterial copper chaperone, CopC, which is structurally similar to azurin and found in the periplasm of Cu resistant bacteria. By analyzing the role of copper in stability and folding of CopC, we hoped to reveal common properties of cupredoxin-like structures; such features could then be applied to azurin-based drug molecules. The thermodynamic *in vitro* work on CopC was described in a paper in *Arch Biochem Biophys* (*44*).

Task 4. ***Use the acquired information on the complex to design small peptide variants that retain the ability to bind and affect p53 like full-length azurin***

The acquired information from the work in Tasks 1-3 will ultimately be used to design peptide variants that mimic azurin's interaction with p53. In contrast to full-length proteins, small peptides are not expected to trigger immunological responses when introduced into a host organism. Moreover, there are strategies to deliver peptides into cells (for example by linkage to a harmless protein that can breach cell membranes) and ways to eliminate peptide vulnerability to degradation (*45-47*).

To date, we have tested a small 13-residue peptide corresponding to azurin's C-terminal sequence, *i.e.*, residues 111-124 with the sequence F**C**TFPG**H**SAL**M**KG (*19, 48*). This peptide contains three key residues involved in azurin's copper site, Cys112, His117 and Met 121 (bold in above sequence). The peptide was tested for p53 and NTD binding with and without the presence of copper (Figure 6). We found that the Cu-loaded peptide binds to p53 in a 1:1 stoichiometry and a K_D of about 100 nM was estimated (pH 8, 20 °C). This is only 25-fold weaker binding than full-length azurin binding to p53. The Cu-peptide complex could also bind to NTD in a 1:1 stoichiometry although the affinity was now reduced to correspond to a K_D of about 2.6 μM. Nonetheless, this is only 10-fold weaker than full-length azurin's affinity for NTD. The peptide binding was reduced if Cu was removed. In the absence of copper, the K_D of the peptide for p53 was 600 nM and no peptide interaction with NTD could be detected (Figure 6). The control experiments testing if copper alone could bind to p53 was negative, indicating no such interaction. Key thermodynamic parameters are listed in Table 1.

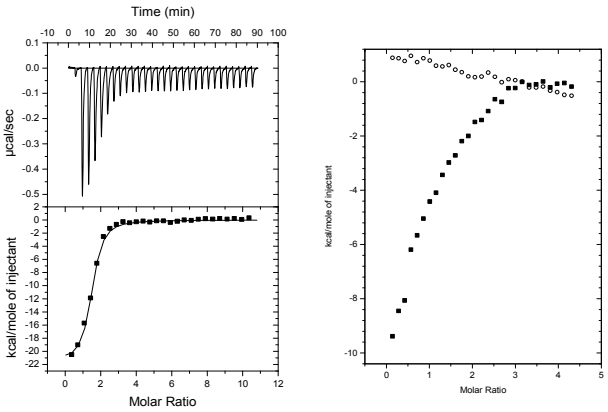

Figure 6. Left. ITC data showing the raw heat injections on top and, below, the thermogram with the integrated enthalpy as a function of peptide:p53 ratio. The solid curve is the best fit to the data. 2 μM p53 (in cell) was titrated with Cu-peptide (in syringe) in a buffer of 100 mM phosphate, pH 8, 20 °C. **Right.** Comparison of thermograms for peptide additions to NTD with (filled symbols) and without (open symbols) pre incubation with Cu.

These results have several implications. First, they suggest that it is the area around the metal site in azurin that interacts with p53. Second, they suggest that metal-induced secondary structure in the peptide is important for tight binding, in agreement with specific binding sites on p53. Third, since peptide binding occurs also to NTD, it strengthens the conclusion that full-length azurin also binds to NTD. Finally, these observations indicate that peptide mimics can reproduce (at least part of) the azurin-p53 interaction.

We have performed cell culture studies (with collaborator Dr. Ananda Chakrabarty) to test the ability of the peptide (+/- copper) to penetrate cancer cells (MCF-7 and Mel-6 cells), interact with p53, and thereby trigger apoptosis. Unfortunately, we found that the peptide itself did not cause much cell death, likely because of poor cell penetration. In the presence of Cu, increased apoptosis was observed although additions of Cu alone or azurin, at the same levels, resulted in higher levels of apoptosis. These experiments imply that in order for the peptide to work *in vivo*, it needs help to go into the cells. This can be done by attachment of another peptide stretch from azurin that was recently shown to act as a 'transduction domain' that enters mammalian cells efficiently (*49*). Therefore, future work will involve studies of a longer peptide with the Cu-site region and the cell-entry part fused by a couple of Gly residues. If peptide-based constructs can be found that enter cells, bind to p53 like full-length azurin and trigger apoptosis *in vivo*, they will be novel leads for the development of new cancer drugs.

We have also analyzed how the crowded environment inside of cells affects protein structure, stability and folding. This is important as azurin (or any drug based on azurin) and p53 will meet in such an environment. To start on this, we used model proteins that had been extensively characterized in dilute solutions. We found that both the α/β protein

flavodoxin and the all α-helical protein VlsE became more structured in the presence of crowding agents. By computer simulations, we revealed where in the proteins the additional ordering was taking place. We reported these findings in *Proc. Natl. Acad. Sci* and *Febs Letters* (*50, 51*). This discovery was surprising as excluded-volume theory assumes that the native state remains the same and that crowding perturbs only the unfolded state. Additional work on azurin in crowding agents revealed that also this protein becomes more ordered in crowded conditions. Future work will involve repetition of the azurin-p53 binding studies in the presence of crowding agents to see if the parameters change.

Table 1. Summary of auzin/peptide interactions with p53/NTD (pH 7.5-8.0, 20 °C).

Azurin variant	Variant of p53	K_D	Stoichiometry
Cu-azurin	p53	40 nM	4:1
Apo-peptide	p53	600 nM	1:1
Cu-peptide	p53	100 nM	1:1
Cu-azurin	NTD	300 nM	2:1
Apo-peptide	NTD	*No binding*	-
Cu-peptide	NTD	2.6 μM	1:1

Key research accomplishments

- Copper-form of azurin binds to NTD domain of p53 with nM affinity
- Stoichiometry of azurin-NTD complex (i.e., 2:1) differs from that of azurin-p53 (i.e., 4:1) indicating that other p53 domains play some role in interaction
- Azurin binding does not increase p53 stability, protect p53 against proteases or affect p53's DNA binding
- Peptide corresponding to copper-binding segment of azurin binds to p53 similarly to full-length azurin; Cu is required for this
- Peptide alone does not enter mammalian cells; transduction domain needed
- Properties of two human copper-metabolism proteins have been identified; these proteins are important as they may cross-react with azurin-based drugs
- The crowded environment inside cells is found to affect protein native structures and thus may influence the azurin-p53 binding reaction

Reportable outcomes

- Six manuscripts published (see Appendix)
- Poster presented at Era of Hope meeting 2008 (see Appendix)

- Training of postdocs; one got a research position at National lab due to this work
- Increased interest to join research group from incoming students
- Initiation of new collaborations; widening of research scope

Conclusion/"So what?"

Reports of regression of cancer in humans infected with microbial pathogens date back more than 100 years (3). However, live bacteria produce significant toxicity, limiting their use. The unprecedented observation that the small bacterial protein *P. aeruginosa* azurin forms a complex with the well-known tumor suppressor protein p53 and triggers cell death provides *a new avenue for cancer research*. Our biophysical project provides key physical, chemical and structural understanding of azurin's interaction with p53 *in vitro*. We propose that the results of our studies may be used to develop small peptide constructs that bind and stabilize p53 like full-length azurin. If these molecules turn out to work *in vivo*, it may be the gateway to an innovative class of new cancer therapeutics.

References

(1) Harris, C. C. (1996) Structure and function of the p53 tumor suppressor gene: clues for rational cancer therapeutic strategies. *J Natl Cancer Inst 88*, 1442-1455.

(2) Adman, E. T. (1991) Copper protein structures. *Adv Protein Chem 42*, 145-197.

(3) Yamada, T., Goto, M., Punj, V., Zaborina, O., Chen, M. L., Kimbara, K., Majumdar, D., Cunningham, E., Das Gupta, T. K., and Chakrabarty, A. M. (2002) Bacterial redox protein azurin, tumor suppressor protein p53, and regression of cancer. *Proc Natl Acad Sci U S A 99*, 14098-14103.

(4) Goto, M., Yamada, T., Kimbara, K., Horner, J., Newcomb, M., Gupta, T. K., and Chakrabarty, A. M. (2003) Induction of apoptosis in macrophages by Pseudomonas aeruginosa azurin: tumour-suppressor protein p53 and reactive oxygen species, but not redox activity, as critical elements in cytotoxicity. *Mol Microbiol 47*, 549-559.

(5) Punj, V., Das Gupta, T. K., and Chakrabarty, A. M. (2003) Bacterial cupredoxin azurin and its interactions with the tumor suppressor protein p53. *Biochem Biophys Res Commun 312*, 109-114.

(6) Yamada, T., Goto, M., Punj, V., Zaborina, O., Kimbara, K., Das Gupta, T. K., and Chakrabarty, A. M. (2002) The bacterial redox protein azurin induces apoptosis in J774 macrophages through complex formation and stabilization of the tumor suppressor protein p53. *Infect Immun 70*, 7054-7062.

(7) Yamada, T., Hiraoka, Y., Ikehata, M., Kimbara, K., Avner, B. S., Das Gupta, T. K., and Chakrabarty, A. M. (2004) Apoptosis or growth arrest: Modulation of tumor suppressor p53's specificity by bacterial redox protein azurin. *Proc Natl Acad Sci U S A 101*, 4770-4775.

(8) Punj, V., Bhattacharyya, S., Saint-Dic, D., Vasu, C., Cunningham, E. A., Graves, J., Yamada, T., Constantinou, A. I., Christov, K., White, B., Li, G., Majumdar, D., Chakrabarty, A. M., and Das Gupta, T. K. (2004) Bacterial cupredoxin azurin as an inducer of apoptosis and regression in human breast cancer. *Oncogene 23*, 2367-2378.

(9) Yamada, T., Hiraoka, Y., Das Gupta, T. K., and Chakrabarty, A. M. (2004) Regulation of mammalian cell growth and death by bacterial redox proteins: relevance to ecology and cancer therapy. *Cell Cycle 3*, 752-755.

(10) Dawson, R., Muller, L., Dehner, A., Klein, C., Kessler, H., and Buchner, J. (2003) The N-terminal domain of p53 is natively unfolded. *J Mol Biol 332*, 1131-1141.

(11) Nichols, N. M., and Matthews, K. S. (2001) Protein-DNA binding correlates with structural thermostability for the full-length human p53 protein. *Biochemistry 40*, 3847-3858.

(12) Bell, S., Klein, C., Muller, L., Hansen, S., and Buchner, J. (2002) p53 contains large unstructured regions in its native state. *J Mol Biol 322*, 917-927.

(13) Kussie, P. H., Gorina, S., Marechal, V., Elenbaas, B., Moreau, J., Levine, A. J., and Pavletich, N. P. (1996) Structure of the MDM2 oncoprotein bound to the p53 tumor suppressor transactivation domain. *Science 274*, 948-953.

(14) Nichols, N. M., and Matthews, K. S. (2002) Human p53 phosphorylation mimic, S392E, increases nonspecific DNA affinity and thermal stability. *Biochemistry 41*, 170-178.

(15) Sakaguchi, K., Sakamoto, H., Lewis, M. S., Anderson, C. W., Erickson, J. W., Appella, E., and Xie, D. (1997) Phosphorylation of serine 392 stabilizes the tetramer formation of tumor suppressor protein p53. *Biochemistry 36*, 10117-10124.

(16) Vijgenboom, E., Busch, J. E., and Canters, G. W. (1997) In vivo studies disprove an obligatory role of azurin in denitrification in Pseudomonas aeruginosa and show that azu expression is under control of rpoS and ANR. *Microbiology 143*, 2853-2863.

(17) Nar, H., Messerschmidt, A., Huber, R., van de Kamp, M., and Canters, G. W. (1992) Crystal structure of Pseudomonas aeruginosa apo-azurin at 1.85 A resolution. *FEBS Lett 306*, 119-124.

(18) Nar, H., Messerschmidt, A., Huber, R., van de Kamp, M., and Canters, G. W. (1991) Crystal structure analysis of oxidized Pseudomonas aeruginosa azurin at pH 5.5 and pH 9.0. A pH-induced conformational transition involves a peptide bond flip. *J Mol Biol 221*, 765-772.

(19) Pozdnyakova, I., Guidry, J., and Wittung-Stafshede, P. (2000) Copper triggered b-hairpin formation. Initiation site for azurin folding? *J AM Chem Soc 122*, 6337-6338.

(20) Pozdnyakova, I., Guidry, J., and Wittung-Stafshede, P. (2001) Probing copper ligands in denatured Pseudomonas aeruginosa azurin: Unfolding His117Gly and His46Gly mutants. *J Biol Inorg Chem 6*, 182-188.

(21) Pozdnyakova, I., Guidry, J., and Wittung-Stafshede, P. (2001) Copper Stabilizes Azurin by Decreasing the Unfolding Rate. *Arch. Biochem. Biophys. 390*, 146-148.
(22) Pozdnyakova, I., Guidry, J., and Wittung-Stafshede, P. (2002) Studies of Pseudomonas aeruginosa azurin mutants: cavities in beta-barrel do not affect refolding speed. *Biophysical Journal 82*, 2645-2651.
(23) Pozdnyakova, I., and Wittung-Stafshede, P. (2001) Biological relevance of metal binding before protein folding. *J Am Chem Soc 123*, 10135-10136.
(24) Pozdnyakova, I., and Wittung-Stafshede, P. (2001) Copper binding before polypeptide folding speeds up formation of active (holo) Pseudomonas aeruginosa azurin. *Biochemistry 40*, 13728-13733.
(25) Pozdnyakova, I., and Wittung-Stafshede, P. (2003) Approaching the speed limit for Greek Key beta-barrel formation: transition-state movement tunes folding rate of zinc-substituted azurin. *Biochim Biophys Acta 1651*, 1-4.
(26) Fuentes, L., Oyola, J., Fernandez, M., and Quinones, E. (2004) Conformational changes in azurin from Pseudomona aeruginosa induced through chemical and physical protocols. *Biophys J 87*, 1873-1880.
(27) Wilson, C. J., and Wittung-Stafshede, P. (2005) Role of structural determinants in folding of the sandwich-like protein Pseudomonas aeruginosa azurin. *Proc Natl Acad Sci U S A 102*, 3984-3987.
(28) Hung, I. H., Casareno, R. L., Labesse, G., Mathews, F. S., and Gitlin, J. D. (1998) HAH1 is a copper-binding protein with distinct amino acid residues mediating copper homeostasis and antioxidant defense. *J Biol Chem 273*, 1749-1754.
(29) Sato, M., and Gitlin, J. D. (1991) Mechanisms of copper incorporation during the biosynthesis of human ceruloplasmin. *J Biol Chem 266*, 5128-5134.
(30) Walker, J. M., Huster, D., Ralle, M., Morgan, C. T., Blackburn, N. J., and Lutsenko, S. (2004) The N-terminal metal-binding site 2 of the Wilson's Disease Protein plays a key role in the transfer of copper from Atox1. *J Biol Chem 279*, 15376-15384.
(31) Strausak, D., Howie, M. K., Firth, S. D., Schlicksupp, A., Pipkorn, R., Multhaup, G., and Mercer, J. F. (2003) Kinetic analysis of the interaction of the copper chaperone Atox1 with the metal binding sites of the Menkes protein. *J Biol Chem 278*, 20821-20827.
(32) van Dongen, E. M., Klomp, L. W., and Merkx, M. (2004) Copper-dependent protein-protein interactions studied by yeast two-hybrid analysis. *Biochem Biophys Res Commun 323*, 789-795.
(33) Minton, A. P. (2001) The influence of macromolecular crowding and macromolecular confinement on biochemical reactions in physiological media. *J Biol Chem 276*, 10577-10580.
(34) Minton, A. P. (2005) Influence of macromolecular crowding upon the stability and state of association of proteins: predictions and observations. *J Pharm Sci 94*, 1668-1675.
(35) Apiyo, D., and Wittung-Stafshede, P. (2005) Unique complex between bacterial azurin and tumor-suppressor protein p53. *Biochem Biophys Res Commun 332*, 965-968.
(36) Nichols, N. M., and Matthews, K. S. (2001) p53 unfolding detected by CD but not by tryptophan fluorescence. *Biochem Biophys Res Commun 288*, 111-115.
(37) Gilardi, G., Mei, G., Rosato, N., Canters, G. W., and Finazzi-Agro, A. (1994) Unique environment of Trp48 in Pseudomonas aeruginosa azurin as probed by site-directed mutagenesis and dynamic fluorescence spectroscopy. *Biochemistry 33*, 1425-1432.
(38) Leckner, J., Wittung, P., Bonander, N., Karlsson, G., and Malmstrom, B. (1997) The effect of redox state on the folding free energy of azurin. *J. Biol. Inorg. Chem. 2*, 368-371.
(39) Bellamine, A., Mangla, A. T., Nes, W. D., and Waterman, M. R. (1999) Characterization and catalytic properties of the sterol 14alpha- demethylase from Mycobacterium tuberculosis. *Proc Natl Acad Sci U S A 96*, 8937-8942.
(40) Van Pouderoyen, G., Mazumdar, S., Hunt, N. I., Hill, A. O., and Canters, G. W. (1994) The introduction of a negative charge into the hydrophobic patch of Pseudomonas aeruginosa azurin affects the electron self-exchange rate and the electrochemistry. *Eur J Biochem 222*, 583-588.
(41) Sedlak, E., and Wittung-Stafshede, P. (2007) Discrete roles of copper ions in chemical unfolding of human ceruloplasmin. *Biochemistry 46*, 9638-9644.
(42) Hussain, F., and Wittung-Stafshede, P. (2007) Impact of cofactor on stability of bacterial (CopZ) and human (Atox1) copper chaperones. *Biochim Biophys Acta 1774*, 1316-1322.
(43) Sedlak, E., Zoldak, G., and Wittung-Stafshede, P. (2008) Role of copper in thermal stability of human ceruloplasmin. *Biophys J 94*, 1384-1391.

(44) Hussain, F., Sedlak, E., and Wittung-Stafshede, P. (2007) Role of copper in folding and stability of cupredoxin-like copper-carrier protein CopC. *Arch Biochem Biophys 467*, 58-66.
(45) Wadia, J. S., Stan, R. V., and Dowdy, S. F. (2004) Transducible TAT-HA fusogenic peptide enhances escape of TAT-fusion proteins after lipid raft macropinocytosis. *Nat Med 10*, 310-315.
(46) Snyder, E. L., and Dowdy, S. F. (2004) Cell penetrating peptides in drug delivery. *Pharm Res 21*, 389-393.
(47) Wadia, J. S., and Dowdy, S. F. (2005) Transmembrane delivery of protein and peptide drugs by TAT-mediated transduction in the treatment of cancer. *Adv Drug Deliv Rev 57*, 579-596.
(48) Marks, J., Pozdnyakova, I., Guidry, J., and Wittung-Stafshede, P. (2004) Methionine-121 coordination determines metal specificity in unfolded Pseudomonas aeruginosa azurin. *J Biol Inorg Chem 9*, 281-288.
(49) Yamada, T., Fialho, A. M., Punj, V., Bratescu, L., Gupta, T. K., and Chakrabarty, A. M. (2005) Internalization of bacterial redox protein azurin in mammalian cells: entry domain and specificity. *Cell Microbiol 7*, 1418-1431.
(50) Stagg, L., Zhang, S. Q., Cheung, M. S., and Wittung-Stafshede, P. (2007) Molecular crowding enhances native structure and stability of alpha/beta protein flavodoxin. *Proc Natl Acad Sci U S A 104*, 18976-18981.
(51) Perham, M., Stagg, L., and Wittung-Stafshede, P. (2007) Macromolecular crowding increases structural content of folded proteins. *FEBS Lett 581*, 5065-5069.

Appendix

Publications (1-6) that acknowledge support from this grant are included in this section, followed by an abstract from the Era of Hope meeting 2008:

1. F Hussain, P Wittung-Stafshede
Impact of Cofactor on Stability of Bacterial (CopZ) and Human (Atox1) Copper Chaperones
Biochem Biophys Acta, 2007, 1774(10):1316-22.

2. E Sedlak, P Wittung-Stafshede
Discrete Roles of Copper Ions in Chemical Unfolding of Human Ceruloplasmin
Biochemistry, 2007, 46(33):9638-44. (Featured in Chem. & Eng. News)

3. F Hussain, E Sedlak, P Wittung-Stafshede
Role of copper in folding and stability of cupredoxin-like copper-carrier CopC
Arch Biochem Biophys, 2007, 467(1):58-66.

4. E Sedlak, P Wittung-Stafshede
Role of copper in thermal stability of human ceruloplasmin
Biophys J, 2008, 94(4), 1384-1391.

5. M Perham, L Stagg, P Wittung-Stafshede
Macromolecular Crowding Increases Structural Content of Folded Proteins
Febs Letters, 2007, 581(26):5065-9.

6. L Stagg, S-Q Zhang, M Cheung, P Wittung-Stafshede
Molecular crowding enhances native structure and stability of α/β protein flavodoxin
Proc Nat Acad Sci USA 2007,104, 18976-18981 (Featured: Rice News; on Rice home page, Kemivarlden)

Abstract Era of Hope 2008:
Title: *Novel Breast Cancer Therapeutics Based on Bacterial Cupredoxin*
(Experimental Therapeutics 1; P16-8)

Available online at www.sciencedirect.com
ScienceDirect
Biochimica et Biophysica Acta 1774 (2007) 1316–1322
Biochimica et Biophysica Acta
BBA
www.elsevier.com/locate/bbapap

Impact of cofactor on stability of bacterial (CopZ) and human (Atox1) copper chaperones

Faiza Hussain [a], Pernilla Wittung-Stafshede [a,b,c,*]

[a] Department of Biochemistry and Cell Biology, Rice University, 6100 Main Street, Houston, TX 77251, USA
[b] Department of Chemistry, Rice University, 6100 Main Street, Houston, TX 77251, USA
[c] Keck Center for Structural Computational Biology, Rice University, 6100 Main Street, Houston, TX 77251, USA

Received 23 May 2007; received in revised form 30 July 2007; accepted 31 July 2007
Available online 19 August 2007

Abstract

Here, we present the first characterization of *in vitro* unfolding and thermodynamic stability of two copper chaperone proteins: *Bacillus subtilis* CopZ and *Homo sapiens* Atox1. We find that the unfolding reactions for apo- and Cu(I)-forms of CopZ and Atox1, induced by the chemical denaturant, guanidine hydrochloride (GuHCl), and by thermal perturbation are reversible two-state reactions. For both proteins, the unfolding midpoints shift to higher GuHCl concentrations and the thermodynamic stability is increased in the presence of Cu(I). Despite the same overall fold, apo-CopZ exhibits much lower thermal stability than apo-Atox1. Although the thermal stability of both proteins is increased in the presence of copper, the stabilizing effect is largest for the less stable variant. Divergent energetic properties of the apo- and holo-forms may be linked to conformational changes that facilitate copper transfer to the target.

Keywords: Protein folding; Metallo-chaperone; Protein stability; Copper metabolism; Spectroscopy

1. Introduction

Copper is one of the most prevalent transition metals in living organisms [1]; its biological function is intimately related to its redox properties. Many proteins that participate in cellular respiration, antioxidant defense, neurotransmitter biosynthesis, connective-tissue biosynthesis and pigment formation use copper as the prosthetic, active group [2–5]. Since free copper is toxic, copper homeostasis in living organisms is tightly controlled by subtle molecular mechanisms [6–8]. In eukaryotes, before cellular uptake via high-affinity copper transporters of the CTR family [5], Cu(II) ions are reduced to Cu(I). During the past decade, an important class of proteins, termed copper-chaperones, has been identified in the cytoplasm that binds Cu(I) with Cys_2 coordination [5,9–12]. These small, soluble proteins guide and protect the copper ions within the cell, delivering them to the appropriate functional protein receptors. P-type ATPases are membrane spanning receptor proteins with cytoplasmic metal-binding domains that transfer Cu(I) through membranes from one cellular compartment to another. In humans, ATP7A (i.e., Menkes disease protein) and ATP7B (i.e., Wilson disease protein) proteins are P-type ATPases involved in copper transport [5,10,13]; in an ATP-dependent process, they translocate copper from the cytoplasm into the Golgi lumen for insertion into enzymes in the secretory pathway [5], such as apo-ceruloplasmin [14].

One hallmark of the copper chaperones is the similarity of the fold between the chaperone and the target metal-binding domains of the ATPases [2,15,16]. Solution NMR and X-ray crystal structures [15–23] demonstrate that these proteins possess a βαββαβ ferredoxin-like fold with the metal ion bound by the two cysteines in a MXCXXC motif in a surface-accessible loop towards the N-terminus (Fig. 1). Despite the wealth of structural data, there is no folding or stability data on copper-transport proteins. Since these proteins switch between apo- and holo-forms as part of their functional cycle, biophysical properties of both states are of biological relevance and may

Abbreviations: CD, circular dichroism; T_m, thermal midpoint; DTT, dithiothreitol

* Corresponding author. Department of Biochemistry and Cell Biology, Rice University, 6100 Main Street, Houston, TX 77251, USA.
E-mail address: pernilla@rice.edu (P. Wittung-Stafshede).

1570-9639/$ – see front matter © 2007 Elsevier B.V. All rights reserved.
doi:10.1016/j.bbapap.2007.07.020

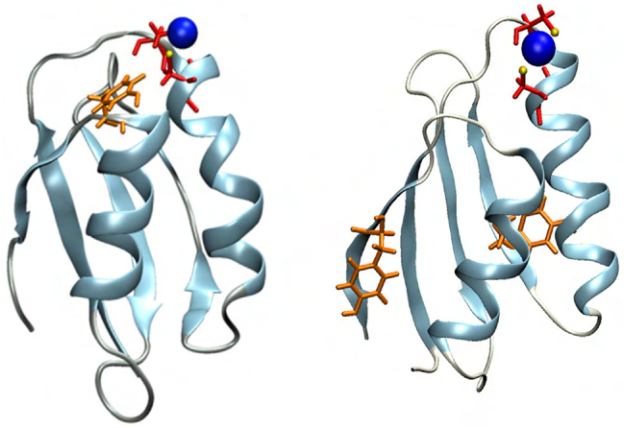

Fig. 1. Structures of CopZ (1KOV; left) and Atox1 (1TL4; right). Copper, blue; metal-binding cysteines, red; tyrosines (Tyr65 in CopZ; Tyr64 and Tyr31 in Atox1), orange.

explain how vectorial copper transport is achieved despite an apparent shallow thermodynamic gradient [24].

To address this issue, we have compared the *in vitro* unfolding processes and thermodynamic stability of homologous copper chaperones from two different organisms: *Bacillus subtilis* CopZ and *Homo sapiens* Atox1. Although these proteins share only 15% sequence identity, they both have the ferredoxin-like fold and the conserved copper-binding motif (Fig. 1). We find that both proteins can unfold in two-state, reversible equilibrium reactions. While Atox1 is more resistant than CopZ to thermal perturbations, in both apo- and holo-forms, the difference in thermodynamic stability between the two homologs at room temperature is small. For both Atox1 and CopZ, the coordination of the Cu(I) cofactor stabilizes the folded state towards perturbations.

2. Materials and methods

2.1. Protein preparation

A pALTER-Ex1 plasmid with the CopZ gene and a pET28a vector with the *H. sapiens* Atox1 gene were expressed in *Escherichia coli*. For both proteins, published purification protocols were followed [24,25] with slight modifications. The proteins were purified in apo-forms. Additional EDTA dialysis was employed to assure no zinc contamination. Protein molecular weights were confirmed by mass spectrometry. Protein samples were stored at −80 °C, in the presence of 1 mM DTT, until use. DTT was removed by extensive dialysis (4 buffer exchanges) to buffer without DTT under argon gas. The presence of the two cysteines in the metal-binding motif was verified with Ellman's assay on samples in the absence of DTT. In copper titrations to apo-CopZ or apo-Atox1, copper was added as $CuCl_2$ in presence/absence of 1 mM DTT as indicated. Unfolding experiments on apo- and Cu(I)-forms of the two proteins were performed in the presence of 1 mM DTT if not otherwise noted.

2.2. Spectroscopy

Far-UV CD was measured in a 1-mm cell between 200 and 300 nm; near-UV CD was measured in a 1-cm cell between 250 and 400 nm (Jasco J-810 spectropolarimeter). Tyrosine fluorescence was measured on a Varian Eclipse fluorometer with excitation at 280 nm and emission monitored between 290 and 400 nm.

2.3. Chemical and thermal unfolding

GuHCl-induced unfolding was performed in 20 mM Tris, pH 7.5, 20 °C, 1 mM DTT, 30 μM protein (apo- or holo-forms of CopZ or Atox1). To obtain the holo-forms, 1 equivalent of copper was added as $CuCl_2$; in the presence of DTT, the Cu(II) is reduced to Cu(I) [25,26]. In some protein samples, DTT was removed before Cu(II) was added (see text). All samples were incubated for 2 h before far-UV CD and fluorescence spectroscopic measurements. There was no time dependence in the reactions for incubation time variations from 30 min to 6 h. Thermal CD and fluorescence data (CD signal at 220 nm and emission at 303 nm) was acquired with a scan rate of 0.5° per min (from 20 to 90 °C). Faster or slower scan rates did not change the thermal profiles and in all cases forward and backward (from 90 to 20 °C) scans overlapped indicating true equilibrium reactions. The chemical unfolding data was fit to standard equations for two-state reactions [27,28] to reveal *m*-values and unfolding-free energies, $\Delta G_U(H_2O)$. Reaction reversibility was tested in all cases. For each protein variant, the far-UV CD (at 220 nm) and tyrosine emission (at 303 nm) data points overlapped in both thermal and chemical reactions. There was no protein-concentration dependence in the transitions (10–50 μM range tested).

3. Results

3.1. Characterization of apo- and holo-forms of CopZ and Atox1

Copper loading of CopZ and target metal-binding domains in Wilson disease protein have been monitored by near-UV CD changes [25,29]. It has been reported that regardless of Cu(II) or Cu(I) additions, the protein-bound form is always Cu(I) [25,30–32]. Thus, the copper-binding site must have a considerable preference for Cu(I) over Cu(II), resulting in a high redox potential for the Cu(II)/Cu(I) couple. This is consistent with the principles of hard/soft acid/base theory, which predicts that soft cysteine-thiol ligands have a preference for soft metals such as Cu(I) [33]. In the presence of a reducing agent such as DTT, copper is reduced prior to protein incorporation. In the absence of DTT or other reducing agents, the source of electrons is not known although copper auto-oxidation/reduction has been proposed [25]. We used Ellman's assay to estimate the amount of reduced cysteine thiols in CopZ after sub-stoichiometric additions of Cu(II) in the absence of DTT. Based on our results, it appears that protein-thiol oxidation may not be the major source of electrons for Cu reduction in the absence of exogenous reducing agents (data not shown).

Copper titrations to apo-CopZ monitored by near-UV CD demonstrate the formation of distinct protein–copper complexes: addition of Cu(II) in the absence of reducing agent results in a holo-protein complex proposed to involve two proteins bridged by copper *via* the cysteine residues [25]. In contrast, addition of 1 equivalent of Cu(II) in the presence of DTT creates a monomeric 1:1 holo-form, perhaps involving DTT as an exogenous copper ligand in addition to the two cysteine thiolates (Fig. 2A) [19,34]. We note that the latter species (i.e., the 1:1 complex) may be the most relevant as the cytoplasmic milieu, where these proteins reside, is reducing. *In vivo*, glutathione may acts as a third copper ligand [35] (instead of DTT) or the metal may be two-coordinated using only the protein cysteines [9].

In CopZ, Tyr65 is positioned close to the copper site, i.e., within 7–8 Å [25,36]. In accord, we found that copper additions to CopZ result in emission quenching until 1:1 stoichiometry is

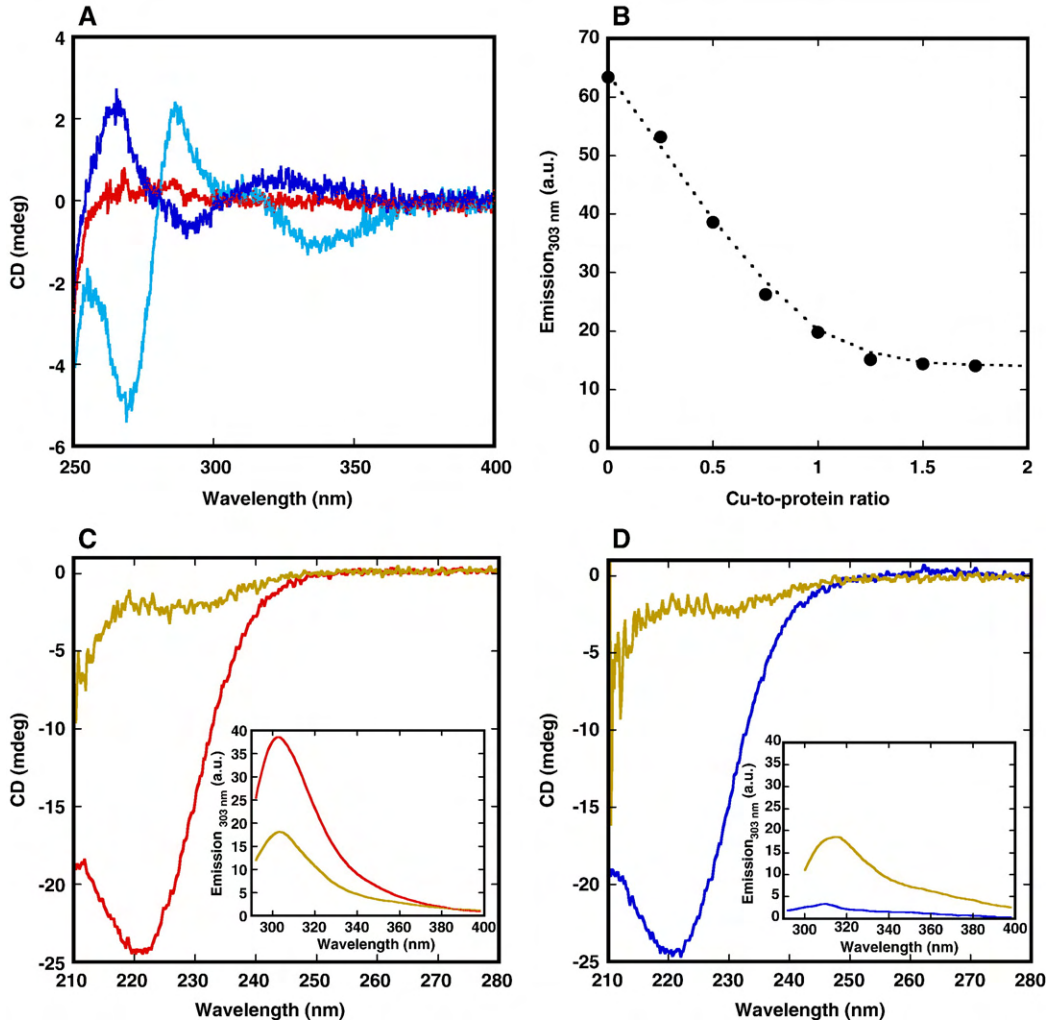

Fig. 2. (A) Near-UV CD of apo-(red) and holo-forms of CopZ: 1:2 (light blue, no DTT) and 1:1 (dark blue, 1 mM DTT) copper-to-protein complexes (pH 7.5, 20 °C). (B) Copper additions to apo-CopZ monitored by fluorescence changes at 303 nm (pH 7.5, 20 °C). (C) Far-UV CD spectra of folded (red; buffer, pH 7.5, 20 °C) and unfolded (gold; 5 M GuHCl, pH 7.5, 20 °C) forms of apo-CopZ. Inset C: fluorescence spectra of folded (red; buffer, pH 7.5, 20 °C) and unfolded (gold; 5 M GuHCl, pH 7.5, 20 °C) forms of apo-CopZ. (D) Far-UV CD spectra of folded (blue; buffer, pH 7.5, 20 °C) and unfolded (gold; 5 M GuHCl, pH 7.5, 20 °C) forms of holo-CopZ. Inset D: fluorescence spectra of folded (blue; buffer, pH 7.5, 20 °C) and unfolded (gold; 5 M GuHCl, pH 7.5, 20 °C) forms of holo-CopZ. Similar CD and emission spectra as in panels C and D were collected for folded and unfolded forms of apo- and holo-Atox1. Whereas the fluorescence decreases for the apo-forms upon unfolding, due to tyrosine exposure to solvent, the emission increases upon unfolding of the holo-forms as the fluorescence is quenched by the copper in the folded state.

reached (with DTT; Fig. 2B). Although copper binding is in essence stoichiometric at these conditions, a protein–copper dissociation constant of about 0.2±0.1 μM (pH 7, 20 °C) could be derived from the fluorescence data. Notably, this value is in good agreement with a previous estimate for CopZ [25].

The copper-binding behavior of apo-Atox1 parallels that of CopZ when monitored by near-UV CD and tyrosine emission changes (data not shown). However, due to the longer distance between the copper site and the tyrosines (see Fig. 1), the emission quenching upon copper binding is less for Atox1 (i.e., emission quenched by ~30% in Atox1 as compared to ~70% in CopZ). Nonetheless, in the presence of DTT, copper binding levels off at 1:1 ratios when monitored by fluorescence and near-UV CD signals, indicative of a 1:1 Cu(I):Atox1 complex. A previous calorimetric study reported 1:1 Cu(I) binding to Atox1 and a dissociation constant for the complex of about 5 μM (in MES buffer, pH 6.5, 22 °C) [24]. In all our experiments with Atox1, therefore, the protein concentration was kept above 20 μM to assure stoichiometric Cu(I) binding. For both Atox1 and CopZ, we verified the presence of stable 1:1 copper-to-protein complexes by dialysis experiments (1 mM DTT, 20 mM Tris, pH 7.5, 20 °C) followed by copper quantification using a biquinoline assay [37].

3.2. Chemical unfolding of CopZ and Atox1

Several buffer conditions were evaluated to assure apo- and holo-forms unfolded reversibly and copper ions did not precipitate (final solvent conditions selected for our work include 20 mM Tris, 1 mM DTT, at pH 7.5). Equilibrium unfolding of CopZ and Atox1 was induced by additions of the chemical denaturant, guanidine hydrochloride (GuHCl). Progress of the reactions was monitored by far-UV CD, probing secondary structure, and tyrosine emission, monitoring tertiary

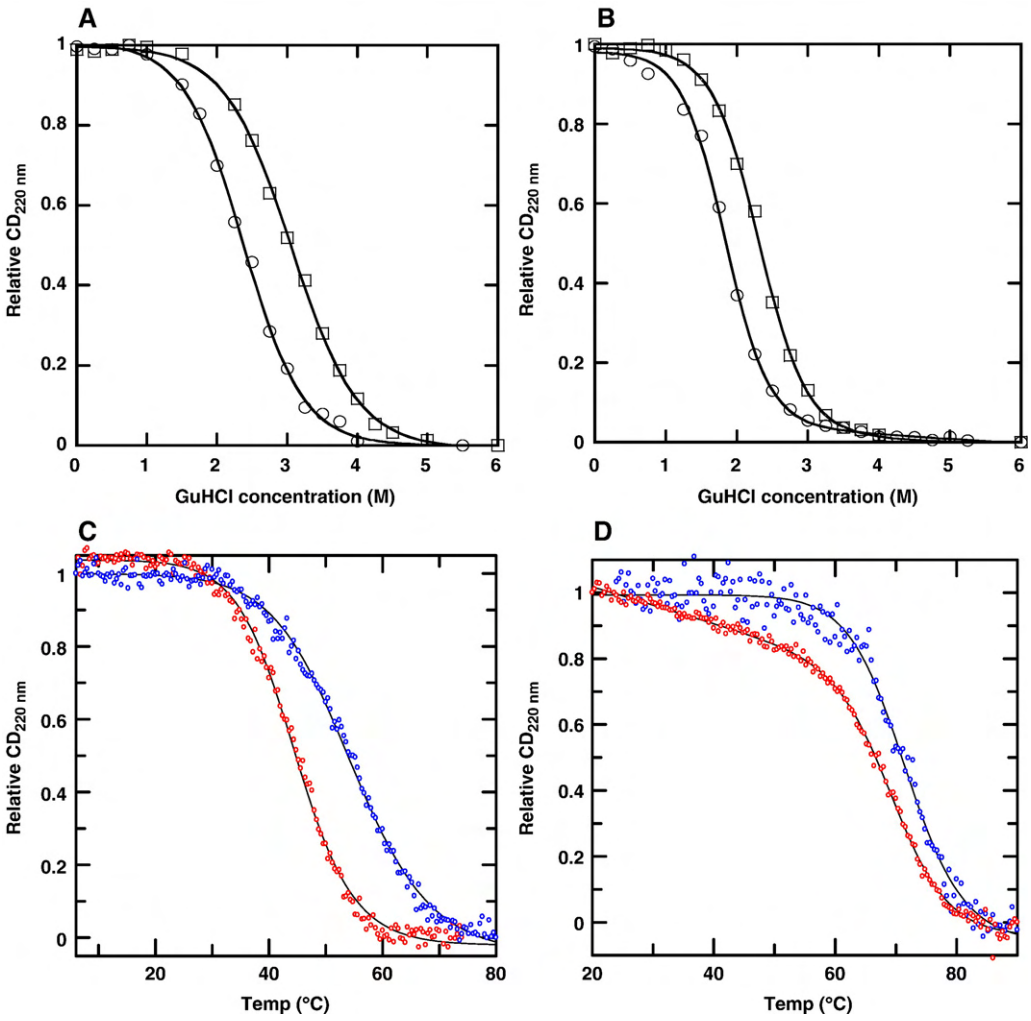

Fig. 3. (A, B) GuHCl-induced unfolding of apo-(circles) and holo-(squares) forms of CopZ (A) and Atox1 (B) monitored by far-UV CD. Solid curves are two-state fits to the data. (C, D) Thermally-induced unfolding of apo-(red) and holo-(blue) forms of CopZ (C) and Atox1 (D) monitored by far-UV CD. In all cases, the holo-form corresponds to 1:1 Cu-to-protein ratio in the presence of 1 mM DTT.

structure (Fig. 2C, D). We found that unfolding of the apo- and monomeric (i.e., 1:1 copper:protein form in the presence of DTT) holo-forms of CopZ and Atox1 are reversible two-state transitions: the CD and fluorescence-detected unfolding data overlap in each case. The holo-forms are more resistant towards chemical perturbation as compared to their corresponding apo-variants (Fig. 3A, B). Both the GuHCl concentrations at the transition midpoints, and the corresponding unfolding-free energies, are increased in the presence of the metal (Table 1). For all GuHCl-induced unfolding reactions, the reversibility was tested by denaturant jumps to lower GuHCl concentrations favoring the folded states. For both Atox1 and CopZ, the reactions were over 90% reversible (data not shown).

Table 1
Thermal and chemical (20 °C) unfolding data for CopZ and Atox1 with and without copper (Fig. 3; 1 mM DTT, 20 mM Tris, pH 7.5)

Protein	T_m	$[GuHCl]_{1/2}$	$\Delta G_U(H_2O)$	m[a]
Apo CopZ	45±1 °C	2.3±0.1 M	13.4±0.5 kJ/mol	5.7
Holo CopZ	55±1 °C	3.0±0.1M	15.5±0.5 kJ/mol	5.1
Apo Atox1	68±1 °C	1.8±0.1M	14.5±0.6 kJ/mol	7.9
Holo Atox1	71±1 °C	2.3±0.1M	16.7±0.7 kJ/mol	7.2

$\Delta G_U(H_2O)$ and m-values were obtained from two-state fits to the data [27,28]; all reactions were reversible. Individual fits to the CD (at 220 nm) and emission (at 303 nm; excitation at 280 nm) data as a function of GuHCl gave identical parameters for each variant (fits to CD data reported here).

[a] Unit is: kJ/(mol·M).

Although the unfolding midpoints appear at higher GuHCl concentrations for CopZ than for Atox1, the lower m-value (corresponding to the relative amount of hydrophobic surface-area exposed upon unfolding [27,28]) results in a lower unfolding-free energy for CopZ as compared to Atox1 (Table 1). This implies that Atox1 has a more well-ordered structure in the native state (regardless of the presence/absence of the metal). This agrees with the NMR data implying more conformational averaging in the apo-form of CopZ than in the apo-form of Atox1 [19,31,36].

3.3. Thermal unfolding of CopZ and Atox1

Equilibrium unfolding of CopZ and Atox1 was also induced by heating; again, progress of the reactions was monitored by far-UV CD and tyrosine emission (Fig. 3C, D). Thermal

unfolding of the apo- and monomeric holo-forms of CopZ and Atox1 are also reversible two-state transitions in the presence of DTT: the CD and fluorescence-detected unfolding data overlap in each case. Interestingly, CopZ is significantly less stable than Atox1 towards thermal perturbation (T_m of 45 vs. 68 °C; Table 1) and the transitions are broader. This agrees with the observation that chemically-induced unfolding of CopZ is less cooperative than of Atox1. Whereas CopZ is stabilized by ~10 °C by the copper, the thermal curves are only shifted by a few degrees when comparing apo- and holo-Atox1 (Fig. 3C, D). Thermal reversibility was investigated by reverse scans from high to low temperatures monitoring the return of the far-UV CD signal. At the solvent conditions used here, all thermal unfolding processes were over 90% reversible. We note that heating without DTT resulted in irreversible protein-unfolding profiles, most likely due to copper-mediated thiol oxidation at high temperatures. Thus, it was not possible to assess the thermal stability of the dimeric holo-CopZ complex formed in the absence of added reducing agent.

4. Discussion

This is the first thermodynamic analysis of copper chaperone unfolding and stability *in vitro*. Depending on copper availability, these proteins cycle between apo- and holo-forms *in vivo.* Therefore, folding and stability properties of both forms are important to understand how these parameters are related to the mechanism of copper transport as well as to diseases caused by mutations in the involved proteins [6,14,38–40]. A recent comparative structural-genomic analysis of metallochaperones and metal-transporting ATPases noted several distinctions in terms of residue substitutions and electrostatic/hydrophobic patterns among these otherwise homologous proteins that were proposed to specify partner recognition [15]. Our biophysical observations on Atox1 and CopZ have several implications for the function of copper-transport proteins, as described below.

First, despite the same overall structure, the apo-form of CopZ has a 23-° lower thermal stability as compared to the apo-form of Atox1. Variations in surface-charges may explain this difference between the proteins on a molecular level [15]. Atox1 and CopZ share only 15% sequence identity; whereas CopZ is acidic, Atox1 has an isoelectric point of about 7 [15]. Moreover, CopZ has a large patch of negative charges on one side that are proposed to be involved in target recognition (i.e., the metal-binding domains of the *B. subtilis* ATPase CopA). In contrast, the electrostatic surface pattern on Atox1 is more varied, involving many small positive and negative areas. The distribution of charges may allow for the formation of stabilizing salt-bridges on the surface of Atox1 but not in the case of CopZ. As charge–charge interactions become stronger, relative to hydrophobic interactions, at high temperatures [41], their effect on protein stability will be more pronounced in the thermal unfolding experiments; in accord, this is the trend that was observed (Table 1). From a functional perspective, the presence of competing copper chaperones in mammalian cells [1] may require a more stable apo-form in eukaryotes as compared to in prokaryotes.

Second, although the copper-site is located in a loop at the protein surface, copper binding favorably affects both thermal (ΔT_m of 3–10°; pH 7.5) and chemical ($\Delta G(H_2O)$ increases by ~15%; pH 7.5, 20 °C) stability of the two proteins. This phenomenon suggests that copper-binding induces rearrangements throughout the protein structure that improves overall stability. This is in accord with the reported solution structures for these proteins. By NMR, major changes in hydrophobic interactions between secondary structure elements as a function of copper were demonstrated in both CopZ [36] and yeast Atx1 [21]. That the stabilizing effect of metallation is not as dramatic in Atox1 as in CopZ is also reasonable. NMR experiments have revealed that, in contrast to the other chaperones, there are only minor alterations in the Atox1 structure upon copper-binding [31]. The effects of copper-binding on protein stability have been found to vary dramatically. For example, the copper in *Pseudomonas aeruginosa* azurin stabilizes the protein towards chemical perturbations by ~30% in its reduced form and by 100% in the oxidized form [42–44]. The copper cofactors also contribute largely to the stability of ascorbate oxidase and Cu, Zn-superoxide dismutase [45,46] whereas, in the multi-domain enzyme ceruloplasmin, the coppers do not contribute at all to the overall stability [47]. On the contrary, copper was found to promote transitions in the prion protein towards less stable conformations [48] and to coordinate to non-native states of beta-2-microglobulin that resulted in native-state destabilization [49].

Third, since copper has a stabilizing effect on both Atox1 and CopZ, albeit the magnitudes differ, we propose that this is a general trend that applies to copper chaperones and target metal-binding domains in most organisms. In support of this idea, unfolding data on the first metal-binding domain of the human Menkes disease protein (with the same fold as CopZ and Atox1) demonstrates that Cu(I) has a stabilizing effect (T_m differs by ~10 °C for apo- and holo-forms; unpublished data). We propose that differential stability of apo- and holo-forms is linked to conformational/dynamic differences in the copper-binding loop and nearby peptide regions that, in turn, provide a mechanism for *in vivo* target recognition. Copper transfer from the holo-form of the chaperone to the apo-form of the target domain may involve partial chaperone unfolding that is coupled to metal release. Based on our CopZ and Atox1 data, it appears that differential stability (and thus flexibility) of the apo-versus holo-forms are fine-tuned by sequence variations to meet the specific need of each organism.

Interestingly, copper-stimulated proteolysis seems to play an important role in the regulation of copper homeostasis in *Enterococcus hirae* [50–52]. *E. hirae* CopZ was found to be more susceptible to degradation in the copper-bound form than in the apo-form [53]. Copper-induced degradation of the copper transporter Ctr1p of *Saccharomyces cerevisiae* and the yeast transcription factor Mac1, involved in high affinity copper uptake, have also been reported [54,55]. It is not clear how preferred degradation of the holo-form of *E. hirae* CopZ occurs and what is the identity of the involved protease [53]. Our biophysical results on *B. subtilis* CopZ imply that a protease-recognition mechanism involving protein unfolding is *not* likely,

as we found the holo-form to be more stable than the apo-form. This is reasonable as many proteins can exist in unfolded forms *in vivo* without degradation. Notably, the apo-form of metallothionein was recently found to be present in high levels in human tissues [56–58]. Moreover, although the apo-form of metallothionein is unfolded [59], the folded metal-form (like holo-CopZ in *E. hirae*) appeared less resistant to proteolysis than the apo-form [57].

Finally, from a technical standpoint, our discovery of metal-dependent fluorescence of these copper-chaperones will allow for real time spectroscopic investigations of metal transfer between CopZ/Atox1 and selected target metal-binding domains (work in progress). Notably, the target metal-binding domains of bacterial CopA as well as the human Wilson and Menkes disease proteins do not have tyrosines at the same positions, i.e., near the metal sites, as in CopZ and Atox1 [15].

Acknowledgements

We thank Dr. N. Le Brun and Dr. A. Rosenzweig for the CopZ and Atox1 plasmid constructs, respectively. Support for this project was provided by the Robert A. Welch Foundation (C-1588) and the USAMRAA (Concept award; W81XWH-06-1-0572).

References

[1] T.V. O'Halloran, V.C. Culotta, Metallochaperones, an intracellular shuttle service for metal ions, J. Biol. Chem. 275 (2000) 25057–25060.
[2] D.L. Huffman, T.V. O'Halloran, Function, structure, and mechanism of intracellular copper trafficking proteins, Annu. Rev. Biochem. 70 (2001) 677–701.
[3] S. Puig, E.M. Rees, D.J. Thiele, The ABCDs of periplasmic copper trafficking, Structure 10 (2002) 1292–1295.
[4] S. Puig, D.J. Thiele, Molecular mechanisms of copper uptake and distribution, Curr. Opin. Chem. Biol. 6 (2002) 171–180.
[5] E.D. Harris, Basic and clinical aspects of copper, Crit. Rev. Clin. Lab. Sci. 40 (2003) 547–586.
[6] P.P. Kulkarni, Y.M. She, S.D. Smith, E.A. Roberts, B. Sarkar, Proteomics of metal transport and metal-associated diseases, Chemistry 12 (2006) 2410–2422.
[7] A.L. Lamb, A.K. Wernimont, R.A. Pufahl, V.C. Culotta, T.V. O'Halloran, A.C. Rosenzweig, Crystal structure of the copper chaperone for superoxide dismutase, Nat. Struct. Biol. 6 (1999) 724–729.
[8] A.L. Lamb, A.S. Torres, T.V. O'Halloran, A.C. Rosenzweig, Heterodimeric structure of superoxide dismutase in complex with its metallochaperone, Nat. Struct. Biol. 8 (2001) 751–755.
[9] M.D. Harrison, C.E. Jones, M. Solioz, C.T. Dameron, Intracellular copper routing: the role of copper chaperones, Trends Biochem. Sci. 25 (2000) 29–32.
[10] I. Hamza, M. Schaefer, L.W. Klomp, J.D. Gitlin, Interaction of the copper chaperone HAH1 with the Wilson disease protein is essential for copper homeostasis, Proc. Natl. Acad. Sci. U. S. A. 96 (1999) 13363–13368.
[11] I.H. Hung, R.L. Casareno, G. Labesse, F.S. Mathews, J.D. Gitlin, HAH1 is a copper-binding protein with distinct amino acid residues mediating copper homeostasis and antioxidant defense, J. Biol. Chem. 273 (1998) 1749–1754.
[12] L.W. Klomp, S.J. Lin, D.S. Yuan, R.D. Klausner, V.C. Culotta, J.D. Gitlin, Identification and functional expression of HAH1, a novel human gene involved in copper homeostasis, J. Biol. Chem. 272 (1997) 9221–9226.
[13] I.H. Hung, M. Suzuki, Y. Yamaguchi, D.S. Yuan, R.D. Klausner, J.D. Gitlin, Biochemical characterization of the Wilson disease protein and functional expression in the yeast *Saccharomyces cerevisiae*, J. Biol. Chem. 272 (1997) 21461–21466.
[14] N.E. Hellman, S. Kono, G.M. Mancini, A.J. Hoogeboom, G.J. De Jong, J.D. Gitlin, Mechanisms of copper incorporation into human ceruloplasmin, J. Biol. Chem. 277 (2002) 46632–46638.
[15] F. Arnesano, L. Banci, I. Bertini, S. Ciofi-Baffoni, E. Molteni, D.L. Huffman, T.V. O'Halloran, Metallochaperones and metal-transporting ATPases: a comparative analysis of sequences and structures, Genome Res. 12 (2002) 255–271.
[16] A.C. Rosenzweig, D.L. Huffman, M.Y. Hou, A.K. Wernimont, R.A. Pufahl, T.V. O'Halloran, Crystal structure of the Atx1 metallochaperone protein at 1.02 A resolution, Structure Fold Des. 7 (1999) 605–617.
[17] T.M. DeSilva, G. Veglia, S.J. Opella, Solution structures of the reduced and Cu(I) bound forms of the first metal binding sequence of ATP7A associated with Menkes disease, Proteins 61 (2005) 1038–1049.
[18] L. Banci, I. Bertini, S. Ciofi-Baffoni, D.L. Huffman, T.V. O'Halloran, Solution structure of the yeast copper transporter domain Ccc2a in the apo and Cu(I)-loaded states, J. Biol. Chem. 276 (2001) 8415–8426.
[19] L. Banci, I. Bertini, R. Del Conte, J. Markey, F.J. Ruiz-Duenas, Copper trafficking: the solution structure of *Bacillus subtilis* CopZ, Biochemistry 40 (2001) 15660–15668.
[20] R.A. Pufahl, C.P. Singer, K.L. Peariso, S.J. Lin, P.J. Schmidt, C.J. Fahrni, V.C. Culotta, J.E. Penner-Hahn, T.V. O'Halloran, Metal ion chaperone function of the soluble Cu(I) receptor Atx1, Science 278 (1997) 853–856.
[21] F. Arnesano, L. Banci, I. Bertini, D.L. Huffman, T.V. O'Halloran, Solution structure of the Cu(I) and apo forms of the yeast metallochaperone, Atx1, Biochemistry 40 (2001) 1528–1539.
[22] L. Banci, I. Bertini, S. Ciofi-Baffoni, L. Gonnelli, X.C. Su, A core mutation affecting the folding properties of a soluble domain of the ATPase protein CopA from *Bacillus subtilis*, J. Mol. Biol. 331 (2003) 473–484.
[23] D. Achila, L. Banci, I. Bertini, J. Bunce, S. Ciofi-Baffoni, D.L. Huffman, Structure of human Wilson protein domains 5 and 6 and their interplay with domain 4 and the copper chaperone HAH1 in copper uptake, Proc. Natl. Acad. Sci. U. S. A. 103 (2006) 5729–5734.
[24] A.K. Wernimont, L.A. Yatsunyk, A.C. Rosenzweig, Binding of copper(I) by the Wilson disease protein and its copper chaperone, J. Biol. Chem. 279 (2004) 12269–12276.
[25] M.A. Kihlken, A.P. Leech, N.E. Le Brun, Copper-mediated dimerization of CopZ, a predicted copper chaperone from *Bacillus subtilis*, Biochem. J. 368 (2002) 729–739.
[26] M. Ralle, S. Lutsenko, N.J. Blackburn, Copper transfer to the N-terminal domain of the Wilson disease protein (ATP7B): X-ray absorption spectroscopy of reconstituted and chaperone-loaded metal binding domains and their interaction with exogenous ligands, J. Inorg. Biochem. 98 (2004) 765–774.
[27] A. Fersht, Structure and mechanism in protein science, W.H. Freeman and Company, New York, 1999.
[28] C.N. Pace, K.L. Shaw, Linear extrapolation method of analyzing solvent denaturation curves, Proteins Suppl. 4 (2000) 1–7.
[29] M. DiDonato, H.F. Hsu, S. Narindrasorasak, L. Que Jr., B. Sarkar, Copper-induced conformational changes in the N-terminal domain of the Wilson disease copper-transporting ATPase, Biochemistry 39 (2000) 1890–1896.
[30] A. Urvoas, B. Amekraz, C. Moulin, L. Le Clainche, R. Stocklin, M. Moutiez, Analysis of the metal-binding selectivity of the metallochaperone CopZ from *Enterococcus hirae* by electrospray ionization mass spectrometry, Rapid Commun. Mass Spectrom. 17 (2003) 1889–1896.
[31] I. Anastassopoulou, L. Banci, I. Bertini, F. Cantini, E. Katsari, A. Rosato, Solution structure of the apo and copper(I)-loaded human metallochaperone HAH1, Biochemistry 43 (2004) 13046–13053.
[32] V. Tanchou, F. Gas, A. Urvoas, F. Cougouluegne, S. Ruat, O. Averseng, E. Quemeneur, Copper-mediated homo-dimerisation for the HAH1 metallochaperone, Biochem. Biophys. Res. Commun. 325 (2004) 388–394.
[33] I. Bertini, H.B. Gary, S.J. Lippard, J.S. Valentine, Bioinorganic Chemistry, University Science Books, Mill Valley, CA, 1994.
[34] M. Ralle, S. Lutsenko, N.J. Blackburn, X-ray absorption spectroscopy of the copper chaperone HAH1 reveals a linear two-coordinate Cu(I) center capable of adduct formation with exogenous thiols and phosphines, J. Biol. Chem. 278 (2003) 23163–23170.

[35] A. Urvoas, M. Moutiez, C. Estienne, J. Couprie, E. Mintz, L. Le Clainche, Metal-binding stoichiometry and selectivity of the copper chaperone CopZ from *Enterococcus hirae*, Eur. J. Biochem. 271 (2004) 993–1003.
[36] L. Banci, I. Bertini, R. Del Conte, Solution structure of apo CopZ from *Bacillus subtilis*: further analysis of the changes associated with the presence of copper, Biochemistry 42 (2003) 13422–13428.
[37] G. Felsenfeld, The determination of cuprous ion in copper proteins, Arch. Biochem. Biophys. 87 (1960) 247–251.
[38] H. Miyajima, Y. Takahashi, T. Kamata, H. Shimizu, N. Sakai, J.D. Gitlin, Use of desferrioxamine in the treatment of aceruloplasminemia, Ann. Neurol. 41 (1997) 404–407.
[39] J.D. Gitlin, Wilson disease, Gastroenterology 125 (2003) 1868–1877.
[40] T.Y. Tao, J.D. Gitlin, Hepatic copper metabolism: insights from genetic disease, Hepatology 37 (2003) 1241–1247.
[41] D. Xu, S. Lin, R. Nussinov, Protein binding versus protein folding: The role of hydrophilic bridges in protein associations, J. Mol. Biol. 265 (1997) 68–84.
[42] J. Leckner, P. Wittung, N. Bonander, G. Karlsson, B. Malmstrom, The effect of redox state on the folding free energy of azurin, J. Biol. Inorg. Chem. 2 (1997) 368–371.
[43] P. Wittung-Stafshede, Role of cofactors in folding of the blue-copper protein azurin, Inorg. Chem. 43 (2004) 7926–7933.
[44] P. Wittung-Stafshede, Role of cofactors in protein folding, Acc. Chem. Res. 35 (2002) 201–208.
[45] J.A. Rodriguez, J.S. Valentine, D.K. Eggers, J.A. Roe, A. Tiwari, R.H. Brown Jr., L.J. Hayward, Familial amyotrophic lateral sclerosis-associated mutations decrease the thermal stability of distinctly metallated species of human copper/zinc superoxide dismutase, J. Biol. Chem. 277 (2002) 15932–15937.
[46] I. Savini, S. D'Alessio, A. Giartosio, L. Morpurgo, L. Avigliano, The role of copper in the stability of ascorbate oxidase towards denaturing agents, Eur. J. Biochem. 190 (1990) 491–495.
[47] E. Sedlak, P. Wittung-Stafshede, Role of copper ions in chemical unfolding of human ceruloplasmin, Biochemistry 46 (2007) 9638–9644.
[48] J. Stockel, J. Safar, A.C. Wallace, F.E. Cohen, S.B. Prusiner, Prion protein selectively binds copper(II) ions, Biochemistry 37 (1998) 7185–7193.
[49] C.M. Eakin, J.D. Knight, C.J. Morgan, M.A. Gelfand, A.D. Miranker, Formation of a copper specific binding site in non-native states of beta-2-microglobulin, Biochemistry 41 (2002) 10646–10656.
[50] Z.H. Lu, C.T. Dameron, M. Solioz, The *Enterococcus hirae* paradigm of copper homeostasis: copper chaperone turnover, interactions, and transactions, Biometals 16 (2003) 137–143.
[51] M. Solioz, Role of proteolysis in copper homoeostasis, Biochem. Soc. Trans. 30 (2002) 688–691.
[52] M. Solioz, J.V. Stoyanov, Copper homeostasis in *Enterococcus hirae*, FEMS Microbiol. Rev. 27 (2003) 183–195.
[53] Z.H. Lu, M. Solioz, Copper-induced proteolysis of the CopZ copper chaperone of *Enterococcus hirae*, J. Biol. Chem. 276 (2001) 47822–47827.
[54] C.E. Ooi, E. Rabinovich, A. Dancis, J.S. Bonifacino, R.D. Klausner, Copper-dependent degradation of the *Saccharomyces cerevisiae* plasma membrane copper transporter Ctr1p in the apparent absence of endocytosis, Embo J. 15 (1996) 3515–3523.
[55] Z. Zhu, S. Labbe, M.M. Pena, D.J. Thiele, Copper differentially regulates the activity and degradation of yeast Mac1 transcription factor, J. Biol. Chem. 273 (1998) 1277–1280.
[56] Y. Yang, W. Maret, B.L. Vallee, Differential fluorescence labeling of cysteinyl clusters uncovers high tissue levels of thionein, Proc. Natl. Acad. Sci. U. S. A. 98 (2001) 5556–5559.
[57] D.H. Petering, J. Zhu, S. Krezoski, J. Meeusen, C. Kiekenbush, S. Krull, T. Specher, M. Dughish, Apo-metallothionein emerging as a major player in the cellular activities of metallothionein, Exp. Biol. Med. (Maywood) 231 (2006) 1528–1534.
[58] A. Krezel, W. Maret, Different redox states of metallothionein/thionein in biological tissue, Biochem. J. 402 (2007) 551–558.
[59] J. Ejnik, J. Robinson, J. Zhu, H. Forsterling, C.F. Shaw, D.H. Petering, Folding pathway of apo-metallothionein induced by Zn2+, Cd2+ and Co2+, J. Inorg. Biochem. 88 (2002) 144–152.

Discrete Roles of Copper Ions in Chemical Unfolding of Human Ceruloplasmin†

Erik Sedlak‡,§ and Pernilla Wittung-Stafshede*,‡,||,⊥

Department of Biochemistry and Cell Biology, Keck Center for Structural Computational Biology, and Department of Chemistry, Rice University, 6100 Main Street, Houston, Texas 77251

Received April 16, 2007; Revised Manuscript Received June 25, 2007

ABSTRACT: Human ceruloplasmin (CP) is a multicopper oxidase essential for normal iron homeostasis. The protein has six β-barrel domains with one type 1 copper in each of domains 2, 4, and 6; the remaining copper ions form a catalytic trinuclear cluster, one type 2 and two type 3 coppers, at the interface between domains 1 and 6. We have characterized urea-induced unfolding of holo- and apo-forms of CP by far-UV circular dichroism, intrinsic fluorescence, 8-anilinonaphthalene-1-sulfonic acid binding, visible absorption, copper content, and oxidase activity probes (pH 7, 23 °C). We find that holo-CP unfolds in a complex reaction with at least one intermediate. The formation of the intermediate correlates with decreased secondary structure, exposure of aromatics, loss of two coppers, and reduced oxidase activity; this step is reversible, indicating that the trinuclear cluster remains intact. Further additions of urea trigger complete protein unfolding and loss of all coppers. Attempts to refold this species result in an inactive apoprotein with molten-globule characteristics. The apo-form of CP also unfolds in a multistep reaction, albeit the intermediate appears at a slightly lower urea concentration. Again, correct refolding is possible from the intermediate but not the unfolded state. Our study demonstrates that in vitro equilibrium unfolding of CP involves intermediates and that the copper ions are removed in stages. When the catalytic site is finally destroyed, refolding is not possible at neutral pH. This implies a mechanistic role for the trinuclear metal cluster as a nucleation point, aligning domains 1 and 6, during CP folding in vivo.

Ceruloplasmin (CP; EC 1.16.3.1)[1] is a circulating copper protein found in vertebrate plasma, which belongs to the family of multicopper oxidases together with ascorbate oxidase and laccases (*1*−*4*). In humans, CP accounts for ∼95% of the plasma copper and plays an important role in iron metabolism due to its ability to oxidize Fe^{2+} to Fe^{3+}, which allows for subsequent incorporation of Fe^{3+} into apotransferrin (*5*−*8*). CP is also believed to function as an antioxidant agent to scavenge free radicals, as an amine oxidase to control levels of biogenic amines, and as a copper transporter to deliver copper to extrahepatic tissues (*8*−*10*). CP is synthesized in hepatocytes and secreted into the plasma after incorporation of six copper ions in the secretory pathway (*5*). Failure to incorporate this metal during biosynthesis results in the secretion of an unstable polypeptide that is rapidly degraded in the plasma (*11*).

CP consists of a 1046 residue polypeptide and six integral copper ions classified into five different sites (*6*, *9*). The crystal structure of CP (*6*, *9*) demonstrates that the polypeptide is folded in six β-barrel domains arranged in three pairs forming a triangular array around a pseudo 3-fold axis (Figure 1). Three copper ions are found in type 1 (T1) mononuclear centers located in domains 2, 4, and 6. Copper in domains 4 (T1B) and 6 (T1A) is coordinated by two His, one Cys, and one Met, whereas the Met is absent in the metal-binding site in domain 2 (T1C) (*6*, *9*). The high reduction potential of the T1C copper indicates that it is permanently reduced and not catalytically relevant (*12*, *13*). The absorption at 610 nm that gives CP its intense blue color is a result of the oxidized coppers T1A and T1B. The remaining three coppers form a trinuclear cluster at the interface of domains 1 and 6. This cluster consists of a mononuclear type 2 (T2) and a binuclear type 3 (T3) copper site. It is envisaged that electrons are donated by substrates

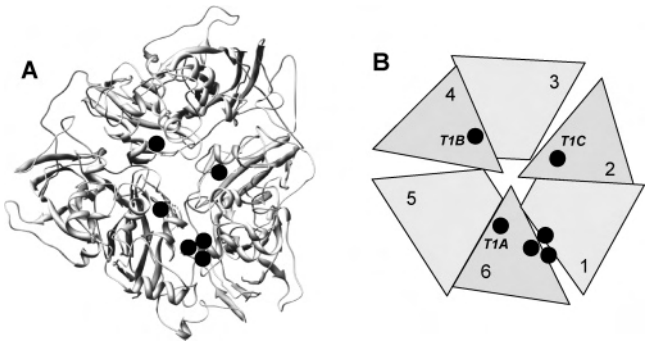

FIGURE 1: (A) Crystal structure of human CP (1kcw, pdb) with highlighted copper ions (circles) bound to the protein (UCSF Chimera). (B) Scheme of holo-CP showing the positions of the coppers (circles) in the six domains. The T1 coppers in domains 2, 4, and 6 are designated as T1C, T1B, and T1A, respectively.

† This work was funded by grants from the Robert A. Welch Foundation (C-1588) and the USAMRAA (Concept award; W81XWH-06-1-0572).

* To whom correspondence should be addressed. Tel: 713-348-4076. Fax: 713-348-5154. E-mail: pernilla@rice.edu.

‡ Department of Biochemistry and Cell Biology.

§ Permanent address: Department of Biochemistry, P.J. Safarik University, Moyzesova 11, 04001 Kosice, Slovakia.

|| Keck Center for Structural Computational Biology.

⊥ Department of Chemistry.

[1] Abbreviations: CP, ceruloplasmin; CD, circular dichroism, ANS, 8-anilinonaphthalene-1-sulfonic acid; CN, cyanide.

10.1021/bi700715e CCC: $37.00
Published on Web 07/28/2007

to T1A or T1B via outer-sphere electron transfer and then transferred to dioxygen at the trinuclear cluster (*6*, *9*, *13*−*15*). The trinuclear cluster is surrounded by four pairs of His residues equally contributed by domains 1 and 6.

Previous studies have indicated that the conformation of apo-CP has molten-globulelike properties (*16*, *17*). For more than 40 years, it has been assumed that apo-CP binds copper in an all-or-none fashion (*18*). In support, recent metabolic-labeling experiments indicated that achieving the final state of CP required occupation of all six copper-binding sites without apparent hierarchy for incorporation at any given site (*5*). On the other hand, there have also been reports that invoke the possibility of partially metallated forms of CP (*19*, *20*). On the basis of cyanide (CN)-dependent metal-removal attempts, it was suggested that the T1 coppers are more sensitive than the T2 and T3 coppers to elimination (*20*, *21*). To probe the role of the coppers in the folding mechanism of human CP, we here compare the chemically induced unfolding reactions of holo- and apo-forms using a set of biophysical tools (pH 7, 23 °C). Our study demonstrates that in vitro unfolding of both CP forms involves populated intermediates; for the holo-form, the partially folded intermediate has lost two coppers and some blue color, but the trinuclear copper cluster remains intact. It appears that this species, and thus early incorporation of the T2 and T3 copper ions, is a necessary requirement for successful in vivo biosynthesis of holo-CP.

MATERIALS AND METHODS

Chemicals and Instruments. Analytical-grade chemicals and *o*-dianisidine were obtained from Sigma-Aldrich. 2,2′-Biquinoline was obtained from Fluka. Human CP (>96% purity, $A_{610}/A_{280} = 0.046$) was obtained from Vital Products (Florida). The concentration of holo- and apo-CP was determined by ϵ_{280nm} of 200 mM^{-1} cm^{-1}. The urea concentration was determined from refractive index measurements. Absorbance, fluorescence, and far-UV circular dichroism (CD) measurements were performed on Varian Cary 50, Cary Eclipse, and Jasco J-810 spectrometers, respectively.

Copper Removal. To prepare apo-CP, 10 mg/mL of CP was dialyzed for 2 h at 23 °C against 30 mM ascorbate in 0.1 M Trizma, pH 7.2. Subsequently, dialysis continued for 20 h at 4 °C against 50 mM NaCN, 10 mM EDTA, and 10 mM ascorbate in 0.1 M Trizma, pH 7.2. The dialysis proceeded for another 24 h at 4 °C (with buffer exchange after 12 h) against 50 mM sodium phosphate buffer, pH 7.0. Alternatively, a more harsh method to prepare apo-CP involved denaturation of holo-CP in 9 M urea with subsequent dialysis against 50 mM phosphate buffer, pH 7.0, to remove the urea and dissociated coppers. The copper content to confirm 100% holo-form, and to reveal loss of copper at different urea concentrations during holo-CP unfolding, was determined according to the method developed by Felsenfeld (*22*).

Unfolding and Refolding Experiments. Samples for unfolding were prepared by suitable mixing of phosphate buffer and urea solution (9.3 M urea in 50 mM phosphate, pH 7.0) and protein (protein solution in phosphate buffer) with a final protein concentration of 2−3 μM. Samples were incubated for 1 h at 23 °C. CD was obtained from the averaged signal at 220 nm collected for 120 s at 23 °C. The same samples were used for determination of the dependence of protein fluorescence on urea concentration. Excitation was at 295 nm, and both intensity and position of emission maximum were determined from spectra obtained by averaging five consecutive scans. The same parameters characterizing 8-anilinonaphthalene-1-sulfonic acid (ANS) fluorescence were obtained from averaged emission spectra (five scans) of protein/urea samples including 200 μM ANS (excitation at 390 nm). To test for reversibility, the protein was incubated in 5.5 or 9.0 M urea, dependent on whether the first or second transition was the target, respectively. The perturbed protein was then mixed with buffer solutions containing the desired (lower) concentration of urea, and spectroscopic measurements were performed as described above. All experiments were performed at 23 °C. Each individual unfolding/refolding transition was analyzed as described in refs *23* and *24* using standard two-state equations that reveal free energies of unfolding in buffer (i.e., ΔG_U) and *m* values [i.e., a measure of cooperativity of the transition or relative exposure of the hydrophobic surface upon unfolding (*23*−*25*)].

CP Oxidase Activity Assay. The oxidase activity of CP was performed by using *o*-dianisidine (an aromatic diamine) as a substrate in accordance with the procedure by Schosinsky et al. (*26*).

Analysis of Far-UV CD Spectra. Far-UV CD spectra (190−260 nm) were recorded at 23 °C; all spectra were averages of 10 scans. Several algorithms available in DICHROWEB (*27*, *28*) were used to analyze the data. The goodness of the fits was based on the NRMSD parameter (*29*), and the best score was provided by CDSSTR (*30*).

RESULTS

Preparing Holo- and Apo-Forms of CP. Our holo-CP stocks were highly pure but sometimes (depending on storage time) contained a fraction of partially metallated protein. The oxidized T1 coppers can be identified from the 610 nm absorption. The T2 and T3 copper sites form the catalytic cluster and thus are probed indirectly via CP oxidase activity. The total number of copper ions in CP can be quantified using the 2,2′-biquinoline assay (*22*). Before each experiment, 100% holo-CP (i.e., the protein coordinating six coppers) was prepared via addition of additional copper ions in the presence of ascorbate followed by extensive dialysis to remove the excess copper (*5*). On the basis of 610 nm absorption and copper quantification, this treatment resulted in a homogeneous sample of 100% holo-CP. Different approaches to preparation of apo-CP have been described (*19*−*21*): CN dialysis under reducing conditions and high-urea treatment. Our experiments revealed that the CN dialysis method is "best" as it does not perturb the protein structure as much as urea treatment (see below). Thus, for our unfolding studies, we prepared apo-CP via CN dialysis. Metal analysis of the protein after this treatment confirmed that all copper ions had been removed.

In Figure 2, we show the far-UV CD (secondary structure) and fluorescence (tryptophan environment; CP has 19 Trp) spectra of apo- and holo-forms of CP. Secondary structure analysis of the CD data for holo-CP agree with the reported crystal structure; the signal is dominated by β-sheets, turns, and random coils, with minimal or no α-helices. Analysis of the spectra for apo-CP (prepared via CN dialysis) suggests

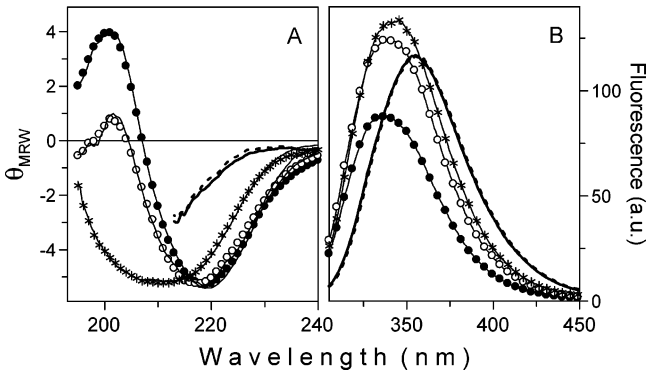

FIGURE 2: (A) Far-UV CD spectra of holo (●), apo(CN) (○), and apo(urea) (*) forms of CP. According to the CDSSTR algorithm, holo-CP contains 5% α-helix, 37% *β*-strands, 23% turns, and 33% unordered secondary structures. Corresponding contents in apo-(CN)-CP are 3% α-helix, 33% *β*-strands, 22% turns, and 41% unordered secondary structures. (B) Tryptophan emission (excitation at 295 nm) of holo (●), apo(CN) (○), and apo(urea) (*) forms of CP. For comparison, CD and fluorescence signals of fully unfolded apo- (dotted curves) and holo-CP (solid curves) (i.e., in 9 M urea) are also shown.

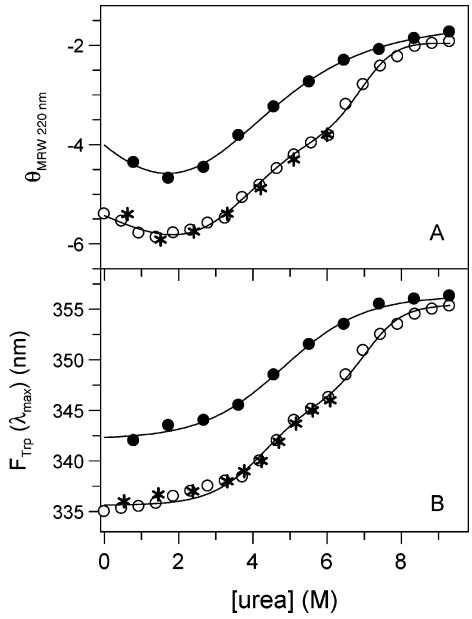

FIGURE 3: Isothermal denaturation of holo-CP followed by (A) CD at 220 nm and (B) tryptophan fluorescence (excitation at 295 nm). Unfolding of native-CP (○), refolding of CP from 5.5 M urea (*), and refolding of CP from 9.0 M urea (●). The continuous lines are fits to the experimental values (Table 1).

that the *β*-sheet content decreases with a subsequent increase in the random coil structure. Analogously, positions of maxima of tryptophan fluorescence of holo- (335 nm) and apo- (340 nm) forms indicate perturbation of the tryptophan environments in the apo-form of CP. Thus, apo-CP is structurally distinct from holo-CP: It appears to have lost some native structural elements. For comparison, CD and fluorescence spectra for fully unfolded forms are also shown in Figure 2.

Unfolding of Holo-CP. Unfolding of holo-CP was induced by urea additions at pH 7 and 23 °C. In Figure 3, we show the far-UV CD and fluorescence signals as a function of urea concentration. It is apparent that the process is not a simple two-state process but involves at least two steps. There appears to be a first transition with a midpoint of ∼4.2 M

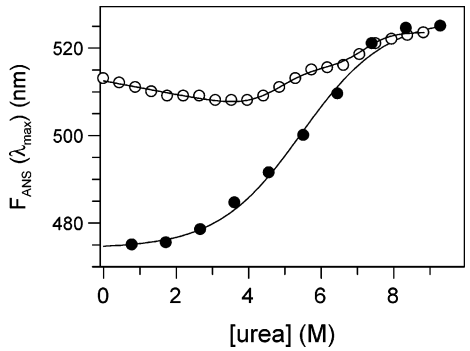

FIGURE 4: Isothermal denaturation of holo-CP followed by ANS fluorescence (excitation at 390 nm). Unfolding of native-CP (○) and refolding of CP from 9.0 M urea (●). The continuous lines are fits to experimental values (Table 1).

urea, resulting in the loss of about 30−40% of the far-UV CD intensity and a shift of the emission maximum toward higher wavelengths (i.e., from 335 to 345 nm) although the intensity does not change much. This first process is followed by a second transition that has a midpoint of ∼7.0 M urea. In this step, the fully unfolded form of the protein is reached according to the far-UV CD and tryptophan emission maximum (now at 355 nm) and intensity changes.

The unfolding reaction of holo-CP induced by urea was also probed via ANS emission (Figure 4). ANS is a fluorophore that emits strongly around 500 nm when bound to hydrophobic surfaces and pockets; it is often used as a tool to detect intermediate species of proteins as it does not significantly bind to either folded or unfolded forms (*31*, *32*). We find that the ANS emission shifts in a biphasic way that matches the two transitions observed for holo-CP with far-UV CD and tryptophan fluorescence. First, there is a small increase in the ANS emission together with a shift of the peak toward a higher maximum wavelength: This transition has a midpoint at ∼4−5 M urea. This change is followed by a further shift toward higher wavelengths of the ANS emission maximum in a second transition with a midpoint at ∼7 M urea. This result supports the presence of an intermediate species at intermediate urea concentrations (i.e., at ∼5.5 M urea).

The fates of the copper ions during urea treatment were tested by visible absorption at 610 nm (probing the oxidized T1 sites), copper analysis (probing total copper content), and oxidase activity (probing the catalytic cluster) as a function of urea (Figure 5). We find ∼50% decrease of 610 nm absorbance (which may correspond to destruction of one of the two oxidized T1 sites) in a first phase that parallels the first CD/fluorescence-detected transition. Copper quantification revealed that in total two copper ions have been removed from the protein at 5.5 M urea. The remaining blue color disappears at higher urea concentrations (6−7 M urea) together with loss of all copper ions (Figure 5). CP's oxidase activity disappears in a three-state transition that matches the disappearance of blue absorption (Figure 5): The first process results in a loss of about 60% activity. This indicates that although the intermediate form of CP at 5.5 M urea has lost some coppers, the catalytic copper cluster is still functional.

The binding site of aromatic diamine substrates such as *o*-dianisidine used here is located in domain 4 near T1B (*6*); thus, if this is the perturbed oxidized T1 site in the

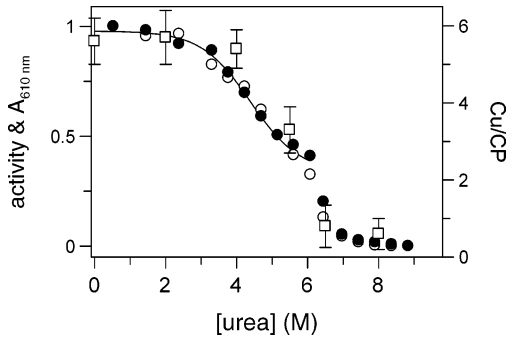

FIGURE 5: Isothermal denaturation of holo-CP followed by oxidase activity (○) monitored by reaction of CP with *o*-dianisidine and by visible absorbance at 610 nm (●). The total copper content in CP at different urea concentrations are also shown. The amount of copper (□) was quantified after dialysis of samples at each specified urea concentration, to remove any dissociated copper ions. The continuous lines are fits to experimental values (Table 1).

intermediate, one may expect less activity. However, also, removal of T1A may affect electron transfer from T1B to the catalytic cluster. On the basis of our data, we cannot distinguish which oxidized T1 site is perturbed. The T1C copper is spectrally invisible as it is permanently reduced (*13*). It is probable that this copper ion, missing one protein ligand as compared to the other T1 sites, will dissociate most readily of all copper cofactors in CP. Thus, it appears reasonable that this copper is one of the two metals removed in the intermediate. We note that the tryptophan fluorescence in folded holo-CP is quenched by the metals; in accord with several metals remaining in the intermediate, the emission stays quenched until ~7 M urea has been added (data not shown).

Next, refolding of holo-CP from the intermediate (i.e., 5.5 M urea) and fully unfolded (i.e., 9 M urea) states was tested. We find that nativelike far-UV CD and Trp fluorescence signals appear upon refolding from the intermediate species (Figure 3). Also, the blue color and oxidase activity return to native-state levels when refolded from the 5.5 M urea state. This suggests that albeit two coppers are gone in the intermediate, these can rebind upon protein refolding.

In contrast, refolding from the unfolded state (9 M urea) results in a protein species distinctly different from the native state. This form has an intermediate-sized far-UV CD signal (and different shape), only partial restoration of the native-like tryptophan emission, no blue color, no copper bound, no oxidase activity, and is found to interact strongly with ANS (Figures 3 and 4). For this species, the ANS emission is increased 3-fold as compared to that for the native-state and 2-fold as compared to that for the intermediate and unfolded states; moreover, the emission maximum is largely red-shifted to 480 nm. Taken together, these properties are indicative of a molten-globulelike species (*33*−*38*). Refolding into the molten-globule species occurs in a broad transition with a midpoint of 4.0−4.5 M urea. Repeated unfolding reveals the same urea-unfolding curve as the one obtained in the refolding experiments from 9 M urea, in accord with reversibility (data not shown). On the basis of the spectroscopic properties, the molten-globulelike CP form is not identical to the apo-form that is prepared via CN dialysis (see below).

The parameters obtained from fits to the different holo-CP unfolding curves are reported in Table 1. It is clear that

Table 1: Parameters Describing the Conformational Transitions of Holo- and Apo-CP as Monitored by Far-UV CD (CD_{220} nm), Tryptophan (F_{Trp}), and ANS (F_{ANS}) Fluorescence Maxima Placement, Blue Copper Absorbance (A_{610} nm), and Oxidase Activity[a]

detection	urea change (M)	ΔG_U (kJ/mol)	*m* (kJ/mol, M)	$[urea]_{1/2}$ (M)
		holo-form		
CD_{220nm}	0 → 5.5	15.3 ± 0.7	3.7 ± 0.2	4.1
CD_{220nm}	5.5 → 9	39.5 ± 3.0	5.7 ± 0.4	6.9
CD_{220nm}	5.5 → 0	−15.2 ± 1.1	3.6 ± 0.3	4.3
CD_{220nm}	9 → 0	−8.6 ± 0.9	1.9 ± 0.2	4.6
F_{Trp}	0 → 5.5	15.2 ± 1.3	3.5 ± 0.2	4.3
F_{Trp}	5.5 → 9	37.4 ± 2.0	5.3 ± 0.4	7.0
F_{Trp}	5.5 → 0	−17.1 ± 1.5	3.8 ± 0.3	4.5
F_{Trp}	9 → 0	−10.9 ± 1.0	2.3 ± 0.2	4.2
F_{ANS}	0 → 5.5			5.0
F_{ANS}	5.5 → 9			7.1
F_{ANS}	9 → 0	−11.7 ± 1.2	2.1 ± 0.2	5.4
activity	0 → 5.5	15.6 ± 1.9	3.6 ± 0.4	4.4
A_{610nm}	0 → 5.5	17.2 ± 1.2	4.1 ± 0.3	4.2
		apo-form		
CD_{220nm}	0 → 5.5	14.4 ± 1.1	3.1 ± 0.3	3.8
CD_{220nm}	5.5 → 9	36.5 ± 3.9	4.8 ± 0.5	7.6
CD_{220nm}	5.5 → 0	−13.2 ± 1.1	3.6 ± 0.3	3.7
F_{Trp}	0 → 5.5	14.6 ± 0.7	4.2 ± 0.2	3.5
F_{Trp}	5.5 → 9	28.8 ± 2.0	4.5 ± 0.3	6.4
F_{Trp}	5.5 → 0	−12.5 ± 3.7	3.7 ± 0.7	3.4
F_{ANS}	0 → 5.5	13.6 ± 1.5	2.9 ± 0.3	4.6

[a] The direction of the urea jump (i.e., unfolding or refolding) is indicated. ΔG_U, *m* values, and $[urea]_{1/2}$ were obtained from two-state fits to individual transitions. (Fit parameters for most of the ANS data were not reliable and are not shown.)

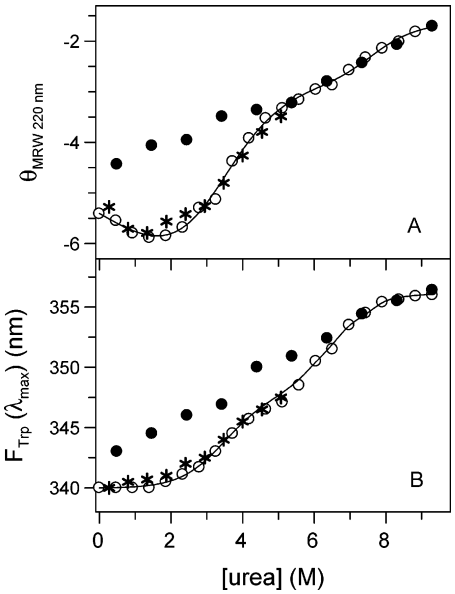

FIGURE 6: Isothermal denaturation of apo-CP followed by (A) CD at 220 nm and (B) tryptophan fluorescence (excitation at 295 nm). Unfolding of native-CP (○), refolding of CP from 5.5 M urea (*), and refolding of CP from 9.0 M urea (●). The continuous lines are fits to experimental values (Table 1).

the parameters for the first transition, from native to intermediate state, match among the five detection methods and correspond to a free-energy change of about 15 kJ/mol (pH 7, 23 °C). The *m* value, indicative of relative exposure of hydrophobic surfaces upon perturbation (*23*−*25*), is low for the protein of this size (120 kDa), supporting that only partial unfolding is involved in the transition. The second

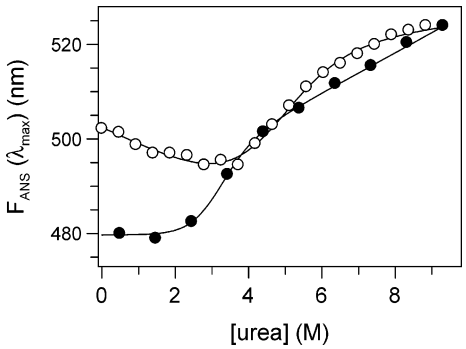

FIGURE 7: Isothermal denaturation of apo-CP followed by ANS fluorescence (excitation at 390 nm). Unfolding of native-CP (○) and refolding of CP from 9.0 M urea (●). The continuous lines are fits to experimental values (Table 1).

step, intermediate to unfolded, is irreversible, and one must use caution when analyzing the fit parameters. Nonetheless, it appears that this transition involves a higher free-energy change and more hydrophobic surface exposure than the first process. The refolding/unfolding of the molten-globule species, which is a reversible transition, corresponds to a free-energy change of about 10 kJ/mol (pH 7, 23 °C) and low cooperativity based on the low *m* value.

Unfolding Apo-CP. Urea-induced unfolding was also investigated with apo-CP prepared by CN dialysis. In Figure 6, far-UV CD and fluorescence curves as a function of urea concentration are shown. Again, unfolding appears in two phases, a first transition with a midpoint of about 3.5 M urea followed by a second transition with a midpoint of about 6−7 M urea. The intermediate species has only ~35% of the original negative far-UV CD signal; the emission maximum is shifted from 340 to 347 nm. ANS binding to apo-CP vs urea concentration was also tested; the results mimic the trends seen above for the holo-protein (Figure 7); again, a biphasic transition is observed when the ANS emission maximum is plotted vs urea concentration.

Whereas refolding of the intermediate species (from 5.5 M urea) results in an apo-protein that is identical to that of the starting form, refolding from 9 M urea again results in the molten-globulelike species that has distinct CD/fluorescence and ANS-binding properties (Figures 6 and 7). As in the case of the fully unfolded holo-protein, refolding of the apo-protein from 9 M urea occurs in a broad transition with a midpoint of ~4.3 M urea. Fits to the different apo-protein unfolding curves are listed in Table 1.

DISCUSSION

The majority of cuproenzymes, including blood-clotting factors, tyrosinase, lysyl oxidase, and CP, are synthesized within the secretory pathway (*39*); copper gains access to this compartment via copper-translocating ATPases present in the *trans*-Golgi membrane (*39*−*41*). Copper incorporation into polypeptides inside this compartment is not clear; it has been proposed that copper ions and proteins meet in vesicular environments before secretion (*5*, *8*). As a first step toward elucidating the interplay between copper uptake and polypeptide folding of cuproproteins made in the secretory pathway, we have characterized the in vitro chemical unfolding reactions of purified apo- and holo-forms of human CP.

Both forms of CP are found to unfold in multistep equilibrium reactions, involving at least one on-pathway intermediate and one misfolded off-pathway species. The

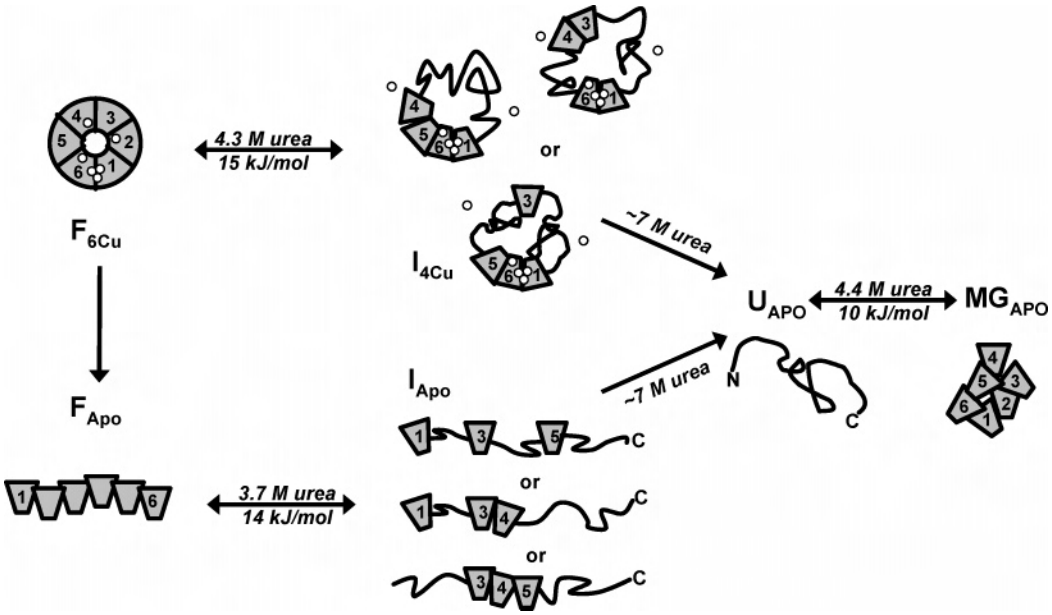

FIGURE 8: Unfolding/refolding pathways of holo- and apo-CP based on the present work. Folded holo-CP containing six bound coppers (circles), F_{6Cu}, undergoes a reversible transition up to ~5.5 M urea, with a midpoint at ~4.3 M, losing two copper ions and about half of the oxidase activity and blue absorption. This intermediate form of holo-CP is termed I_{4Cu}. This intermediate may have T1C and T1B coppers removed (see text) and two domains unfolded, perhaps involving those harboring the destroyed copper sites; the catalytic cluster and therefore domains 1 and 6 are likely intact in the intermediate. Three possible structures of I_{4Cu} are shown. A further increase in urea concentration leads to full CP unfolding accompanied by dissociation of all coppers, U_{Apo}. Analogously, F_{Apo} (prepared via CN dialysis) undergoes a reversible urea-induced transition with a midpoint at ~3.7 M (forming I_{Apo}; three possible structures are shown), followed by an irreversible transition to U_{Apo} completed at 9.3 M urea. The final unfolded state of apo-CP is similar to that obtained when starting from holo-CP. U_{Apo} undergoes a reversible off-pathway transition to a molten globulelike state, MG_{Apo}, with a midpoint at 4.4 M urea. Double-headed arrows indicate reversibility; single-headed arrows depict transitions that only go in one direction. Midpoints and stabilities are from Table 1.

proposed folding/unfolding landscape for holo- and apo-forms of CP (i.e., F_{6Cu} and F_{apo}) in urea (pH 7, 23 °C), and tentative structural aspects of the intermediates, are summarized in Figure 8. First, the activity data suggest that the holo-intermediate (i.e., I_{4Cu}) has an intact trinuclear copper cluster; thus, the interface between domains 1 and 6 where this site is located is likely intact; therefore, domains 1 and 6 remain folded. Because the holo-intermediate has lost about 30−40% of its secondary structure (which equals two out of six domains) and two coppers, one being an oxidized T1 copper (based on the blue color change), it is possible that domains 2 (containing silent T1C) and 4 (containing T1B) are unfolded in I_{4Cu}. Notably, the disulfide bonds in domains 2 and 4 link different β-strands as compared to the disulfide bonds in domains 1, 3, and 5 (*6*, *9*); this may account for differential domain stability. Earlier work (*19*) gives support that T1B, and not T1A, is the oxidized T1 copper removed in the unfolding intermediate. It was reported that upon loss of two coppers via CN dialysis, CP lost half of its blue color and most of its oxidase activity (substrate binding near T1B) disappeared whereas most of the dismutase activity (substrate binding near T1A) remained (*19*). That a few domains are unfolded and a few remain folded is in agreement with the ANS data, which do not indicate that the whole protein is partially folded [if so, we would observe a dramatic increase in ANS emission and a red shift of its maximum (*25*)]. Further additions of urea result in complete polypeptide unfolding and loss of all coppers (i.e., U_{apo}).

The apo-form of CP (i.e., F_{apo}) has been proposed to adopt a folded but extended form in which the interface between domains 1 and 6 is absent (*21*); the domains may be depicted as beads on a string with domain 1 spatially distant from domain 6. Conversion of apo-CP to the intermediate state (i.e., I_{apo}) again appears to involve selective unfolding of some of the domains based on the spectroscopic signals. Further perturbation of the apo-intermediate results in a fully unfolded state with all domains unfolded (i.e., U_{apo}). Refolding of U_{apo} (obtained from complete unfolding of both holo- and apo-forms of CP) occurs, reversibly, into an off-pathway copper-lacking molten globule (i.e., MG_{apo}). This form may have several domains folded, as it has a significant secondary structure content, but the arrangement of the domains in three-dimensional space, and interdomain interactions, may be incorrect, prohibiting copper incorporation and proper folding.

Several biological implications can be drawn from our findings. First, it is clear that, in contrast to small proteins where bound cofactors often have large effects on protein stability (*42*−*49*), the coppers in CP contribute minimally to the overall protein stability. The transition midpoints are found at roughly the same urea concentrations for both apo- and holo-forms (Table 1). Furthermore, because apo-CP may have a more extended conformation, it appears that the individual domains, and not the domain−domain interactions, govern most of the protein's stability. Second, our experiments suggest a mechanistic role for the trinuclear copper cluster in proper alignment of domains 1 and 6; only when this interface/metal site is in place is correct CP folding possible in our experiments. In agreement, several demetalation studies have demonstrated that if all six coppers are removed from CP, reconstitution is not possible at neutral and oxidizing conditions (*19*, *21*). Reconstitution of apo-CP has only been achieved in some special conditions, that is, in the presence of ascorbate at pH 5.6 and only partially via Cu(I)-glutathione in the presence of Mg-ATP at pH 7 (*5*, *17*, *50*). Third, our findings provide mechanistic insight into the recently proposed CP biosynthesis pathway (*5*). It was demonstrated via metabolic labeling and gel shift experiments that copper incorporation into CP is an all-or-none process, although the possibility of unstable, "hidden" intermediates was mentioned (*5*). We propose that the intermediate detected here with an intact trinuclear copper site is such a hidden intermediate not resolved by the methods used in ref *5*. This intermediate may form for several of the copper-site mutants studied in ref *5*, but their low stability causes them to return to the apo-form if the remaining T1 copper ions are not incorporated (due to mutations of copper ligands).

Finally, our study implies that the CP polypeptide can adopt a molten-globule form that is not on the path to the native state. Thus, timely copper incorporation, before apoprotein misfolding occurs, may be crucial for successful in vivo biosynthesis of CP. Notably, we have earlier shown that for *Pseudomonas aeruginosa* azurin, copper binding readily occurs in the unfolded state (*51*, *52*). Additional studies using strategic CP mutants and solvent conditions mimicking the biological environment in the secretory pathway will be of importance from a fundamental point of view, as it may apply to other cuproproteins made in the secretory pathway, and also from a medical aspect, as it may facilitate new approaches to incorporate copper into copper-lacking CP variants found in affected patients.

REFERENCES

1. Holmberg, C. G., and Laurell, C. B. (1948) Investigations in serum copper II: Isolation of the copper-containing protein and a description of some of its properties, *Acta Physiol. Scand. 2*, 550−556.
2. Palmer, A. E., Quintanar, L., Severance, S., Wang, T. P., Kosman, D. J., and Solomon, E. I. (2002) Spectroscopic characterization and O2 reactivity of the trinuclear Cu cluster of mutants of the multicopper oxidase Fet3p, *Biochemistry 41*, 6438−6448.
3. Quintanar, L., Gebhard, M., Wang, T. P., Kosman, D. J., and Solomon, E. I. (2004) Ferrous binding to the multicopper oxidases Saccharomyces cerevisiae Fet3p and human ceruloplasmin: Contributions to ferroxidase activity, *J. Am. Chem. Soc. 126*, 6579−6589.
4. Wang, T. P., Quintanar, L., Severance, S., Solomon, E. I., and Kosman, D. J. (2003) Targeted suppression of the ferroxidase and iron trafficking activities of the multicopper oxidase Fet3p from Saccharomyces cerevisiae, *J. Biol. Inorg. Chem. 8*, 611−620.
5. Hellman, N. E., Kono, S., Mancini, G. M., Hoogeboom, A. J., De Jong, G. J., and Gitlin, J. D. (2002) Mechanisms of copper incorporation into human ceruloplasmin, *J. Biol. Chem. 277*, 46632−46638.
6. Zaitsev, V. N., Zaitseva, I., Papiz, M., and Lindley, P. F. (1999) An X-ray crystallographic study of the binding sites of the azide inhibitor and organic substrates to ceruloplasmin, a multi-copper oxidase in the plasma, *J. Biol. Inorg. Chem. 4*, 579−587.
7. Osaki, S., Johnson, D. A., and Frieden, E. (1966) The possible significance of the ferrous oxidase activity of ceruloplasmin in normal human serum, *J. Biol. Chem. 241*, 2746−2751.
8. Hellman, N. E., and Gitlin, J. D. (2002) Ceruloplasmin metabolism and function, *Annu. Rev. Nutr. 22*, 439−458.
9. Lindley, P. F. (2001) Ceruloplasmin, *Handb. Metalloproteins*, 1369−1380.
10. Musci, G., Bellenchi, G. C., and Calabrese, L. (1999) The multifunctional oxidase activity of ceruloplasmin as revealed by anion binding studies, *Eur. J. Biochem. 265*, 589−597.
11. Gitlin, J. D., Schroeder, J. J., Lee-Ambrose, L. M., and Cousins, R. J. (1992) Mechanisms of caeruloplasmin biosynthesis in normal and copper-deficient rats, *Biochem. J. 282* (Part 3), 835−839.

12. Machonkin, T. E., Zhang, H. H., Hedman, B., Hodgson, K. O., and Solomon, E. I. (1998) Spectroscopic and magnetic studies of human ceruloplasmin: identification of a redox-inactive reduced Type 1 copper site, *Biochemistry 37*, 9570−9578.
13. Machonkin, T. E., and Solomon, E. I. (2000) The thermodynamics, kinetics and molecular mechanism of intramolecular electron transfer in human ceruloplasmin, *J. Am. Chem. Soc. 122*, 12547−12560.
14. Mukhopadhyay, C. K., Mazumder, B., Lindley, P. F., and Fox, P. L. (1997) Identification of the prooxidant site of human ceruloplasmin: A model for oxidative damage by copper bound to protein surfaces, *Proc. Natl. Acad. Sci. U.S.A. 94*, 11546−11551.
15. Calabrese, L., Carbonaro, M., and Musci, G. (1989) Presence of coupled trinuclear copper cluster in mammalian ceruloplasmin is essential for efficient electron transfer to oxygen, *J. Biol. Chem. 264*, 6183−6187.
16. De Filippis, V., Vassiliev, V. B., Beltramini, M., Fontana, A., Salvato, B., and Gaitskhoki, V. S. (1996) Evidence for the molten globule state of human apo-ceruloplasmin, *Biochim. Biophys. Acta 1297*, 119−123.
17. Sato, M., and Gitlin, J. D. (1991) Mechanisms of copper incorporation during the biosynthesis of human ceruloplasmin, *J. Biol. Chem. 266*, 5128−5134.
18. Isen, P., and Morell, A. G. (1965) Physical and chemical studies on ceruloplasmin. 3. A stabilizing copper-copper interaction in ceruloplasmin, *J. Biol. Chem. 240*, 1974−1978.
19. Vassiliev, V. B., Kachurin, A. M., Beltramini, M., Rocco, G. P., Salvato, B., and Gaitskhoki, V. S. (1997) Copper depletion/repletion of human ceruloplasmin is followed by the changes in its spectral features and functional properties, *J. Inorg. Biochem. 65*, 167−174.
20. Musci, G., Fraterrigo, T. Z., Calabrese, L., and McMillin, D. R. (1999) On the lability and functional significance of the type 1 copper pool in ceruloplasmin, *J. Biol. Inorg. Chem. 4*, 441−446.
21. Vachette, P., Dainese, E., Vasyliev, V. B., Di Muro, P., Beltramini, M., Svergun, D. I., De Filippis, V., and Salvato, B. (2002) A key structural role for active site type 3 copper ions in human ceruloplasmin, *J. Biol. Chem. 277*, 40823−40831.
22. Felsenfeld, G. (1960) The determination of cuprous ion in copper proteins, *Arch. Biochem. Biophys. 87*, 247−251.
23. Santoro, M. M., and Bolen, D. W. (1992) A test of the linear extrapolation of unfolding free energy changes over an extended denaturant concentration range, *Biochemistry 31*, 4901−4907.
24. Santoro, M. M., and Bolen, D. W. (1988) Unfolding free energy changes determined by the linear extrapolation method. 1. Unfolding of phenylmethanesulfonyl α-chymotrypsin using different denaturants, *Biochemistry 27*, 8063−8068.
25. Fersht, A. (1999) *Structure and Mechanism in Protein Science*, W. H. Freeman and Company, New York.
26. Schosinsky, K. H., Lehmann, H. P., and Beeler, M. F. (1974) Measurement of ceruloplasmin from its oxidase activity in serum by use of *o*-dianisidine dihydrochloride, *Clin. Chem. 20*, 1556−1563.
27. Lobley, A., Whitmore, L., and Wallace, B. A. (2002) DICHROWEB: An interactive website for the analysis of protein secondary structure from circular dichroism spectra, *Bioinformatics 18*, 211−212.
28. Whitmore, L., and Wallace, B. A. (2004) DICHROWEB, an online server for protein secondary structure analyses from circular dichroism spectroscopic data, *Nucleic Acids Res. 32*, W668−W673.
29. Mao, D., Wachter, E., and Wallace, B. A. (1982) Folding of the mitochondrial proton adenosinetriphosphatase proteolipid channel in phospholipid vesicles, *Biochemistry 21*, 4960−4968.
30. Manavalan, P., and Johnson, W. C., Jr. (1987) Variable selection method improves the prediction of protein secondary structure from circular dichroism spectra, *Anal. Biochem. 167*, 76−85.
31. Apiyo, D., Guidry, J., and Wittung-Stafshede, P. (2000) No cofactor effect on equilibrium unfolding of Desulfovibrio desulfuricans flavodoxin, *Biochim. Biophys. Acta 1479*, 214−224.
32. Muralidhara, B. K., and Wittung-Stafshede, P. (2005) FMN binding and unfolding of Desulfovibrio desulfuricans flavodoxin: "Hidden" intermediates at low denaturant concentrations, *Biochim. Biophys. Acta 1747*, 239−250.
33. Redfield, C., Smith, R. A., and Dobson, C. M. (1994) Structural characterization of a highly-ordered 'molten globule' at low pH, *Nat. Struct. Biol. 1*, 23−29.
34. Ptitsyn, O. (1996) How molten is the molten globule? [news], *Nat. Struct. Biol. 3*, 488−490.
35. Gast, K., Damaschun, H., Misselwitz, R., Muller-Frohne, M., Zirwer, D., and Damaschun, G. (1994) Compactness of protein molten globules: Temperature-induced structural changes of the apomyoglobin folding intermediate, *Eur. Biophys. J. 23*, 297−305.
36. Eliezer, D., and Wright, P. E. (1996) Is apomyoglobin a molten globule? Structural characterization by NMR, *J. Mol. Biol. 263*, 531−538.
37. Dobson, C. M. (1994) Protein folding. Solid evidence for molten globules, *Curr. Biol. 4*, 636−640.
38. Baum, J., Dobson, C. M., Evans, P. A., and Hanley, C. (1989) Characterization of a partly folded protein by NMR methods: Studies on the molten globule state of guinea pig alpha-lactalbumin, *Biochemistry 28*, 7−13.
39. Harris, E. D. (2003) Basic and clinical aspects of copper, *Crit. Rev. Clin. Lab. Sci. 40*, 547−586.
40. Hung, I. H., Suzuki, M., Yamaguchi, Y., Yuan, D. S., Klausner, R. D., and Gitlin, J. D. (1997) Biochemical characterization of the Wilson disease protein and functional expression in the yeast Saccharomyces cerevisiae, *J. Biol. Chem. 272*, 21461−21466.
41. Hamza, I., Schaefer, M., Klomp, L. W., and Gitlin, J. D. (1999) Interaction of the copper chaperone HAH1 with the Wilson disease protein is essential for copper homeostasis, *Proc. Natl. Acad. Sci. U.S.A. 96*, 13363−13368.
42. Wilson, C. J., Apiyo, D., and Wittung-Stafshede, P. (2004) Role of cofactors in metalloprotein folding, *Q. Rev. Biophys. 37*, 285−314.
43. Winkler, J. R., Wittung-Stafshede, P., Leckner, J., Malmstrom, B. G., and Gray, H. B. (1997) Effects of folding on metalloprotein active sites, *Proc. Natl. Acad. Sci. U.S.A. 94*, 4246−4249.
44. Wittung-Stafshede, P. (2004) Role of cofactors in folding of the blue-copper protein azurin, *Inorg. Chem. 43*, 7926−7933.
45. Goedken, E. R., Keck, J. L., Berger, J. M., and Marqusee, S. (2000) Divalent metal cofactor binding in the kinetic folding trajectory of *Escherichia coli* ribonuclease HI, *Protein Sci. 9*, 1914−1921.
46. Filimonov, V. V., Prieto, J., Martinez, J. C., Bruix, M., Mateo, P. L., and Serrano, L. (1993) Thermodynamic analysis of the chemotactic protein from *Escherichia coli*, CheY, *Biochemistry 32*, 12906−12921.
47. Bollen, Y. J., Nabuurs, S. M., van Berkel, W. J., and van Mierlo, C. P. (2005) Last in, first out: The role of cofactor binding in flavodoxin folding, *J. Biol. Chem. 280*, 7836−7844.
48. Hargrove, M. S., and Olson, J. S. (1996) The stability of holomyoglobin is determined by heme affinity, *Biochemistry 35*, 11310−11318.
49. Feng, Y. Q., and Sligar, S. G. (1991) Effect of heme binding on the structure and stability of *Escherichia coli* apocytochrome b562, *Biochemistry 30*, 10150−10155.
50. Musci, G., Di Marco, S., Bellenchi, G. C., and Calabrese, L. (1996) Reconstitution of ceruloplasmin by the Cu(I)-glutathione complex. Evidence for a role of Mg2+ and ATP, *J. Biol. Chem. 271*, 1972−1978.
51. Pozdnyakova, I., and Wittung-Stafshede, P. (2001) Biological relevance of metal binding before protein folding, *J. Am. Chem. Soc. 123*, 10135−10136.
52. Pozdnyakova, I., and Wittung-Stafshede, P. (2001) Copper binding before polypeptide folding speeds up formation of active (holo) *Pseudomonas aeruginosa* azurin, *Biochemistry 40*, 13728−13733.

BI700715E

Available online at www.sciencedirect.com
ScienceDirect
Archives of Biochemistry and Biophysics 467 (2007) 58–66
ABB
www.elsevier.com/locate/yabbi

Role of copper in folding and stability of cupredoxin-like copper-carrier protein CopC

Faiza Hussain [a], Erik Sedlak [a,1], Pernilla Wittung-Stafshede [a,b,c,*]

[a] Department of Biochemistry and Cell Biology, Rice University, 6100 Main Street, Houston, TX 77251, USA
[b] Keck Center for Structural, Computational Biology, Rice University, 6100 Main Street, Houston, TX 77251, USA
[c] Department of Chemistry, Rice University, 6100 Main Street, Houston, TX 77251, USA

Received 20 June 2007, and in revised form 6 August 2007
Available online 29 August 2007

Abstract

CopC is a periplasmic copper carrier that, in contrast to cytoplasmic copper chaperones, has a β-barrel fold and two metal-binding sites distinct for Cu^{II} and Cu^{I}. The copper sites are located in each end of the molecule: the Cu^{I} site involves His and Met coordination whereas the Cu^{II} site consists of charged residues. To reveal biophysical properties of this protein, we have explored the effects of the cofactors on CopC unfolding *in vitro*. We demonstrate that Cu^{II} coordination affects both protein stability and unfolding pathway, whereas Cu^{I} has only a small effect on stability. Apo–CopC unfolds in a two-state reaction between pH 4 and 7.5 with maximal stability at pH 6. In contrast, Cu^{II}–CopC unfolds in a three-state reaction at pH $\geqslant$ 6 that involves a partly folded intermediate that retains Cu^{II}. This intermediate exhibits high thermal and chemical stability. Unique energetic and structural properties of different metalated CopC forms may help facilitate metal transport to many partners *in vivo*.

Keywords: Protein folding; Unfolding intermediate; Copper chaperone; Periplasm; Spectroscopy; Calorimetry

Copper is one of the most prevalent transition metals in living organisms; its biological function is intimately related to its redox properties. Many proteins that participate in cellular respiration, antioxidant defense, neurotransmitter biosynthesis, connective-tissue biosynthesis and pigment formation use copper as the prosthetic, active group [1–4]. Since free copper is toxic, copper homeostasis in living organisms is tightly controlled by subtle molecular mechanisms [5–7]. In eukaryotes, before cellular uptake *via* high-affinity copper transporters of the CTR family [4], Cu^{II} ions are reduced to Cu^{I}. During the past decade, an important class of proteins, termed copper chaperones, has been identified in the cytoplasm that binds Cu^{I} with Cys_2 coordination [4,8–11]. Recently, an atypical Cys_2His coordination was also found for Cu^{I} in a copper-chaperone from cyanobacteria [12,13]. These small, soluble proteins guide and protect the copper ions within the cell, delivering them to the appropriate functional protein receptors. P-type ATPases are membrane spanning receptor proteins with cytoplasmic metal-binding domains that transfer Cu^{I} through membranes from one cellular compartment to another. In humans, the Menkes and Wilson disease proteins are P-type ATPases involved in copper transport [4,9,14]; in an ATP-dependent process, they translocate copper from the cytoplasm into the Golgi network for loading into proteins. Solution NMR and crystal structures [15–22] have been reported for various metal-bound and/or apo-forms of cytoplasmic copper chaperones and metal-binding domains of P-type ATPases from a range of different organisms. In all structures, the proteins possess an αβ ferredoxin-like fold and a conserved MXCXXC motif.

* Corresponding author. Address: Department of Biochemistry and Cell Biology, Rice University, 6100 Main Street, Houston, TX 77251, USA. Fax: +1 713 348 5154.
E-mail address: pernilla@rice.edu (P. Wittung-Stafshede).
[1] Present address: Department of Biochemistry, P.J. Safarik University, Moyzesova 11, 04001 Kosice, Slovakia.

0003-9861/$ - see front matter © 2007 Elsevier Inc. All rights reserved.
doi:10.1016/j.abb.2007.08.014

In addition to the cytoplasmic Cu^{I}-trafficking proteins, other proteins have recently been identified that are involved in bacterial resistance to high copper concentrations [23,24]. Since copper is particularly toxic to lower organisms such as bacteria, copper based bactericides are extensively used in agriculture to control plant pathogens. Copper resistant strains of *Pseudomonas syringae* pathovar *tomato* are characterized by a 35-kb plasmid that contains an operon (*cop*) encoding four proteins, CopABCD, acting under a copper inducible promoter requiring the regulatory genes, CopR and CopS, coded directly downstream from CopD [23–26]. This plasmid is able to confer copper resistance to the host strains of Gram-negative bacteria and protects the cells by sequestering the excess copper in the periplasm and in the outer membrane. Upon exposure to high copper concentrations, *P. syringae* cells turn blue and up to 12% of the dry weight of the cells may be copper [27]. CopA and CopC are soluble proteins present in the oxidizing environment of the periplasm, CopB and CopD appear to be membrane-bound copper pumps while CopS and CopR form part of copper sensing and gene induction systems. It is not yet clear how these proteins interact with each other to facilitate copper resistance.

The CopC protein is proposed to be a copper-carrier protein but in contrast to the cytoplasmic copper chaperones, it lacks cysteine residues and has two copper binding sites that are separated by 30 Å [25,26,28–30]. One metal site is specific for Cu^{I} and the other for Cu^{II}: the protein can be either simultaneously loaded with Cu^{I} and Cu^{II} or with one copper in either site. CopC has a β-sandwich structure comprised of β-strands arranged in a Greek Key topology similar to that of blue-copper proteins (*e.g.,* azurin) and domains of multi-copper oxidases (*e.g.,* ceruloplasmin) (Fig. 1). The suggested ligand environment based on EXAFS and NMR data is tetragonal $Cu^{I}(His)(Met)_3$ and tetrahedral $Cu^{II}(His)_2(Asp)(Glu)(OH_2)$ [28]. Whereas the Cu^{I} site is situated in a disordered loop near the C-terminus, the position of the Cu^{II} site is similar to that of the metal sites in blue-copper proteins. Solution and X-ray structures of apo- and various Cu^{I}/Cu^{II}-forms of CopC have been reported [27–30]. Although the core of the molecule is identical in all structures, the presence of metal affects the conformation of loop regions in both ends of the molecule. Based on crystal structures of the holo-forms at pH 4.6 and 7.5, it was suggested that the N-terminus is a Cu^{II} ligand at the higher but not the lower pH [27]. Notably, N-terminal Cu^{II} coordination has only been observed in a few proteins and peptides before (*e.g.,* albumins and neuromedins) [31–33]. The fundamental chemistry of copper binding and transfer in CopC was recently explored in depth *in vitro* [27]. CopC has high-affinity for both copper ions although the Cu^{II} site has the highest affinity ($\sim 10^{13}\ M^{-1}$). Inter-protein copper transfer reactions between sites, with or without involvement of copper-redox change, were demonstrated [27]. Thus, CopC may interact with different partner proteins *in vivo* and act as a "redox switch".

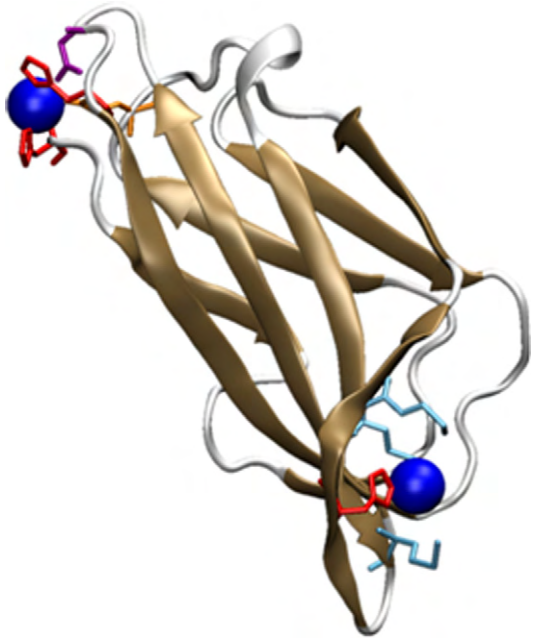

Fig. 1. Crystal structure of CopC (2C9Q) at pH 7.5 revealing the β-sandwich fold and the two copper sites. Cu(II) interacts with His1 (red), His91 (red), Glu27 (orange), Asp89 (purple) and the N-terminus (red) in a tetragonal environment forming a type-II copper site. Cu(I) interacts with a His48 (red) and several methionine (blue) sulfurs in a disordered loop.

To elucidate thermodynamic properties of CopC, and assess how they are linked to the occupation of the copper sites, we have here investigated CopC thermodynamic stability and unfolding as a function of copper loading and solvent conditions *in vitro*. We find that the two copper ions have different effects on the protein: whereas the Cu^{II} changes the unfolding mechanism and stabilizes an intermediate CopC species, the Cu^{I}-form behaves more like the apo-form. The diverging thermodynamic properties of various metalated forms of CopC may explain how this protein interacts with different partner proteins *in vivo* depending on copper levels and redox state.

Materials and methods

Protein expression and purification

Escherichia coli BL21(DE3) pLysS cells, transformed with the CopC gene cloned into the vector pAT2, were grown in LB media (37 °C) to an OD_{600nm} of 0.6 followed by protein expression induction with 0.4 mM IPTG. Cells were harvested after 6 h. Protein was extracted by freeze-thaw cycles into extraction buffer (20 mM Tris, pH 8.0, 1 mM PMSF, 1 mM EDTA). The cell lysate was then loaded on an anion exchange column (DEAE) pre-equilibrated with 20 mM Tris, 1 mM EDTA, pH 8.0. The flow-through fractions containing CopC were pooled and dialyzed against 20 mM MES, 1 mM EDTA, pH 6.0 and loaded onto a cation exchange column (SP) pre-equilibrated with the same buffer. CopC was eluted from the column with 20 mM MES, 1 mM EDTA, 0.5 M NaCl, pH 6.0 and then dialyzed into 20 mM Tris, pH 7.5. Purity was monitored by SDS–PAGE at each step. CopC was purified in its apo-form. Protein concentration was determined using $\varepsilon_{280nm} = 8700\ M^{-1}\ cm^{-1}$. The Cu^{II}-form is prepared by Cu^{II} ($CuCl_2$) addition (1 equivalent); the Cu^{I}-form is made by

the addition of Cu^{II} in the presence of the reducing agent ascorbate, as described [27]. In the μM range of protein, the Cu^{I} and the Cu^{II}-forms, respectively, are obtained stoichiometrically [27]. Absorbance, fluorescence and far-UV circular dichroism (CD)[2] measurements were performed on Varian Cary 50, Cary Eclipse and Jasco J-810 spectrometers, respectively.

pH titration

Apo– and Cu^{II}–CopC, initially at pH 7.5, were titrated with either concentrated HCl (for acidic pHs) or concentrated NaOH (for basic pHs) and the effect was monitored by far-UV circular dichroism (CD) (200–300 nm, 1 mm cell) and tryptophan fluorescence (excitation at 295 nm; emission from 300 to 400 nm) at 20 °C (40 μM protein). The data (CD/fluorescence versus pH) was fit to the following equation [34]:

$$Y_{obs} = (Y_B + Y_A \times 10^{n(pK_a - pH)})/(1 + 10^{n(pK_a - pH)})$$

where Y_{obs} is the measured signal (CD or fluorescence), Y_B and Y_A correspond to the signal before and after the transition, respectively. In this equation, the n value is the number of protons (protonizable groups) involved in the transition and correlates with the steepness of the curve at the inflection point.

Chemical unfolding experiments

Urea-induced unfolding of apo- and Cu^{II}-forms of CopC was performed at different pH conditions at 20 °C in separate experiments. The urea concentration was determined from refractive index measurements. The buffers were as follows: 20 mM acetate, pH 4.0, 20 mM acetate, pH 5.0, 20 mM cacodylate, pH 6.0, and 20 mM Tris, pH 7.5, all with 15 μM protein. All samples were incubated for 1 h before CD and emission measurements. There was no time dependence in the reactions for incubation times between 30 min and 48 h. The CD data was obtained from the averaged signal at 218 nm collected for 120 s. For fluorescence, emission was collected from 303 to 500 nm (excitation at 295 nm; averaging three consecutive scans). To test for reversibility, protein samples were incubated in 8 M urea for 1 h and then mixed with buffer solutions containing lower concentrations of urea and spectroscopic measurements were conducted as described above. Unfolding transitions were analyzed as described by Santoro and Bolen [35,36]. Unfolding experiments with the Cu^{I}-form of CopC induced by urea were unsuccessful due to partial oxidation of Cu^{I} over time. For Cu^{I}–CopC, only thermal unfolding experiments using DSC (and anaerobic conditions) were reliable.

Thermal unfolding experiments

Thermal unfolding data for apo- and Cu^{II}-forms of CopC (30 μM) was acquired by monitoring the CD signal at 235 nm as a function of temperature, scan rate of 1 deg/min. Thermal experiments were performed at different pH conditions, 4, 4.5, 5, 6, and 7.5 using the buffers above. All thermal profiles were >90% reversible, as determined from reverse scans to the starting temperature. The thermal scan rates were varied between 0.5 and 2 °C per min without any significant change in the profiles (for either apo- or holo-forms); this indicates that the thermal reactions are at thermodynamic equilibrium. Data were fitted to two-state equations (except in a few cases where three states were required) to elucidate T_m values.

Differential scanning calorimetry (DSC)

DSC experiments on apo-, Cu^{II}- and Cu^{I}-forms of CopC (35 μM) were performed on a MicroCal VP-DSC calorimeter at a scan rate of 1 deg/min. The experiments were performed at different pH conditions, 4, 5, 6, 7, and 7.5 using the buffers above. For the Cu^{I}-form, 1 mM ascorbate was included in the buffer. Prior to measurements, the sample and reference solutions were properly degassed in a vacuum chamber for 10 min at room temperature. An overpressure of 2 atm was kept in the cells throughout the measurements to prevent degassing during heating. Baseline scans collected with buffer in both cells were subtracted from each scan. The reversibility of the thermal transition was checked by examining the reproducibility of the calorimetric trace in a second heating of the sample immediately after cooling from the first scans. Excess heat capacity curves were analyzed using the Origin software (MicroCal) to obtain calorimetric and van't Hoff enthalpies and T_m values.

[2] *Abbreviations used:* CD, circular dichroism; DTT, dithiothreitol; DSC, differential scanning calorimetry; T_m, thermal unfolding midpoint.

Results

Characteristics of apo- and holo-forms of CopC

The structural state of CopC can be monitored by far-UV CD and fluorescence methods. Folded CopC (apo- and various holo-forms) exhibits a negative CD signal around 210–220 nm that is characteristic of β-sheet structure (Fig. 2a); the aromatic emission is dominated by Trp83 and is centered at 320 nm in agreement with a hydrophobic position. Trp83 is situated near the Cu^{II} site; thus, in the Cu^{II}-form, the emission is quenched as compared to in the apo-form (Fig. 2b). Upon chemical or thermal perturbations to CopC, the far-UV CD and fluorescence (both intensity and wavelength maxima) signals change in accord with the formation of unfolded polypeptides (Fig. 2). We find that apo–CopC is folded in a wide range of pH values (3–11) as measured by the integrity of the far-UV CD and fluorescence signals (Fig. 3). Cu^{I} and Cu^{II} have been shown to bind tightly to the folded state of CopC; since the Cu^{I}–Cu^{II}-form of CopC was crystallized at pH 4.6 [27], the copper ions can bind in a wide range of pH values. Whereas Cu^{II}-form is prepared by simple Cu^{II} addition, the Cu^{I}-form can be made by the addition of Cu^{II} in the presence of the reducing agent, ascorbate [27]. It has been demonstrated by these procedures, the Cu^{I} and the Cu^{II}-forms, respectively, are made cleanly and stoichiometrically [27]. Notably, we found that using DTT (instead of ascorbate) as the reducing agent abolishes Cu^{I}–CopC complex formation (see below).

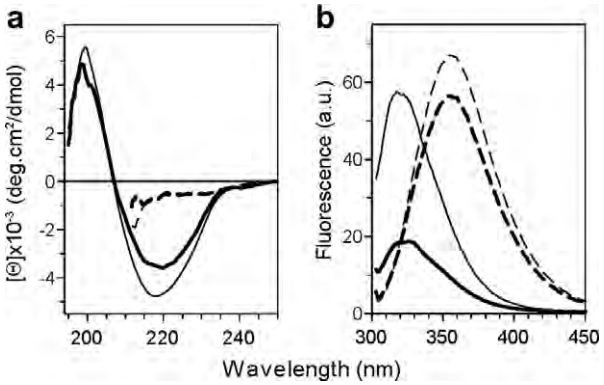

Fig. 2. Signals for folded (solid curves) and unfolded (dashed curves) forms of apo- (thin curves) and holo- (thick curves) forms of CopC as probed by far-UV CD (a) and fluorescence (b). In the folded Cu^{II}-form, both CD and fluorescence signals are quenched due to the copper ion.

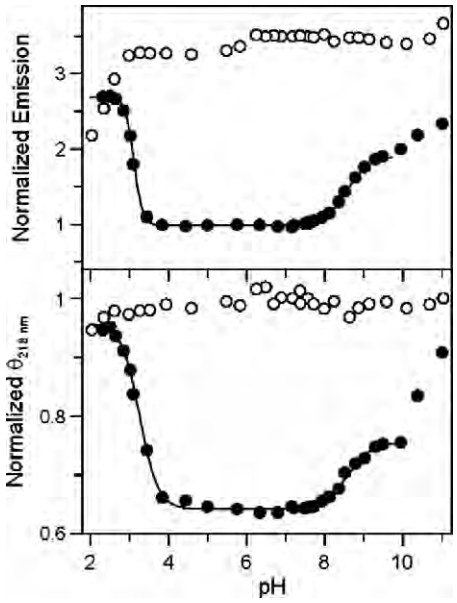

Fig. 3. Emission at 320 nm (top) and CD at 218 nm (bottom) for apo (open symbols) and Cu^{II} (filled symbols) forms of CopC as a function of pH (room temperature). All signals are normalized to that for apo–CopC at pH 7.5. Whereas the apo-form is intact in the pH range 3–11, fitting of the holo data reveals low-pH (pK_a at ~3.3) and high-pH (one pK_a at ~8.5) transitions that likely involve Cu dissociation (See Materials and methods section for equation).

To establish the pH range in which Cu^{II} is bound to CopC, we probed the far-UV CD and fluorescence signals as a function pH, starting from pH 7.5 conditions (Fig. 3). Notably, the negative far-UV CD signal is reduced by about 30% for the holo-complex as compared to the signal of the apo-protein. This is likely not due to less secondary structure in the holo-form but because of changes in electronic coupling due to the copper ion [37,38]. We find that Cu^{II}–CopC is destabilized at lower pH values in a transition that corresponds to a pK_a of about 3.3 and involvement of 2–4 protons (Fig. 3). This agrees with copper dissociation and protonation of the coordinating residues (likely two His, an Asp, and a Glu). Going to higher pH values, changes start to occur at pH values above 8. The holo-form appears to be destabilized in a bi-phasic reaction when the conditions gradually turn more basic (Fig. 3). The first of the basic transitions has a pK_a of ~8.5 and involves one proton; this process may be linked to de-protonation of a backbone amide that may become a Cu ligand at pH > 8.5 [39,40]. Due to the limited data, the very high-pH transition (probably correlating to Cu dissociation) could not be further analyzed. Nonetheless, we conclude that at least between pH values 4 and 8, the Cu^{II}–CopC form is intact in solution.

Urea-induced unfolding of apo– and holo–CopC

The thermodynamic stability of apo- and Cu^{II}-forms of CopC was tested in urea-induced unfolding experiments at four different pH values (4, 5, 6, and 7.5; 20 °C). We find that the apo-form unfolds in two-state equilibrium reactions when monitored by fluorescence and far-UV CD changes (Fig. 4a and c). The unfolding profiles obtained with the two detection methods roughly overlap at each pH, in support of two-state processes. The unfolding reaction is 100% reversible (inset, Fig. 4a). Apo–CopC is less stable at the lower two pH values; the urea-concentrations at the transition midpoints are higher, and similar to each other, at pH 6 and 7.5 (Table 1).

The corresponding urea-experiments with Cu^{II}–CopC revealed some differences. Whereas the pH 4 unfolding curves obtained by CD and fluorescence are similar to those collected for the apo-protein, the unfolding curves at higher pH values differ in distinct ways from the data for the apo-form. First, at pH 5, the unfolding-transition midpoints for Cu^{II}–CopC are shifted to higher urea-concentrations, but the transitions are broader than those for the apo-protein (Fig. 4b and d). At pH 6 and 7.5, instead, the unfolding profiles obtained for Cu^{II}–CopC appear to involve two sequential transitions. This indicates that the equilibrium-unfolding reactions are three state, involving an intermediate species populated at 3 to 4 M urea at these pH conditions (Fig. 4b and d). At pH 4 and 5, the far-UV CD and fluorescence data overlap, in accord with two-state reactions. At pH 6 and 7.5, both fluorescence and CD curves reveal three-state reactions and the midpoints for each transition agree between the detection methods, although the intermediate species has more native-like Trp emission than native-like far-UV CD signal (at pH 7.5; intermediate has 75% native-like CD and 90% native-like emission signals). Since the Trp emission in the intermediate is quenched almost as much as in the native holo-state, it is reasonable that Cu^{II} remains coordinated in the intermediate species. Like the apo-protein, the Cu^{II}–CopC unfolding reactions are 100% reversible. The pH 4 and 5 unfolding curves were fit to two-state transitions, whereas the pH 6 and 7.5 transitions were fit to two sequential two-state transitions *i.e.,* involving folded, intermediate, and unfolded species (Table 1).

To test if the Cu^{II} ion dissociates in the unfolded state of holo–CopC, we performed urea-induced unfolding experiments with Cu^{II}–CopC in the presence of 20-fold excess copper (data not shown). If copper dissociation is directly coupled to protein unfolding, there should be an apparent stabilizing effect by the presence of excess copper; however, if copper remains bound, no effect would be observed by excess copper. We found the latter scenario to be the case for Cu^{II}–CopC, the unfolding curve in presence of excess copper is not shifted to higher urea concentration. In addition, dialysis experiments of Cu^{II}–CopC samples in high concentrations of urea (8 M) also imply that the metal remains bound to the fully unfolded protein. Despite extensive dialysis for days, 90% of the copper remains with the protein fraction when quantified by the biquinoline assay (data not shown). The copper may coordinate to a subset of the native-state ligands His1, Glu27, Asp89 and His91 in the unfolded state. Peptide studies have shown Cu^{II} to

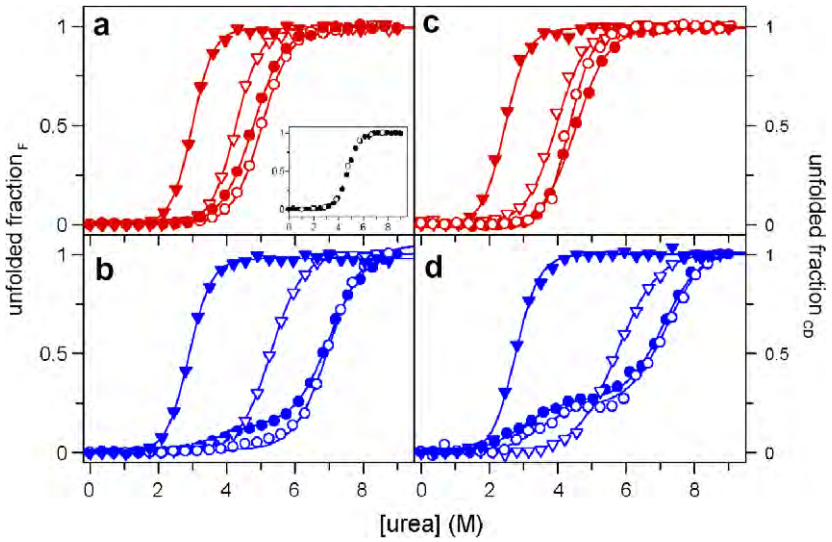

Fig. 4. Urea-induced unfolding (room temperature) of CopC monitored by fluorescence 356/320 nm ratio (a and b) and CD at 218 nm (c and d) for apo (a and c) and Cu^{II} (b and d) forms at different pH conditions (filled triangles, pH 4; open triangles, pH 5; filled circles, pH 6; open circles, pH 7.5). Inset a: refolding data points for apo–CopC starting from 8 M urea conditions (open symbols) together with the direct unfolding data (filled symbols).

Table 1
Thermodynamic data for various forms of CopC from urea-induced unfolding experiments at different pH values (20 °C)

Form of CopC	pH		$[Urea]_{1/2}$ (M)	$\Delta G_U(H_2O)$ (kJ/mol)
Apo	4		2.5	18.0 ± 0.5
	5		4.0	22.6 ± 0.5
	6		4.5	23.3 ± 0.5
	7.5		4.5	23.1 ± 0.5
Cu^{II}	4		2.7	19.7 ± 0.5
	5		5.7	23.3 ± 0.5
	6	F–I	3.5	17.6 ± 0.5
		I–U	7.2	32.9 ± 0.5
	7.5	F–I	3.0	12.8 ± 0.5
		I–U	7.1	33.6 ± 0.5

$\Delta G_U(H_2O)$ was obtained from two-state fits (F–U) to the data, for Cu^{II}–CopC at pH 6 and 7.5, a three-state model, involving two sequential two-state reactions were used (F–I–U). All reactions are reversible. Data from CD transitions are shown.

interact strongly with short peptides containing Glu, Asp, and His residues [41].

Thermally induced unfolding of apo– and holo–CopC

The thermal stability of apo–CopC was tested as a function of pH conditions (Fig. 5a). Like in urea, thermal unfolding of apo–CopC is a two-state reaction in which far-UV CD and fluorescence detected curves overlap. At all pH values, thermal unfolding of apo–CopC was over 90% reversible. The maximum stability of apo–CopC towards heat is found at pH 5–6, corresponding to a T_m of about ~67 °C (Table 2). The same experiments were repeated for the Cu^{II}-form of CopC. At pH values between 4 and 6, the thermal reaction appears as two-state transi-

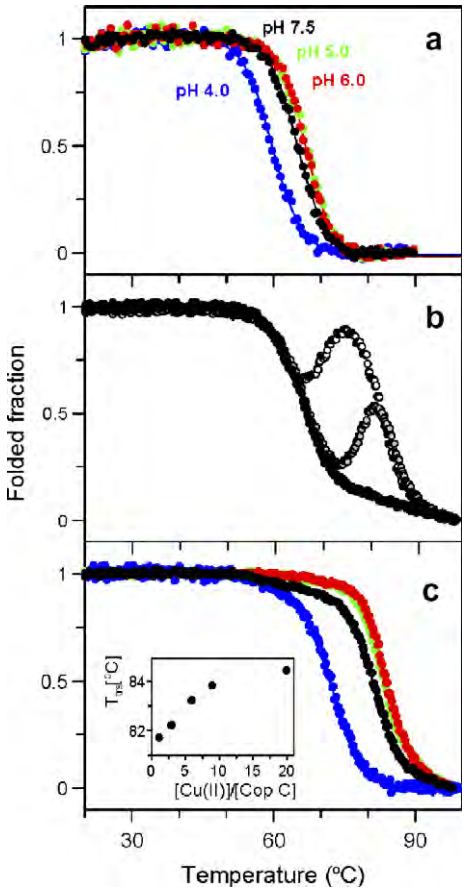

Fig. 5. Thermal unfolding monitored by CD for apo (a) and Cu^{II} (c) forms at different pH values (pH 4, blue; pH 5, green; pH 6, red; pH 7.5, black). (b) Thermal unfolding curves for CopC in the presence of 1 equivalent of copper and 0.18 (white), 0.25 (grey), 0.5 (black) mM DTT (pH 7.5). Inset c: T_{trs} for the major (second) transition versus excess Cu present in the solutions for Cu^{II}–CopC at pH 7.5.

Table 2
Thermal midpoints (T_m) for various forms of CopC at different pH values obtained by far-UV CD or calorimetric measurements

Form of CopC	pH	Detection		T_m (°C)	$\Delta H_{cal}/\Delta H_{vH}$
Apo	4	CD		59.9	—
	5	CD		67.0	—
	6	CD		66.9	—
	7.5	CD		65.1	—
	4	DSC		59.0	1.4
	5	DSC		65.8	1.1
	6	DSC		65.1	1.1
	7	DSC		62.9	1.2
	7.5	DSC		63.8	0.9
Cu^{II}	4	CD		72.0	—
	4.3	CD		79.4	—
	4.6	CD		81.4	—
	5	CD		83.6	—
	6	CD		83.9	—
	7.5	CD	F–I	~62	—
			I–U	81.7	—
	4	DSC		71.7	1.5
	5	DSC		81.6	1.4
	6	DSC		81.7	1.2
	7	DSC	F–I	~63	—
			I–U	79.0	1.3
	7.5	DSC	F–I	~60	—
			I–U	80.0	1.1
Cu^{I}	5	DSC		74.9	n.d.
	6	DSC		73.4	n.d.
	7.5	DSC		72.8	1.1

ΔH_{vH} was obtained from assuming two-state transitions (F–U), ΔH_{cal} is the calorimetric heat from the DSC measurements. For Cu^{II}–CopC at pH 7 and 7.5, a three-state model, involving two sequential two-state reactions was used (F–I–U). All reactions are reversible. For the Cu^{I}-form at pH 5 and 6, the DSC data revealed the presence of some apo-protein in the samples; therefore, enthalpy analysis was not reliable (the listed T_m values at those conditions are for the Cu^{I}-form). n.d., not determined. Errors in T_m are less than ±0.5 °C in all cases.

tions with midpoints that are 10–15 °C higher than the corresponding midpoints for the apo-form (Fig. 5c and Table 2). At pH 7.5, the thermal reaction for Cu^{II}–CopC is best fit by a bi-phasic process. There is a first broad transition, corresponding to about 10–15% change in far-UV CD, that occurs at a low-temperature (T_m of ~63 °C) followed by a second, major transition with a T_m of about 80 °C (Fig. 5c). The observation of a three-state thermal behavior at pH 7.5 matches the findings in urea, which implied the presence of an intermediate under high-pH urea-induced unfolding (*cf.* Fig. 4). We note that the pH 4 thermal profile also has a small shoulder at lower temperatures; here, it is likely due to the presence of a small fraction of apo-protein (see DSC section).

To assess if the pH 7.5 thermal intermediate retains Cu^{II} and if complete unfolding promotes Cu^{II} dissociation, we performed a set of thermal unfolding experiments with Cu^{II}–CopC at pH 7.5 in the presence of various Cu^{II} excess (3-, 6-, 9-, and 20-fold excess). Since the T_m of the 2nd transition (but not the first) shifts towards higher temperatures as a function of increasing Cu^{II} concentration (Fig. 5c; inset), it supports that the intermediate retains copper, but that the metal dissociates in parallel with protein unfolding at the higher temperatures (in contrast to urea-induced unfolding, where the metal remained bound after holo–CopC unfolding).

Apo–CopC refolding triggered by Cu^{II} binding

In our efforts to probe thermal unfolding of the Cu^{I}-form of CopC, we instead found conditions at which Cu^{II} binding triggered protein folding. Upon testing solvent conditions including various amounts of DTT (as an alternative with less absorption than ascorbate) to keep Cu^{I} reduced throughout the heating cycle, we ended up performing a set of far-UV CD experiments in which Cu^{I} oxidation (due to DTT depletion) was followed by metal uptake to the Cu^{II} site in partially unfolded apo–CopC. Upon Cu^{II} binding, the newly formed holo-protein refolded and its unfolding was then detected at higher temperatures matching those for Cu^{II}–CopC (Fig. 5b). Depending on the DTT concentration, Cu^{I} oxidation started at different temperatures, some where apo–CopC was almost fully unfolded; however, when the DTT concentration was increased to 0.5 mM, no Cu^{II}–CopC was detected during heating and the thermal unfolding profile matched that obtained for apo–CopC (Table 2). These observations indicate (a) that Cu^{I} does not bind to apo–CopC in the presence of DTT and, (b) that Cu^{II} binding can trigger protein refolding. To assure Cu^{I}–CopC complex formation, ascorbate was used as the reducing agent, as reported previously [27]. Due to the high absorption of ascrobate, we only performed thermal experiments with Cu^{I}–CopC using calorimetry and anaerobic conditions (see below).

Unfolding probed by differential scanning calorimetry

Thermal unfolding of apo-, Cu^{II}- and Cu^{I}-forms of CopC was analyzed by differential scanning calorimetry (DSC) at different pH values (Fig. 6 and Table 2). All DSC scans for CopC samples were reversible as subsequent scans (after cooling) revealed the same transitions as the 1st scan (data not shown). The DSC experiments demonstrate that the apo-form of CopC exhibits two-state-like thermal transitions at all studied pH conditions with maximal thermal stability found at pH 5–6. The calorimetric traces for the Cu^{II}-form of CopC at pH 4, 5, and 6 also appear two state, although a fraction of apo-protein is detected at pH 4. The DSC data at pH 7.0 and 7.5 reveal a major transition that corresponds to a thermal midpoint around 82 °C but, in addition, there is a small, distinct peak/shoulder at about 62 °C. The low-temperature feature may report on the formation of the Cu^{II}-intermediate of CopC, as the midpoint temperature matches that for the 1st transition in the far-UV CD-detected thermal scans at the same pH values. For both apo- and Cu^{II}-forms of CopC, the thermal midpoints obtained from the DSC data equal the CD-derived values (Table 2). The integrated calorimetric enthalpies from the DSC scans agree with the van't Hoff

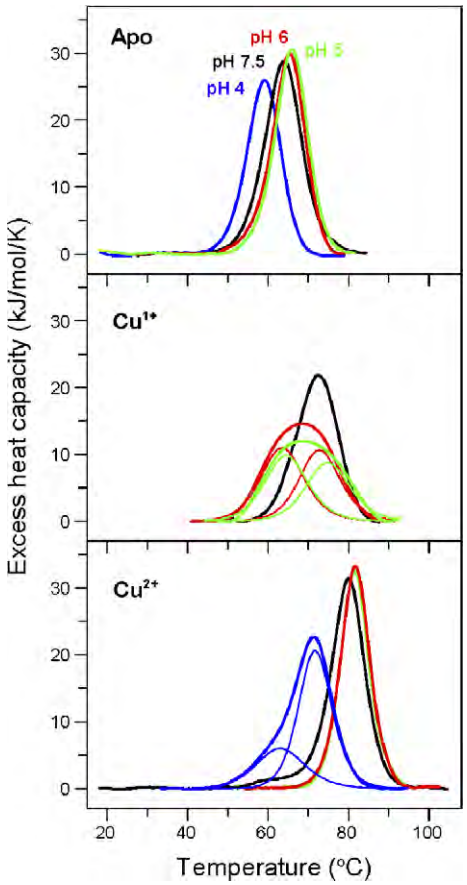

Fig. 6. Calorimetric transitions for apo (top), Cu^{I} (center), and Cu^{II} (bottom) forms at different pH values (pH 4, blue; pH 5, green; pH 6, red; pH 7.5, black curves). Parameters reported in Table 2. For transitions displaying non-two-state behavior, the fits are also shown (thin curves). For Cu^{I} at pH 5 and 6 and Cu^{II} at pH 4, the low-temperature transitions correspond to apo-protein.

enthalpies for most conditions, in agreement with two-state reactions.

For Cu^{I}–CopC (in the presence of ascorbate and extensive degassing), a two-state thermal transition is detected at pH 7.5 with a T_m of 73 °C. This value is higher than the T_m for apo–CopC (64 °C at pH 7.5) but lower than that for the Cu^{II}-form (80 °C at pH 7.5). At lower pH values, the DSC traces for Cu^{I}–CopC were best fit by two thermal transitions; one that matched the data for the apo-protein at the corresponding pH condition and one that was at a higher temperature, likely being the Cu^{I}-form. The appearance of some apo-protein at lower pH values may reflect partial protonation of His48, one of the ligands involved in Cu^{I} coordination.

Discussion

The understanding of copper homeostasis has become increasingly important as the metal could be involved in the pathogenesis of neurological disorders such as Alzheimer's and prion diseases [4,39,42–44]. However, while cellular mechanisms for Cu^{I} transport have been widely described [4,8–11], trafficking pathways for Cu^{II} remain largely unknown. The CopC protein from *P. syringae* pathovar *tomato* is expressed as one of four proteins encoded by the CopABCD operon and is proposed to act in chaperoning Cu^{II} in the oxidizing environment of the periplasm [28–30]. In contrast to cytoplasmic chaperones, CopC has a Greek key β-barrel fold and is capable of binding Cu^{I} and Cu^{II} at two distinct sites, occupied individually or simultaneously [27–30]. Oxidation of Cu^{I}–CopC or reduction of Cu^{II}–CopC causes migration of the Cu from one site to the other. The copper binding sites have been characterized by EXAFS, NMR and crystallographic studies; they both represent novel coordination environments for copper in proteins [27–30]. To learn about the biophysical properties of CopC, we have studied chemical and thermal unfolding *in vitro* as a function of copper and pH using spectroscopic and calorimetric methods.

Apo–CopC unfolds in a two-state process with a stability of ~27 kJ/mol (20 °C, pH 6) and a thermal midpoint of about 67 °C (pH 6). These values are very similar to the corresponding data for *Pseudomonas aeruginosa* apo-azurin, which is a blue-copper protein with the same β-barrel fold as CopC [45,46]. Whereas CopC has one strand less than azurin, the topological arrangement of the strands is the same although CopC has a Met rich region (where the Cu^{I} binds) at the position of azurin's helix. The Cu^{II} site is at the same position in both proteins, although the ligand environment differs. Notably, a recent structural alignment study reported that all β-sandwich proteins contain an interlocked pair of strands with eight positions highly conserved [47]. These residues have been identified and characterized in azurin [48]. Alignment of CopC and azurin reveals that the conserved positions are also present in CopC (data not shown). Thus, the hydrophobic core of the two proteins is similar, which suggests that core stability defines the overall apo-protein stability. Also, thermal and chemical stability values of other apo-forms of cupredoxins, such as plastocyanin and pseudo-azurin are similar to the apo–CopC parameters [49–51].

We find that the Cu^{II} ion largely affects CopC thermal and chemical stability in a pH dependent manner (Tables 1 and 2). The Cu^{I} ion also has a stabilizing effect but not as large as that of Cu^{II} at the same pH condition. The difference between Cu^{II} and Cu^{I} effects is reasonable as the affinity for the reduced metal is lower than for Cu^{II}. Also, the fact that the Cu^{I} site consists of residues all nearby in sequence in a disordered loop region correlates with less impact on overall protein properties. The stabilizing trend of copper in CopC is similar to the behavior of metals bound to *Pseudomonas aeruginosa* azurin. Cu^{I}, Cu^{II}, and Zn can all bind in the active site and stabilize azurin by 10, 23, and 13 kJ/mol, respectively [45,46,52]. In addition, thermal stability is increased to 84, 86, and 89 °C for Cu^{I}, Cu^{II}, and Zn forms of azurin, although the transitions are not reversible [49,53]. Since the thermal reactions of Cu^{II}–CopC (and Cu^{I}–CopC) are reversible, this suggests

that the presence of cysteines (CopC does not have any cysteines), and their oxidation at higher temperatures, is responsible for the thermal irreversibility of other cupredoxins [49].

The metal cofactor remains bound to unfolded azurin in chemical denaturants [45,46,52]; this seems to be the case also for the copper in urea-unfolded Cu^{II}–CopC. This is reasonable as some of the ligands involved in Cu^{II} coordination in CopC are near each other in the sequence (*i.e.,* residues 1 and 27, and residues 89 and 91). In azurin, the metal ligands in the unfolded state are three of the five native-state ligands that are close in the amino-acid sequence (*i.e.,* residues 112, 117, and 121) [54–56]. Assuming a closed thermodynamic cycle, we estimated the Cu^{II} affinity for the unfolded CopC polypeptide (pH 7.5, 20 °C), using the reported K_D of 10^{-13} M [27] for the folded state at pH 7.5 and our unfolding-free energies for the apo- and the holo-forms (23 and 46 kJ/mol, respectively, Table 1), to be in the low nM range. Notably, this value falls between the high-affinity of copper for unfolded azurin [57] and the somewhat weaker Cu^{II} affinities for a range of smaller peptides [39,41,58,59]. CopC may thus be able to protect the copper ion (*i.e.,* keep it bound) during *in vivo* stress that promote polypeptide unfolding.

Interestingly, the presence of Cu^{II} facilitates the formation of a stable holo–CopC intermediate species at neutral and higher pH values upon small perturbations. This intermediate is as stable as the native Cu^{II} protein at lower pH values (Table 1). The intermediate appears rather native-like in terms of spectroscopic signals; with at least 75% of the native CD signal and 90% of the native emission signal intact (Fig. 4). It is possible that the CopC intermediate resembles an equilibrium intermediate observed for a mutant form of pseudo-azurin, another protein with the same β-barrel fold as CopC [60]. Also, kinetic intermediates have been reported for proteins with the cupredoxin fold indicating that this structural motif is poised to intermediate formation [61].

Although structural details of the CopC intermediate cannot be resolved from our experiments, it is clear that the presence of Cu^{II} and a pH of 6, or higher, are necessary requirements. The crystal structures of the Cu^{II}–Cu^{I}-form of CopC at high- and low-pH values provide some clues to why this may be the case [27]. Whereas the N-terminus is a Cu^{II} ligand in the pH 7.5 structure, it is not in the crystal structure of holo–CopC at the lower pH value. We propose that in the native Cu^{II}-form at neutral pH in solution, like in the crystal, the N-terminus coordinates the copper in the folded state together with His1, His91, and Asp89. In support, it has been proposed that Cu interaction can lower the pK_a of the N-terminus to allow it to be de-protonated at neutral pH [39,40]. We speculate that upon minor urea or thermal perturbations to Cu^{II}–CopC at pH 6–7.5 conditions, the Cu interaction with the N-terminus readily falls apart (in parallel with protonation of N-terminus) along with some secondary structure elements (25% of total; i.e., 1–2 β-strands). The Cu^{II} likely remains bound to the other ligands (*i.e.,* His1, His91, Asp89, and H_2O) in the intermediate species. This scenario agrees with the observation that the intermediate has a changed far-UV CD signal but almost native-like Trp83 emission, as will be the case if the Cu site remains in essence intact.

It is possible that the high Cu^{II} affinity in CopC (K_D of 10^{-13} M at pH 7 [27]) is due to the N-terminal coordination acting as a 'lid' that protects Cu^{II} from being transferred to other proteins. Low pH or other external perturbations may switch off the N-terminus (causing formation of the intermediate species), revealing a metal site in CopC with lower Cu^{II} affinity; this may be the relevant form of CopC that is involved in Cu^{II} transfer *in vivo*. Our preliminary K_D estimates for Cu^{II} binding to apo–CopC at low-pH conditions, where the N-terminus is not a Cu^{II} ligand, support this hypothesis (K_D of 1.1 μM determined at pH 4, 20 °C; data not shown). Since the periplasm can vary in its pH value and solvent composition, intermediate as well as the unfolded forms of CopC may be populated at different times during the bacterial life cycle.

Conclusions

We here report the thermodynamic stability and unfolding mechanisms for apo- and holo-forms of CopC, a cupredoxin-like metal carrier that binds Cu^{I} and Cu^{II} in different sites. We find that occupation of the two metal sites has different effects on CopC stability. The Cu^{II}-form of CopC readily adopts a native-like intermediate structure upon minor perturbations that may mimic various stress/growth conditions *in vivo*. We propose that structural, dynamic and thermodynamic differences between apo- and various singly/doubly metalated CopC forms, including the partly folded Cu^{II}-intermediate at high-pH, may be a delicate way to facilitate copper transfer to different partner proteins in the periplasm, as appropriate depending on copper levels and environment pH. CopC may transfer Cu^{II} to CopD for delivery to the cytoplasm, or *via* redox-coupling to CopA/CopB for export out of the cell. CopC may also interact with itself, in a head-to tail fashion [27], to transfer Cu^{I}, or Cu^{II}, to the other site and thereby alter the metal-redox state.

Acknowledgments

This work was funded by grants from the Robert A. Welch Foundation (C-1588) and the USAMRAA (Concept award; W81XWH-06-1-0572). We thank Profs. I. Bertini, L. Banci and Dr. Z. Xiao for providing the CopC plasmid.

References

[1] D.L. Huffman, T.V. O'Halloran, Annu. Rev. Biochem. 70 (2001) 677–701.
[2] S. Puig, E.M. Rees, D.J. Thiele, Structure 10 (10) (2002) 1292–1295.
[3] S. Puig, D.J. Thiele, Curr. Opin. Chem. Biol. 6 (2) (2002) 171–180.
[4] E.D. Harris, Crit. Rev. Clin. Lab. Sci. 40 (5) (2003) 547–586.
[5] P.P. Kulkarni et al., Chemistry 12 (9) (2006) 2410–2422.

[6] A.L. Lamb et al., Nat. Struct. Biol. 6 (8) (1999) 724–729.
[7] A.L. Lamb et al., Nat. Struct. Biol. 8 (9) (2001) 751–755.
[8] M.D. Harrison et al., Trends Biochem. Sci. 25 (1) (2000) 29–32.
[9] I. Hamza et al., Proc. Natl. Acad. Sci. USA 96 (23) (1999) 13363–13368.
[10] I.H. Hung et al., J. Biol. Chem. 273 (3) (1998) 1749–1754.
[11] L.W. Klomp et al., J. Biol. Chem. 272 (14) (1997) 9221–9226.
[12] L. Banci et al., J. Biol. Chem. 279 (26) (2004) 27502–27510.
[13] G.P. Borrelly et al., Biochem. J. 378 (Pt 2) (2004) 293–297.
[14] I.H. Hung et al., J. Biol. Chem. 272 (34) (1997) 21461–21466.
[15] F. Arnesano et al., Genome Res. 12 (2) (2002) 255–271.
[16] T.M. DeSilva, G. Veglia, S.J. Opella, Proteins 61 (4) (2005) 1038–1049.
[17] L. Banci et al., J. Biol. Chem. 276 (11) (2001) 8415–8426.
[18] L. Banci et al., Biochemistry 40 (51) (2001) 15660–15668.
[19] A.C. Rosenzweig et al., Struct. Fold Des. 7 (6) (1999) 605–617.
[20] F. Arnesano et al., Biochemistry 40 (6) (2001) 1528–1539.
[21] L. Banci et al., J. Mol. Biol. 331 (2) (2003) 473–484.
[22] D. Achila et al., Proc. Natl. Acad. Sci. USA 103 (15) (2006) 5729–5734.
[23] S.M. Lee et al., Biochem. Biophys. Res. Commun. 295 (3) (2002) 616–620.
[24] D.A. Cooksey, FEMS Microbiol. Rev. 14 (4) (1994) 381–386.
[25] S. Silver, L.T. Phung, Annu. Rev. Microbiol. 50 (1996) 753–789.
[26] J.S. Cha, D.A. Cooksey, Proc. Natl. Acad. Sci. USA 88 (20) (1991) 8915–8919.
[27] L. Zhang et al., J. Am. Chem. Soc. 128 (17) (2006) 5834–5850.
[28] F. Arnesano et al., Proc. Natl. Acad. Sci. USA 100 (7) (2003) 3814–3819.
[29] F. Arnesano et al., Structure 10 (10) (2002) 1337–1347.
[30] M. Koay et al., Inorg. Chem. 44 (15) (2005) 5203–5205.
[31] L.W. Donaldson et al., J. Am. Chem. Soc. 123 (40) (2001) 9843–9847.
[32] G. Gasmi et al., J. Pept. Res. 49 (6) (1997) 500–509.
[33] P.F. Predki et al., Biochem. J. 287 (Pt 1) (1992) 211–215.
[34] M. Stupak et al., Biochim. Biophys. Acta 1764 (1) (2006) 129–137.
[35] M.M. Santoro, D.W. Bolen, Biochemistry 31 (20) (1992) 4901–4907.
[36] M.M. Santoro, D.W. Bolen, Biochemistry 27 (21) (1988) 8063–8068.
[37] T.M. Cooper, R.W. Woody, Biopolymers 30 (7–8) (1990) 657–676.
[38] M.C. Manning, R.W. Woody, Biopolymers 31 (5) (1991) 569–586.
[39] C.D. Syme et al., J. Biol. Chem. 279 (18) (2004) 18169–18177.
[40] T. Kowalik-Jankowska et al., J. Inorg. Biochem. 95 (4) (2003) 270–282.
[41] C. Kallay et al., J. Inorg. Biochem. 99 (7) (2005) 1514–1525.
[42] J. Stockel et al., Biochemistry 37 (20) (1998) 7185–7193.
[43] C.S. Atwood et al., J. Biol. Chem. 273 (21) (1998) 12817–12826.
[44] C. Ha, J. Ryu, C.B. Park, Biochemistry 46 (20) (2007) 6118–6125.
[45] J. Leckner et al., Biochim. Biophys. Acta 1342 (1) (1997) 19–27.
[46] J. Leckner et al., J. Biol. Inorg. Chem. 2 (1997) 368–371.
[47] A.E. Kister, A.V. Finkelstein, I.M. Gelfand, Proc. Natl. Acad. Sci. USA 99 (22) (2002) 14137–14141.
[48] C.J. Wilson, P. Wittung-Stafshede, Proc. Natl. Acad. Sci. USA 102 (11) (2005) 3984–3987.
[49] A. Sandberg et al., Biochemistry 41 (3) (2002) 1060–1069.
[50] A. Sandberg, D.J. Harrison, B.G. Karlsson, Biochemistry 42 (34) (2003) 10301–10310.
[51] A.P. Capaldi, S.J. Ferguson, S.E. Radford, J. Mol. Biol. 286 (5) (1999) 1621–1632.
[52] P. Wittung-Stafshede, Inorg. Chem. 43 (25) (2004) 7926–7933.
[53] I. Pozdnyakova, P. Wittung-Stafshede, FEBS Lett. 531 (2) (2002) 209–214.
[54] I. Pozdnyakova, J. Guidry, P. Wittung-Stafshede, J. Am. Chem. Soc. 122 (2000) 6337–6338.
[55] I. Pozdnyakova, J. Guidry, P. Wittung-Stafshede, J. Biol. Inorg. Chem. 6 (2001) 182–188.
[56] I. Pozdnyakova, P. Wittung-Stafshede, J. Am. Chem. Soc. 123 (41) (2001) 10135–10136.
[57] J. Marks et al., J. Biol. Inorg. Chem. 9 (3) (2004) 281–288.
[58] D. Sanna et al., Dalton Trans. (17) (2004) 2702–2707.
[59] J.H. Viles et al., Proc. Natl. Acad. Sci. USA 96 (5) (1999) 2042–2047.
[60] S. Jones et al., Biochemistry 39 (19) (2000) 5672–5682.
[61] J.S. Reader et al., Protein Sci. 10 (6) (2001) 1216–1224.

Role of Copper in Thermal Stability of Human Ceruloplasmin

Erik Sedlák,* Gabriel Žoldák,† and Pernilla Wittung-Stafshede*‡§

*Department of Biochemistry and Cell Biology, Rice University, Houston, Texas 77251; †Laboratorium für Biochemie, Universität Bayreuth, D-95440 Bayreuth, Germany; ‡Keck Center for Structural Computational Biology, Rice University, Houston, Texas 77251; and §Department of Chemistry, Rice University, Houston, Texas 77251

ABSTRACT Human ceruloplasmin (CP) is a multicopper oxidase essential for normal iron homeostasis. The protein has six domains with one type-1 copper in each of domains 2, 4, and 6; the remaining coppers form a catalytic trinuclear cluster at the interface between domains 1 and 6. To assess the role of the coppers in CP thermal stability, we have probed the thermal unfolding process as a function of scan rate of holo- and apo-forms using several detection methods (circular dichroism, aromatic and 8-anilino-naphthalene-1-sulfonic acid fluorescence, visible absorption, activity, and differential scanning calorimetry). Both species of CP undergo irreversible thermal reactions to denatured states with significant residual structure. For identical scan rates, the thermal midpoint appears at temperatures 15–20° higher for the holo- as compared with the apo- form. The thermal data for both forms were fit by a mechanistic model involving two consecutive, irreversible steps ($N \rightarrow I \rightarrow D$). The holo-intermediate, *I*, has lost one oxidized type-1 copper and secondary structure in at least one domain; however, the trinuclear copper cluster remains intact as it is functional in oxidase activity. The activation parameters obtained from the fits to the thermal transitions were used to assess the kinetic stability of apo- and holo-CP at physiological temperatures (i.e., at 37°C). It emerges that native CP (i.e., with six coppers) is rather unstable and converts to *I* in $<$1 day at 37°C. Nonetheless, this form remains intact for more than 2 weeks and may thus be a biologically relevant state of CP in vivo. In contrast, apo-CP unfolds rapidly: the denatured state is reached in $<$2 days at 37°C.

INTRODUCTION

Ceruloplasmin (CP; EC 1.16.3.1) is a multicopper protein widely distributed in vertebrates. It occurs mainly in the plasma and plays an important role in iron homeostasis (1,2). Other roles include its participation in the antioxidant defense (3–6) or in oxidative damage mechanisms (7,8) and its involvement in a number of processes related to the metabolism of copper (9), biogenic amines (10), and nitric oxide (11).

Human ceruloplasmin is a single chain of 1046 amino acids (12) with a carbohydrate content of 7–8% and six integral copper ions. The x-ray structure has shown that CP is composed of six compact β-barrel domains with large loop insertions and that the six copper ions are distributed in one trinuclear copper cluster (involving type-2 and type-3 copper ions) located at the border between domains 1 and 6 and possessing ligands from each domain, and in three mononuclear type-1, or ''blue'', sites (13). The mononuclear copper sites located in domains 4 and 6 of CP are typical type-1 sites, like that in ascorbate oxidase (14), and have four ligands (two histidines, one cysteine, and one methionine) arranged in a distorted tetrahedral geometry. The type-1 copper site located in domain 2 is instead a tricoordinated type-1 site in that it lacks an axial Met ligand. This position is replaced by Leu in CP, like blue-copper sites in some laccases (15), and in Fet3 (16). The type-1 copper in domain 2 has been found to be permanently reduced and is not involved in catalytic activity (17,18). CP is synthesized in hepatocytes and secreted into the plasma after incorporation of six copper ions in the secretory pathway (19). Failure to incorporate copper during biosynthesis results in the secretion of an unstable polypeptide that is rapidly degraded in the plasma (20). In Wilson's disease, the absence or impaired function of a copper-transporting ATPase disrupts copper translocations into the secretary pathway, resulting in decreased serum levels of CP in affected patients (21). Aceruloplasminemia, an autosomal recessive neurodegenerative disease, is associated with mutations in the CP gene and accompanied by absence of CP oxidase activity (22).

Previous studies have indicated that the conformation of apo-CP is different from that of the holoprotein (23,24). It was proposed that the apo- form has molten-globule-like properties, although a significant amount of residual tertiary structure remained (23). For more than 40 years, the working model has assumed that CP binds copper in an all-or-none fashion (25). In support, recent metabolic labeling experiments indicated that achieving the final state of CP required occupation of all six copper-binding sites, with no apparent hierarchy for incorporation at any given site (19). On the other hand, there have also been a number of reports that invoke the possibility of partially metalated forms of CP (26,27). Based on cyanide-dependent metal-removal attempts, it was suggested that the type-1 coppers are more sensitive than the type-2 and type-3 coppers to elimination (27,28). Very recently, we showed that chemically induced equilibrium denaturation of CP at room temperature proceeds through an intermediate (*I*) that has lost two copper ions (29). Whereas the *I* forms reversibly, complete unfolding and loss of all copper ions result in an irreversibly

Submitted May 29, 2007, and accepted for publication October 3, 2007.

Address reprint requests to P. Wittung-Stafshede, Tel.: 713-348-4076; Fax: 713-348-5154; E-mail: pernilla@rice.edu.

The permanent address for Erik Sedlák and Gabriel Žoldák is Dept. of Biochemistry, P. J. Safarik University, Moyzesova 11, 04001 Kosice, Slovakia.

Editor: Jonathan B. Chaires.

0006-3495/08/02/1384/08 $2.00

doi: 10.1529/biophysj.107.113696

denatured state. Attempts to refold this species at pH 7 result in the formation of a misfolded molten globule, regardless of the presence or absence of copper ions (29).

To analyze the role of copper in thermal stability, we have investigated the thermal denaturation reactions of holo- and apo- forms of human CP by circular dichroism (CD), fluorescence, visible absorption, oxidase activity, and differential scanning calorimetry (DSC) methods. The thermal reactions were analyzed according to Lyubarev and Kurganov's model (30) for two consecutive irreversible steps. The data reveal the presence of a partially folded intermediate, with (for the holo- form) an intact trinuclear site but loss of one or two type-I coppers at intermediate temperatures. The activation parameters extracted from fits to thermal transitions at different scan rates were used to predict the kinetic behavior of CP at 37°C (pH 7). It emerges that the native, six-copper form of CP is rather unstable at this temperature (half-life of 14 h), whereas the intermediate form remains intact for weeks; the latter species may therefore be present during in vivo CP circulation.

EXPERIMENTAL PROCEDURES

Chemicals and instruments

Analytical-grade chemicals and *o*-dianisidine were obtained from Sigma-Aldrich (St. Louis, MO). 2,2′- Biquinoline was obtained from Fluka (Seelze, Germany). Human CP (>95% purity, $A_{610}/A_{280} = 0.046$) was obtained from Vital Products (Boynton Beach, FL). Concentration of holo- and apo-CP was determined by ε_{280nm} of 200 $mM^{-1}cm^{-1}$. Absorbance and far-UV CD measurements were performed on Varian Cary 50 and Jasco J-810 spectrometers, respectively.

Copper removal

To prepare apo-CP, 5 mg/ml of CP was dialyzed for 2 h at 4°C against 50 mM ascorbate in 0.1 M TrisHCl, pH 7.2. Subsequently, dialysis continued for 12–14 h at 4°C against 50 mM NaCN, 10 mM EDTA, and 10 mM ascorbate in 0.1 M TrisHCl, pH 7.2. The dialysis proceeded for another 16 h at 4°C (with buffer exchange after 8 h) against 50 mM sodium phosphate buffer, pH 7.0. The final apo- form of CP prepared this way contained 0.6 ± 0.4 coppers/CP, as determined by the method developed by Felsenfeld (31).

Activity assay

Oxidase activity of CP was tested using *o*-dianisidine as a substrate in accordance with the procedure by Schosinsky et al. (32). CP activity as a function of temperature was determined as follows: a sample with CP was heated at a rate of 1 K/min; after the desired temperature was reached, a 25-μl aliquot of CP solution was transferred into 100 μl 100 mM acetate, pH 5.0, and cooled on ice. The activity was measured at 23°C.

DSC

DSC experiments were performed on a VP-DSC differential scanning microcalorimeter (Microcal, Northampton, MA) at scan rate of 1.0 K/min. Protein concentration was 3–4 μM (pH 7). Before measurements, sample and reference solutions were properly degassed in an evacuated chamber for 5 min at room temperature and carefully loaded into the cells to avoid bubble formation. Exhaustive cleaning of the cells was undertaken before each experiment. A pressure of 2 atm was kept in the cells throughout the heating cycles to prevent degassing. A background scan collected with buffer in both cells was subtracted from each scan. The reversibility of the transitions was assessed by the reproducibility of the calorimetric trace in a second heating cycle performed immediately after cooling from the first scan. Excess heat capacity curves were plotted using Origin software supplied by Microcal.

CD

CD spectra in the far-UV range (190–250 nm) were recorded on a Jasco-810 instrument with cell path of 1 mm and protein concentrations of 0.3–0.4 μM. Each spectrum is an average of 10 scans. All spectra were background-corrected and converted to mean residue ellipticity (deg·cm^2/dmol). The thermal CD experiments were monitored at 210 nm using a constant heating rate of 0.5, 1, or 1.5 K/min in separate experiments.

Fluorescence

Samples of the holo- or apo- form (~3 μM) of CP were mixed with 200 μM 8-anilino-naphthalene-1-sulfonic acid (ANS) and incubated for 1 h at 23°C. The sample temperature was increased at a constant scan rate (0.5, 1, or 1.5 K/min in separate experiments). The same sample was monitored both for tryptophan and ANS fluorescence at 335 nm (excitation at 295 nm) and 510 nm (excitation at 390 nm), respectively.

Data analysis

DSC-, fluorescence-, and CD-monitored thermal transitions were analyzed according to the model by Lyubarev and Kurganov involving two consecutive irreversible steps of reaction:

$$N \xrightarrow{k_1} I \xrightarrow{k_2} D, \tag{1}$$

where N, I, and D are native, partially denatured, and denatured states, respectively, and k_1 and k_2 are rate constants of corresponding reactions (30). This model is described by a set of differential equations (see Results). Differential equations were solved numerically, and the sum of squared differences between experimental and generated points was minimized. Standard deviations were calculated using 10 sets of the generated data with added Gaussian white noise. Distribution moments of the noise were modeled according to the resulting distribution of the residuals. The correlation coefficient (R) was calculated as:

$$R = \sqrt{1 - \sum_{i=1}^{n}(y_i - y_i^{calc})^2 / \sum_{i=1}^{n}(y_i - y_i^{m})^2}, \tag{2}$$

where y_i and y_i^{calc} are, respectively, the experimental and calculated values of C_p^{ex}; y_i^m is the mean of the experimental values of C_p^{ex} and n is the number of points (e.g., (33)).

Time dependence of the mole fractions γ_N, γ_I, and γ_D of the three different forms of CP (N, I, and D) at 37°C were obtained from the following analytical equations:

$$\gamma_N = \exp(-k_1 t) \tag{3}$$

$$\gamma_I = \frac{k_1}{k_2 - k_1}[\exp(-k_1 t) - \exp(-k_2 t)] \tag{4}$$

$$\gamma_D = 1 + \frac{1}{k_1 - k_2}[k_2 \exp(-k_1 t) - k_1 \exp(-k_2 t)], \tag{5}$$

where the rate constants at any given temperature can be obtained from the Arrhenius equation, $k = A\exp(-E_a/RT)$, where A is the preexponential factor, E_a is the energy of activation, and R is the gas constant. It is convenient to use an alternative form of the Arrhenius equation where the parameter

T^* (temperature at which rate constant equals 1 min^{-1}) is used instead of the parameter A:

$$k = \exp[E_a/R(1/T^* - 1/T)]. \quad (6)$$

RESULTS

Thermal denaturation of CP monitored by far-UV CD

Thermal denaturation of holo- (i.e., six copper) and apo- (i.e., no copper) forms of CP was first monitored by far-UV CD. These experiments show that 1), the thermal transitions of both apo- and holo- forms of CP are irreversible, and 2), they proceed to a state characterized by significant negative ellipticity in the 200- to 210-nm range (Fig. 1). The latter finding indicates that there is residual structure in the thermally denatured state of both apo- and holo-forms. In contrast, chemically denatured CP (at 20°C) has much less negative ellipticity (29), and the far-UV CD spectrum instead matches that of an unfolded protein (Fig. 1). The irreversibility of the thermal transition is not caused by protein aggregation because no signs of aggregation or precipitation were observed. The thermal denaturation processes for both holo- and apo- forms of CP depend on the heating rate: the faster the rate, the higher the apparent thermal midpoint (Fig. 2). Comparing thermal curves at identical scan rates (three different scan rates tested) reveals that the holo- form of CP is more resistant to thermal perturbation than the apo-form by ~15–20°C.

Thermal denaturation of CP monitored by DSC

To obtain more insight into thermal denaturation of CP we next turned to DSC experiments. In Fig. 2, we show DSC data as a function of temperature for both forms of CP at three different scan rates. We note that the transitions observed by CD and DSC at the same scan rate correspond well with each other. The DSC scans clearly demonstrate that the thermal transitions for both forms include at least two steps. From various cooling experiments, we found (as in the CD experiments) that both transitions appear irreversible under our conditions.

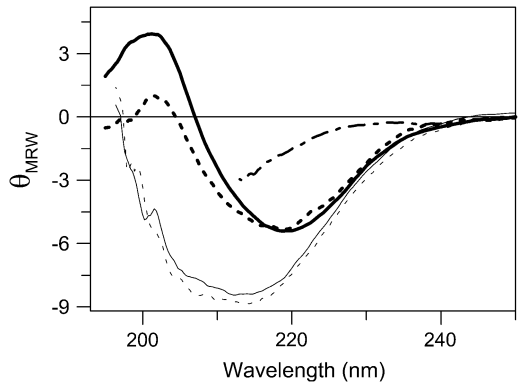

FIGURE 1 CD spectra of N (*thick lines*, at 20°C, pH 7.0) and D (*thin line*, at 70°C, pH 7.0) forms of holo-CP (*solid lines*) and apo-CP (*dotted lines*). For comparison, GuHCl-perturbed CP (at 20°C, pH 7.0) is also shown (*dash-dot line*). CD spectra of 3Cu-CP N and D forms are indistinguishable of those of holo-CP.

Two consecutive irreversible transitions can be described by Eq. 1 in Materials section: $N \xrightarrow{k_1} I \xrightarrow{k_2} D$. This model can be considered a particular case of the Lumry-Eyring model in which the rate of the reverse reaction of the first step is much slower than the rate of the second step (34). Analysis of DSC data using the model of two consecutive irreversible steps has been described in detail by Lyubarev and Kurganov (30). Briefly, the kinetic behavior of the system is described by the following differential equations:

$$\frac{d\gamma_N}{dt} = -k_1\gamma_N \quad (7a)$$

$$\frac{d\gamma_I}{dt} = k_1\gamma_N - k_2\gamma_I \quad (7b)$$

where γ_N and γ_I are the mole fractions of native and partially unfolded protein, respectively. After substituting $dt = dT/\nu$, where ν is the scan rate, and solving the equations, the following is obtained:

$$\gamma_N = \exp\left(-\frac{1}{\nu}\int_{T_0}^{T} k_1 dT\right). \quad (8)$$

$$\gamma_I = \frac{1}{\nu}\exp\left(-\frac{1}{\nu}\int_{T_0}^{T} k_2 dT\right)\int_{T_0}^{T}\left[k_1\exp\left(\frac{1}{\nu}\int_{T_0}^{T}(k_2 - k_1)dT\right)\right]dT. \quad (9)$$

The excess heat capacity, which is the parameter measured in the DSC experiments, is then expressed by the equation:

$$C_p^{ex} = \frac{d\langle\Delta H\rangle}{dT} = \frac{\Delta H_1 k_1}{\nu}\gamma_N + \frac{\Delta H_2 k_2}{\nu}\gamma_I, \quad (10)$$

where ΔH_1 and ΔH_2 are molar enthalpy changes for the first and second steps, respectively. The rate constants, k, are related to E_a and T^* via Eq. 6. The DSC data in Fig. 2 were fitted to Eq. 10, and the resulting six parameters (ΔH_1, ΔH_2, E_{a1}, E_{a2}, T_1^*, and T_2^*) are listed in Table 1.

In analogy, the temperature dependences of the CD and fluorescence signals were fitted by the following equation:

$$S_{obs} = S_N\gamma_N + S_I\gamma_I + S_D(1 - \gamma_N - \gamma_I), \quad (11)$$

where S_{obs}, S_N, S_I, and S_D are measured signal and signals of native, partially denatured, and denatured states, respectively. In combination with the expressions for each mole fraction given in the equations above (using CD signals instead of enthalpy changes), and the relation among k, E_a, and T^* provided by Eq. 6, the key parameters (i.e., E_a and T^* values) could be obtained from fits to the CD-detected profiles (Table 1). The parameters for the first transition (N to I) obtained from CD differ somewhat from those obtained from DSC. This is likely an effect of the poor separation of the two thermal steps when probed by CD, causing unreliable fits. The theoretical

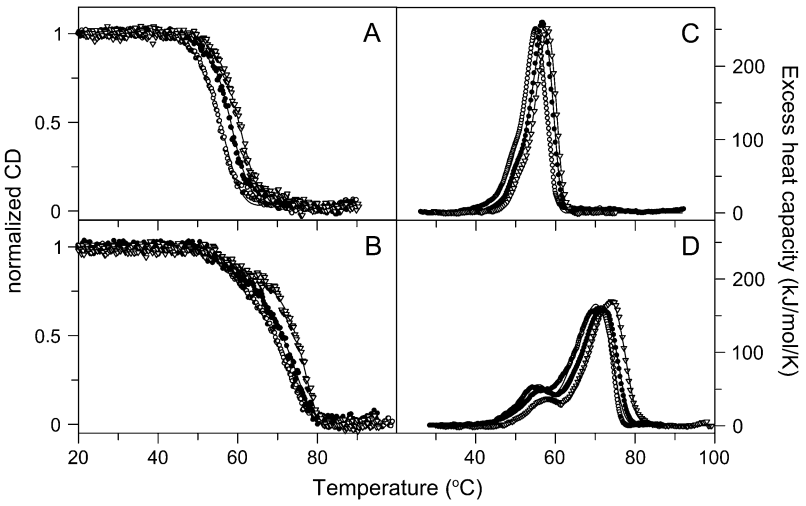

FIGURE 2 Thermal transitions of apo- (*A* and *C*) and holo- (*B* and *D*) forms of CP monitored by CD and DSC. Ellipticity dependence monitored at 210 nm is shown as normalized ellipticity. Measurements were performed at three different scan rates (from *left*: 0.5, 1.0, and 1.5 K/min) at pH 7.0. DSC scans were performed at three different scan rates (from *left*: 0.5, 1.0, and 1.5 K/min) at pH 7.0. Experimental data are shown as points; theoretical fits based on Eqs. 10 and 11 are shown as solid lines.

DSC and CD curves based on the fitted parameters are shown in Fig. 2 and are in good agreement with the actual data. This supports the two-step irreversible mechanism as an appropriate assumption.

Thermal denaturation of CP monitored by other methods

To further investigate the thermal reactions of CP, tryptophan fluorescence and fluorescence of ANS were probed as a function of temperature. CP has 19 tryptophans that are scattered throughout the six domains. Normalized tryptophan and ANS fluorescence signals of apo- and holo- forms of CP as a function of temperature are shown in Fig. 3 for three different scan rates. Whereas the data for apo-CP adopt an asymmetrical sigmoidal shape (Fig. 3 *A*), holo-CP fluorescence data clearly show three-state behavior (Fig. 3 *B*). For both holo- and apo-forms, the tryptophan-emission changes as a function of temperature were not affected by the presence or absence of ANS. Thus, ANS in itself did not have any effect on CP thermal

TABLE 1 Calculated parameters based on two-step analysis of the data shown in Figs. 2 and 3 describing the irreversible thermal transitions of holo- and apo- forms of human CP

CP form	E_{a1} (kJ/mol)	T^*_1 (K)	ΔH_1 (kJ/mol)	E_{a2} (kJ/mol)	T^*_2 (K)	ΔH_2 (kJ/mol)	R	T_{obs}† (°C)
Apo								**1st/2nd**
DSC 0.5 K/min	222	332	407	275	334	1571	0.9980	50.9/55.5
DSC 1.0 K/min	273	328	365	326	333	1593	0.9975	52.7/57.0
DSC 1.5 K/min	267	330	394	323	333	1401	0.9994	53.9/58.0
Average	254	330	389	308	333	1521		
F_{Trp} 0.5 K/min	238	334	–	240	334	–	0.9999	54.1
F_{Trp} 1.0 K/min	274	334	–	331	335	–	0.9997	55.6
F_{Trp} 1.5 K/min	239	334	–	322	331	–	0.9999	56.6
CD 0.5 K/min	181	341	–	176	335	–	0.9991	55.3
CD 1.0 K/min	167	341	–	298	332	–	0.9985	57.9
CD 1.5 K/min	187	340	–	265	332	–	0.9979	59.9
Holo								
DSC 0.5 K/min	268	334	420	219	353	1917	0.9934	55.0/71.6
DSC 1.0 K/min	219	335	443	230	351	1801	0.9989	56.5/72.4
DSC 1.5 K/min	275	333	381	232	351	1930	0.9990	57.4/74.0
Average	254	334	415	227	351	1883		
F_{Trp} 0.5 K/min	275	334	–	175	358	–	0.9996	54.1/70.0
F_{Trp} 1.0 K/min	278	333	–	213	354	–	0.9998	56.4/72.6
F_{Trp} 1.5 K/min	232	336	–	221	355	–	0.9998	58.5/75.9
CD 0.5 K/min	174	347	–	210	357	–	0.9995	56.7/71.1
CD 1.0 K/min	152	348	–	235	354	–	0.9986	59.0/73.1
CD 1.5 K/min	118	354	–	337	352	–	0.9987	61.6/75.0

T^* values are the temperatures at which the rate constant for the specific reaction is 1/min. Index 1 corresponds to the first *N*-to-*I* transition, and index 2 corresponds to the subsequent *I*-to-*D* process. The DSC data are most reliable and were used to derive average values for each parameter. R is the correlation coefficient (see Eq. 4).

†Observed thermal midpoints; for some apo-CP data, only the midpoint of the major transition is reported.

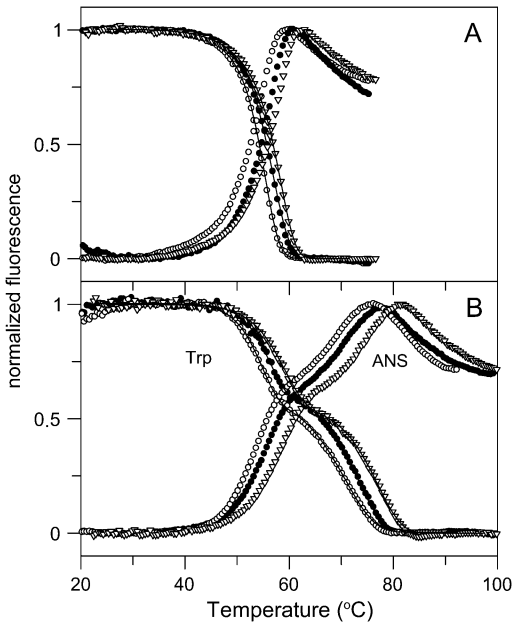

FIGURE 3 Thermal transitions of apo- (*A*) and holo- (*B*) forms of CP monitored by tryptophan fluorescence (emission wavelength 335 nm) and ANS fluorescence (emission wavelength 510 nm). Fluorescence is shown as normalized ellipticity. Measurements were performed at three different scan rates (from *left*: 0.5, 1.0, and 1.5 K/min) at pH 7.0. Experimental data are shown as points; theoretical fits based on Eq. 11 are shown as solid lines.

stability. The obtained parameters from fits to the tryptophan fluorescence, again assuming a two-step, irreversible reaction mechanism, are in good agreement with the parameters obtained from the DSC data (Table 1). The ANS emission increases on CP denaturation, with the *I* species having an intermediate-sized signal. This implies that *I* is not a partially folded molten-globule-like species, as such structures tend to bind ANS strongly, causing orders of magnitude higher ANS emission. (The ANS emission data were not analyzed further because of the nonlinearity of the posttransition regions.)

For holo-CP, 610-nm absorbance was also investigated as a function of temperature (Fig. 4). Absorbance at 610 nm monitors the two oxidized type-1 copper sites in CP, i.e., the coppers in domains 4 and 6. The high reduction potential of

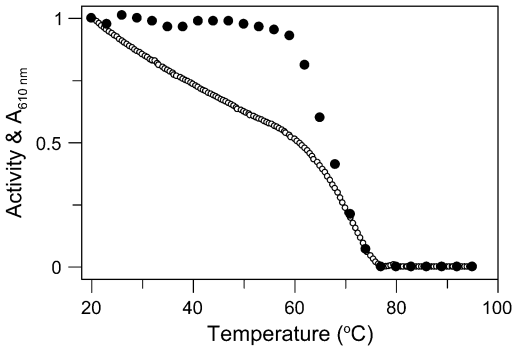

FIGURE 4 Thermal dependence of absorbance of holo-CP at 610 nm (○) and oxidase activity at 20°C (●) after heating to the indicated temperatures.

the type-1 copper in domain 2 has indicated that it is permanently reduced; thus, it does not contribute to the blue color, nor is it catalytically relevant (17,18). We find that 610-nm absorption of holo-CP decreases gradually with temperature up to ~60°C, where it adopts a signal that is ~50% of its original value at 20°C. At higher temperatures, the remaining visible absorption rapidly decreases toward zero. This result indicates perturbation (and likely metal dissociation) of the two type-1 copper sites in two phases as a function of temperature; one copper goes in the first step, the other in the second step. The first phase correlates with the formation of the *N*-to-*I* step as detected by CD, fluorescence, and DSC; the second phase correlates with the *I*-to-*D* step detected by the other methods.

Also CP's oxidase activity parameters were obtained as a function of temperature (Fig. 4). Aromatic diamine (*o*-dianisidine) oxidation by CP requires an intact trinuclear copper site, which is situated on the interface between domains 1 and 6. The type-1 copper site in domain 4 is likely the entry point of the electrons from this substrate before transfer to the catalytic cluster (10). When CP solutions heated to different temperatures were cooled to 23°C and oxidase activity was measured, native-like activity was found for samples heated to temperatures up to 60°C. This indicates that the structural changes of the first phase (*N* to *I*) include distortion of parts of the protein not involved in catalytic activity. Further increase in temperature leads to irreversible inhibition of CP oxidase activity with an apparent transition midpoint at 68°C. This process correlates with the second step (i.e., *I* to *D*) observed by DSC and the spectral methods. Based on these results, we conclude that the trinuclear site is destroyed in the *I*-to-*D* step.

DISCUSSION

Human CP is a key protein in copper/iron metabolism (35,36). It is linked to diseases such as aceruloplasminemia and Wilson's disease. From a biophysical point, it is an intriguing, complex protein with six integral coppers distributed in a structure of six β-sandwich domains. We recently reported chemical unfolding data on apo- and holo- forms of human CP. We found that urea-induced unfolding involves an intermediate with loss of about two type-1 coppers (one being the permanently reduced one in domain 2). Complete unfolding was irreversible because attempts to refold from this starting point resulted in a dead-end molten globule species (29). Less is known about CP thermal unfolding. Thermal denaturation of sheep CP was reported to be irreversible and to have a T_{trs} of >70°C (37). However, for irreversible reactions, a high melting temperature does not guarantee that a protein will remain in its native state for a given time at a certain temperature (38). In such cases, information about the structural integrity of proteins can only be obtained from kinetic parameters. The physical basis of protein kinetic stability is, however, poorly understood, and no structural consensus has been found to explain this phenomenon (39).

In this study, we assessed the thermal reaction of human CP in its apo- and copper-loaded forms to reveal details about kinetic stability and specific roles of the coppers. Previously, copper has been found to add to both equilibrium and kinetic stability of some proteins (i.e., azurin, ascorbate oxidase, Cu, Zn-superoxide dismutase) (40–44). However, it has also been shown that copper can decrease the stability of proteins. For example, copper ions 1), promote transitions in the prion protein toward less thermally stable conformations (45), 2), limit the reversibility of thermal transitions of blue-copper proteins (46–48), and 3), bind specifically to nonnative states of β_2-microglobulin, resulting in a destabilization of the native state (49). Our work presented here reveals that in the case of human CP, the protein is thermally and kinetically stabilized by its copper cofactors.

We have found that the thermal reaction of CP (both apo- and holo- forms) is irreversible and involves two phases. An irreversible two-step model was therefore used to analyze thermal data collected by a set of different detection methods (i.e., CD, fluorescence, and DSC). The similar parameters derived from data collected by the different detection methods, and for data collected with different scan rates, strongly support the validity of the assumed denaturation mechanism. Based on the spectroscopic data (Fig. 2), the holo-intermediate species has slightly perturbed secondary structure and exposes 50–70% of its tryptophans to the solvent (Fig. 3). The enthalpy data (Table 1) suggest that formation of the intermediate corresponds to about one-sixth of the overall enthalpy change associated with the overall reaction (ΔH_1 is about one-sixth of total enthalpy change for holo-CP). These numbers suggest that the intermediate has one or two domains (of the six) unfolded. Because there is no significant increase in ANS emission at the conditions favoring the thermal intermediate, a partially folded species is disfavored over a species with most domains fully folded and a few (or one) domains fully unfolded.

The blue color experiments (Fig. 4) indicate that the holo-intermediate has lost one oxidized type-1 copper, and the activity experiments imply that the trinuclear cluster is intact in the intermediate species. The oxidized type-1 copper that is removed in the intermediate could be the one in either domain 4 or 6. We propose that it is more likely that it is the one in domain 4, as disruption of the type-1 site in domain 6 (for example, through domain unfolding) would likely also perturb the interface between domains 6 and 1 and therefore affect the trinuclear copper site. It is also possible that the copper loss in the first unfolding step corresponds to a small disruption of the metal site and that the affected protein domain (i.e., domain 4 or 6) remains folded. In analogy with the urea-induced holo-CP intermediate observed at room temperature that had lost two coppers (one oxidized and one reduced) (29), we suggest that the reduced type-1 copper in domain 2 is also absent in the thermal holointermediate of CP. We propose that domain 2 is an unfolded domain in the intermediate; if so, the parts of CP involved in oxidase activity are not affected (which is in agreement with our observations) (Fig. 4).

The transition $I \rightarrow D$ is most likely accompanied by structural perturbation in all domains and loss of the trinuclear copper cluster. Based on its CD spectrum, the final thermal state, D, corresponds to a molten-globule species for both apo- and holo-CP (Fig. 1). This species appears similar to the dead-end molten globule detected on refolding attempts in urea from the completely unfolded states of apo- and holo-CP at room temperature (29). The starting state of apo-CP has an open structure and no interactions between domains 1 and 6 (28). Because the $N \rightarrow I$ transition for apo-CP involves a similarly low ΔH_1 as in the case of holo-CP, it is likely that the same domain is perturbed as in the holointermediate. In Fig. 5, a tentative scheme for thermal perturbations of holo- and apo-forms of CP that is based on our data is shown.

Inspection of the parameters from the fits (Table 1) reveals that although the first transition (N to I) is only somewhat stabilized in the holo- form (T_1* increases by 4°), the second step (I to D) is much stabilized in the holo- form (T_2* increases by 18°) as compared with the apo-form data. This implies that although the trinuclear copper cluster (and thus the interactions between domains 1 and 6) contributes to the thermal stability of holo-CP, the type-1 coppers have almost no such effect.

The activation/rate parameters obtained from the fits to the DSC data enabled us to predict the time dependences of the populations of γ_N, γ_I, and γ_D at 37°C (and any other temperature) for apo- and holo- forms of CP via Eq. 5 (Fig. 6). We find that the native state of holo-CP is relatively unstable at

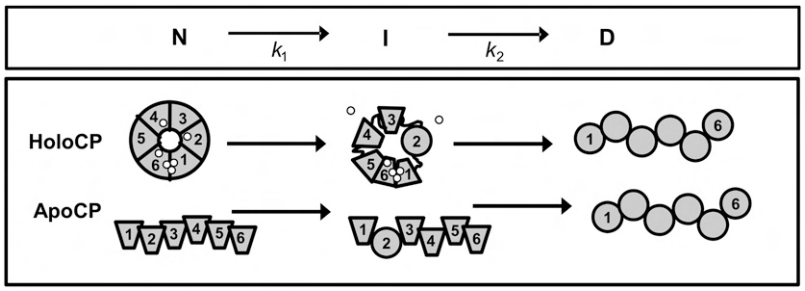

FIGURE 5 Tentative scheme for thermal unfolding of holo- and apo- forms of CP based on our work (*trapezoid* indicates intact domain, and *circle* molten-globule-like domain). We propose that the first *N*-to-*I* transition involves unfolding of one or two domains, perhaps domain 2 as shown here. For holo-CP, the *N*-to-*I* step also couples to type-I copper release. One oxidized type-1 copper is lost (the one in domain 4 is shown, but it could also be the one in domain 6). If domain 2 is unfolded in *I*, it appears reasonable that the reduced type-1 copper in this domain is also lost (as shown here). This was previously concluded to be the case for the urea-induced CP intermediate (29). The last step involves destruction of the trinuclear copper cluster and structural perturbations in all domains.

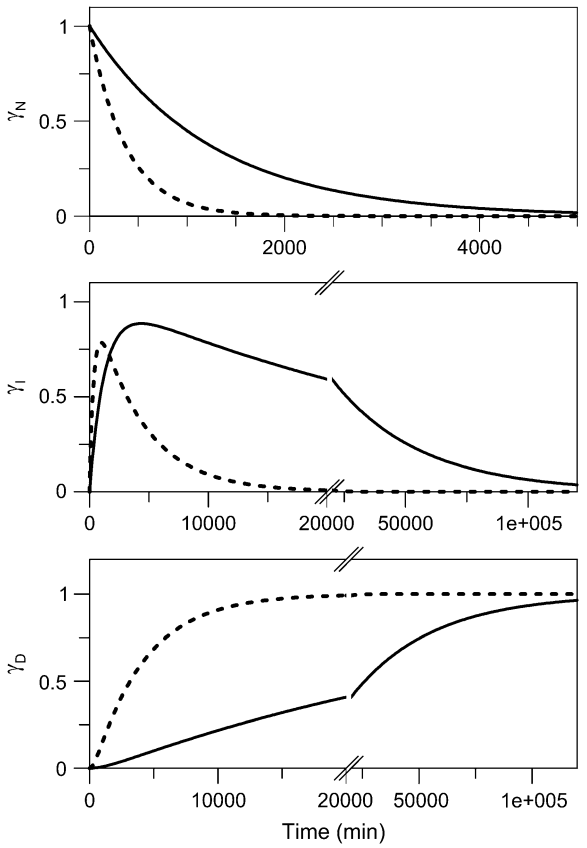

FIGURE 6 Time dependence of mole fractions γ_N, γ_I, and γ_D of holo- (*solid lines*), and apo- (*dotted lines*) forms of CP at 37°C. The kinetics were obtained from Eq. 5 using the average parameters from DSC experiments; i.e., for the holo- form ($E_{a,1} = 254$ kJ/mol, $T_1^* = 334$ K, $E_{a,2} = 227$ kJ/mol, $T_2^* = 352$ K): $k_1 = 8.0 \times 10^{-4}$ min^{-1}, and $k_2 = 2.8 \times 10^{-5}$ min^{-1}; and for the apo- form ($E_{a,1} = 254$ kJ/mol, $T_1^* = 330$ K, $E_{a,2} = 308$ kJ/mol, $T_2^* = 333$ K): $k_1 = 2.7 \times 10^{-3}$ min^{-1}, and $k_2 = 2.5 \times 10^{-4}$ min^{-1}, respectively.

physiological temperatures (i.e., 37°C): it transforms to the *I* state with a half-time of ~13.8 h at this temperature. The *I* form of holo-CP is more kinetically stable: its half-life is ~17 days, pH 7, 37°C. Because the ($N \rightarrow I$) conversion occurs on a biologically relevant time scale (i.e., hours at 37°C), both *N* and *I* forms of holo-CP may be present in vivo depending on conditions and copper levels. Removal of copper results in an apoprotein that has less kinetic stability at 37°C. The rate of disappearance of ''native'' apo-CP corresponds to a half-life of 4.3 h (threefold faster than holo-CP). The intermediate species of apo-CP disappears in 1.9 days (i.e., ninefold faster than the holo- form). Notably, direct kinetic unfolding experiments measured by fluorescence of apo- and holo-CP on jumping to different final temperatures (between 42°C and 60°C) matched the values of k_1 and k_2 predicted from the DSC parameters at each temperature (Supplementary Material). This agreement between physical measurements and predictions supports the conclusion that the assumed two-step mechanism is appropriate and thus that the predicted kinetic parameters at 37°C are valid.

CONCLUSIONS

In summary, we show that despite an apparent high thermal stability (observed midpoint at 70–75°C depending on conditions), holo-CP with six intact coppers is a kinetically unstable protein at physiological temperatures (i.e., at 37°C, pH 7). Within hours at this temperature, it converts to a much more inert intermediate species that has lost one or two of the type-1 copper ions. We propose that this intermediate may be present in vivo under some conditions. Our earlier urea experiments (pH 7, 20°C) revealed a similar holo-*I* species that formed reversibly on minor perturbations of the six-copper, fully loaded state of CP (29). In the absence of all coppers, CP is even more unstable; apo-CP is completely unfolded in <2 days at 37°C. The low kinetic stability of the apo- form of CP may correlate with its rapid degradation in vivo in various disease conditions (36).

SUPPLEMENTARY MATERIAL

To view all of the supplemental files associated with this article, visit www.biophysj.org.

This work was funded by grants from the Robert A. Welch Foundation (C-1588) and the US Army Medical Research Acquisition Activity (Concept award W81XWH-06-1-0572).

REFERENCES

1. Frieden, E., and H. S. Hsieh. 1976. Ceruloplasmin: the copper transport protein with essential oxidase activity. *Adv. Enzymol. Relat. Areas Mol. Biol.* 44:187–236.
2. Gitlin, J. D. 1998. Aceruloplasminemia. *Pediatr. Res.* 44:271–276.
3. Gutteridge, J. M. C. 1983. Antioxidant properties of caeruloplasmin towards iron- and copper-dependent oxygen radical formation. *FEBS Lett.* 157:37–40.
4. Miyajima, H., Y. Takahashi, M. Serizawa, E. Kaneko, and J. D. Gitlin. 1996. Increased plasma lipid peroxidation in patients with aceruloplasminemia. *Free Radic. Biol. Med.* 20:757–760.
5. Cha, M. K., and I. H. Kim. 1999. Ceruloplasmin has a distinct active site for the catalyzing glutathione-dependent reduction of alkyl hydroperoxide. *Biochemistry.* 38:12104–12110.
6. Inoue, K., T. Akaike, Y. Miyamoto, T. Okamoto, T. Sawa, M. Otagiri, S. Suzuki, T. Yoshimura, and H. Maeda. 1999. Nitrosothiol formation catalyzed by ceruloplasmin. Implication for cytoprotective mechanism in vivo. *J. Biol. Chem.* 274:27069–27075.
7. Swain, J., and J. M. C. Gutteridge. 1995. Prooxidant iron and copper, with ferroxidase and xanthine oxidase activities in human atherosclerotic material. *FEBS Lett.* 368:513–515.
8. Mukhopadhyay, C. K., B. Mazumder, P. F. Lindley, and P. L. Fox. 1997. Identification of the prooxidant site of human ceruloplasmin: a model for oxidative damage by copper bound to protein surfaces. *Proc. Natl. Acad. Sci. USA.* 94:11546–11551.
9. Harris, E. D. 1993. The transport of copper. *Prog. Clin. Biol. Res.* 380: 163–179.
10. Zaitsev, V. N., I. Zaitseva, M. Papiz, and P. F. Lindley. 1999. An x-ray crystallographic study of the binding sites of the azide inhibitor and organic substrates to ceruloplasmin, a multi-copper oxidase in the plasma. *J. Biol. Inorg. Chem.* 4:579–587.
11. Bianchini, A., G. Musci, and L. Calabrese. 1999. Inhibition of endothelial nitric-oxide synthase by ceruloplasmin. *J. Biol. Chem.* 274:20265–20270.

12. Ortel, T. L., N. Takahashi, and F. W. Putnam. 1984. Structural model of human ceruloplasmin based on internal triplication, hydrophilic/hydrophobic character, and secondary structure of domains. *Proc. Natl. Acad. Sci. USA.* 81:4761–4765.

13. Zaitseva, I., V. Zaitsev, G. Card, K. Moshkov, B. Bax, A. Ralph, and P. Lindley. 1996. The x-ray structure of human serum ceruloplasmin at 3.1 Å: nature of the copper centres. *J. Biol. Inorg. Chem.* 1:15–23.

14. Messerschmidt, A., R. Ladenstein, R. Huber, M. Bolognesi, L. Avigliano, R. Petruzzelli, A. Rossi, and A. Finazzi-Agro. 1992. Refined crystal structure of ascorbate oxidase at 1.9 A resolution. *J. Mol. Biol.* 224:179–205.

15. Solomon, E. I., U. M. Sundaram, and T. E. Machonkin. 1996. Multicopper oxidases and oxygenases. *Chem. Rev.* 96:2563–2606.

16. Hassett, R. F., D. S. Yuan, and D. J. Kosman. 1998. Spectral and kinetic properties of the Fet3 protein from *Saccharomyces cerevisiae*, a multinuclear copper ferroxidase enzyme. *J. Biol. Chem.* 273:23274–23282.

17. Machonkin, T. E., H. H. Zhang, B. Hedman, K. O. Hodgson, and E. I. Solomon. 1998. Spectroscopic and magnetic studies of human ceruloplasmin: identification of a redox-inactive reduced Type 1 copper site. *Biochemistry.* 37:9570–9578.

18. Machonkin, T. E., and E. I. Solomon. 2000. The thermodynamics, kinetics, and molecular mechanism of intramolecular electron transfer in human ceruloplasmin. *J. Am. Chem. Soc.* 122:12547–12560.

19. Hellman, N. E., S. Kono, G. M. Mancini, A. J. Hoogeboom, G. J. De Jong, and J. D. Gitlin. 2002. Mechanisms of copper incorporation into human ceruloplasmin. *J. Biol. Chem.* 277:46632–46638.

20. Gitlin, J. D., J. J. Schroeder, L. M. Lee-Ambrose, and R. J. Cousins. 1992. Mechanisms of caeruloplasmin biosynthesis in normal and copper-deficient rats. *Biochem. J.* 282:835–839.

21. Gitlin, J. D. 2003. Wilson disease. *Gastroenterology.* 125:1868–1877.

22. Harris, Z. L., L. W. J. Klomp, and J. D. Gitlin. 1998. Aceruloplasminemia: an inherited neurodegenerative disease with impairment of iron homeostasis. *Am. J. Clin. Nutr.* 67 Suppl.:972S–977S.

23. De Filippis, V., V. B. Vassiliev, M. Beltramini, A. Fontana, B. Salvato, and V. S. Gaitskhoki. 1996. Evidence for the molten globule state of human apo-ceruloplasmin. *Biochim. Biophys. Acta.* 1297:119–123.

24. Sato, M., and J. D. Gitlin. 1991. Mechanisms of copper incorporation during the biosynthesis of human ceruloplasmin. *J. Biol. Chem.* 266: 5128–5134.

25. Aisen, P., and A. G. Morell. 1965. Physical and chemical studies on ceruloplasmin. 3. A stabilizing copper-copper interaction in ceruloplasmin. *J. Biol. Chem.* 240:1974–1978.

26. Vassiliev, V. B., A. M. Kachurin, M. Beltramini, G. P. Rocco, B. Salvato, and V. S. Gaitskhoki. 1997. Copper depletion/repletion of human ceruloplasmin is followed by the changes in its spectral features and functional properties. *J. Inorg. Biochem.* 65:167–174.

27. Musci, G., T. Z. Fraterrigo, L. Calabrese, and D. R. McMillin. 1999. On the lability and functional significance of the type 1 copper pool in ceruloplasmin. *J. Biol. Inorg. Chem.* 4:441–446.

28. Vachette, P., E. Dainese, V. B. Vasyliev, P. Di Muro, M. Beltramini, D. I. Svergun, V. De Filippis, and B. Salvato. 2002. A key structural role for active site type 3 copper ions in human ceruloplasmin. *J. Biol. Chem.* 277:40823–40831.

29. Sedlak, E., and P. Wittung-Stafshede. 2007. Discrete roles of copper ions in chemical unfolding of human ceruloplasmin. *Biochemistry.* 46: 9638–9644.

30. Lyubarev, A. E., and B. I. Kurganov. 1998. Modeling of irreversible thermal protein denaturation at varying temperature. I. The model involving two consecutive irreversible steps. *Biochemistry (Mosc.).* 63: 434–440.

31. Felsenfeld, G. 1960. The determination of cuprous ion in copper proteins. *Arch. Biochem. Biophys.* 87:247–251.

32. Schosinsky, K. H., H. P. Lehmann, and M. F. Beeler. 1974. Measurement of ceruloplasmin from its oxidase activity in serum by use of *o*-dianisidine dihydrochloride. *Clin. Chem.* 20:1556–1563.

33. Pina, D. G., A. V. Shnyrova, F. Gavilanes, A. Rodriguez, F. Leal, M. G. Roig, I. Y. Sakharov, G. G. Zhadan, E. Villar, and V. L. Shnyrov. 2001. Thermally induced conformational changes in horseradish peroxidase. *Eur. J. Biochem.* 268:120–126.

34. Sanchez-Ruiz, J. M., J. L. Lopez-Lacomba, M. Cortijo, and P. L. Mateo. 1988. Differential scanning calorimetry of the irreversible thermal denaturation of thermolysin. *Biochemistry.* 27:1648–1652.

35. Musci, G. 2001. Ceruloplasmin, the unique multi-copper oxidase of vertebrates. *Protein Pept. Lett.* 8:159–169.

36. Hellman, N. E., and J. D. Gitlin. 2002. Ceruloplasmin metabolism and function. *Annu. Rev. Nutr.* 22:439–458.

37. Bonaccorsi di Patti, M. C., G. Musci, A. Giartosio, S. D'Alessio, and L. Calabrese. 1990. The multidomain structure of ceruloplasmin from calorimetric and limited proteolysis studies. *J. Biol. Chem.* 265:21016–21022.

38. Plaza del Pino, I. M., B. Ibarra-Molero, and J. M. Sanchez-Ruiz. 2000. Lower kinetic limit to protein thermal stability: a proposal regarding protein stability in vivo and its relation with misfolding diseases. *Proteins.* 40:58–70.

39. Manning, M., and W. Colon. 2004. Structural basis of protein kinetic stability: resistance to sodium dodecyl sulfate suggests a central role for rigidity and a bias toward beta-sheet structure. *Biochemistry.* 43:11248–11254.

40. Baker, D., and D. A. Agard. 1994. Kinetics versus thermodynamics in protein folding. *Biochemistry.* 33:7505–7509.

41. Milardi, D., D. M. Grasso, M. P. Verbeet, G. W. Canters, and C. La Rosa. 2003. Thermodynamic analysis of the contributions of the copper ion and the disulfide bridge to azurin stability: synergism among multiple depletions. *Arch. Biochem. Biophys.* 414:121–127.

42. Pozdnyakova, I., J. Guidry, and P. Wittung-Stafshede. 2001. Copper stabilizes azurin by decreasing the unfolding rate. *Arch. Biochem. Biophys.* 390:146–148.

43. Savini, I., S. D'Alessio, A. Giartosio, L. Morpurgo, and L. Avigliano. 1990. The role of copper in the stability of ascorbate oxidase towards denaturing agents. *Eur. J. Biochem.* 190:491–495.

44. Rodriguez, J. A., J. S. Valentine, D. K. Eggers, J. A. Roe, A. Tiwari, R. H. Brown, Jr., and L. J. Hayward. 2002. Familial amyotrophic lateral sclerosis-associated mutations decrease the thermal stability of distinctly metallated species of human copper/zinc superoxide dismutase. *J. Biol. Chem.* 277:15932–15937.

45. Stockel, J., J. Safar, A. C. Wallace, F. E. Cohen, and S. B. Prusiner. 1998. Prion protein selectively binds copper(II) ions. *Biochemistry.* 37:7185–7193.

46. Sandberg, A., J. Leckner, Y. Shi, F. P. Schwarz, and B. G. Karlsson. 2002. Effects of metal ligation and oxygen on the reversibility of the thermal denaturation of *Pseudomonas aeruginosa* azurin. *Biochemistry.* 41:1060–1069.

47. Sandberg, A., D. J. Harrison, and B. G. Karlsson. 2003. Thermal denaturation of spinach plastocyanin: effect of copper site oxidation state and molecular oxygen. *Biochemistry.* 42:10301–10310.

48. Stirpe, A., L. Sportelli, and R. Guzzi. 2006. A comparative investigation of the thermal unfolding of pseudoazurin in the Cu(II)-holo and apo form. *Biopolymers.* 83:487–497.

49. Eakin, C. M., J. D. Knight, C. J. Morgan, M. A. Gelfand, and A. D. Miranker. 2002. Formation of a copper specific binding site in non-native states of beta-2-microglobulin. *Biochemistry.* 41:10646–10656.

FEBS Letters 581 (2007) 5065–5069

Macromolecular crowding increases structural content of folded proteins

Michael Perham[a,1], Loren Stagg[b,1], Pernilla Wittung-Stafshede[a,b,c,*]

[a] Department of Chemistry, Rice University, 6100 Main Street, Houston, TX 77251, United States
[b] Department of Biochemistry and Cell Biology, Rice University, 6100 Main Street, Houston, TX 77251, United States
[c] Keck Center for Structural Computational Biology, Rice University, 6100 Main Street, Houston, TX 77251, United States

Received 27 August 2007; revised 19 September 2007; accepted 20 September 2007

Available online 1 October 2007

Edited by Hans Eklund

Abstract Here we show that increased amount of secondary structure is acquired in the folded states of two structurally-different proteins (α-helical VlsE and α/β flavodoxin) in the presence of macromolecular crowding agents. The structural content of flavodoxin and VlsE is enhanced by 33% and 70%, respectively, in 400 mg/ml Ficoll 70 (pH 7, 20 °C) and correlates with higher protein-thermal stability. In the same Ficoll range, there are only small effects on the unfolded-state structures of the proteins. This is the first *in vitro* assessment of crowding effects on the *native-state* structures at physiological conditions. Our findings imply that for proteins with low intrinsic stability, the functional structures *in vivo* may differ from those observed in dilute buffers.

Keywords: Macromolecular crowding; Excluded volume effect; Circular dichroism; Secondary structure

1. Introduction

The intracellular environment is crowded due to the presence of high concentrations of macromolecules including proteins, nucleic acids, ribosomes, and carbohydrates [1]. This means that a significant fraction of the intracellular space is not available to other macromolecular species. It has been estimated that the concentration of macromolecules in the cytoplasm is in the range of 80–400 mg/ml [2,3] corresponding to a volume occupancy of up to 40%. Due to excluded volume effects, any reaction that amplifies the available volume will be stimulated by macromolecular crowding [4–7]. It is proposed that the major result of macromolecular crowding, or space confinement, is a stabilizing effect on the folded protein that originates in lowered entropy of the unfolded state because of polypeptide compaction. Experimental and theoretical work has demonstrated large effects of crowding on the thermodynamics and kinetics of many biological processes *in vitro*, including protein binding, folding, and aggregation [2,8–11].

Crowded conditions can be created experimentally by adding inert synthetic or natural macromolecules, termed crowding agents, to the systems *in vitro*. Experimental studies of crowding effects on folding have mostly involved large, complex proteins and often at extreme solvent conditions (such as acidic pH) [2,8,12,13]. A few studies have focused on the ability of crowding agents to induce conformational changes in unfolded states of proteins. For example, unfolded cytochrome *c* was found to adopt a molten globule state in crowding agents at low pH, [14] and two intrinsically unstructured proteins (FlgM and a variant of RNase T1) were discovered to fold in crowded conditions [15,16]. No *in vitro* studies have focused on the effects of macromolecular crowding agents on the folded structures of small, single-domain proteins at physiological conditions.

To address this issue, here we investigate the native- and unfolded-state structures of two model proteins (*Borrelia burgdorferi* VlsE and *Desulfovibrio desulfuricans* flavodoxin) as a function of macromolecular crowding *in vitro* (*i.e.*, using synthetic crowding agents). The two proteins were strategically selected to include contrasting folds and sizes: VlsE (341 residues) has 50% α-helices and the rest is mostly unstructured loops [17,18], whereas flavodoxin (148 residues) has a mixed α/β topology with a flavin mononucleotide (FMN) cofactor (Fig. 1) [19]. Both proteins have been characterized previously in our laboratory in terms of chemical and thermal unfolding behaviors in dilute solutions [17,20,21]; both proteins have rather low thermal (T_m of ~50 °C; pH 7) and thermodynamic (ΔG_U of 15–20 kJ/mol; pH 7, 20 °C) stabilities. Ficoll 70 (*i.e.*, a highly branched copolymer of sucrose and epichlorohydrin building blocks) and dextran 70 (*i.e.*, a flexible long-chain poly(D-glucose) with sparse and short branches) are polysaccharides that are inert, polar and do not interact with proteins. Ficoll behaves like a semi-rigid sphere (radius ~55 Å) whereas dextran is best modeled as a rod-like particle [22,23]. Both polymers are attractive mimics of macromolecules that may be present in the biological setting where proteins normally fold.

2. Materials and methods

Proteins were prepared as described [17,21]. Ficoll 70, dextran 70, polyethylene glycol (PEG1,450), GuHCl and urea (Sigma) were of highest purity; special care was taken to mix all solutions due to the high viscosity of some samples. Equilibration times (at 20 °C) were checked before measurements; 2–16 h were sometimes needed. Aggregation was not detected in these mixtures as assessed by manual inspection and by light scattering at 300 nm. Far-UV CD (Jasco J-810 instrument) was measured in a 1-mm cell (200–300 nm); 10 mM HEPES or phosphate buffer, pH 7, with/without GuHCl/urea as indicated. In most experiments, 20 μM flavodoxin or 10 μM VlsE was

*Corresponding author. Address: Department of Chemistry, Rice University, 6100 Main Street, Houston, TX 77251, United States.
E-mail address: pernilla@rice.edu (P. Wittung-Stafshede).

[1]These authors contributed equally to this work.

0014-5793/$32.00
doi:10.1016/j.febslet.2007.09.049

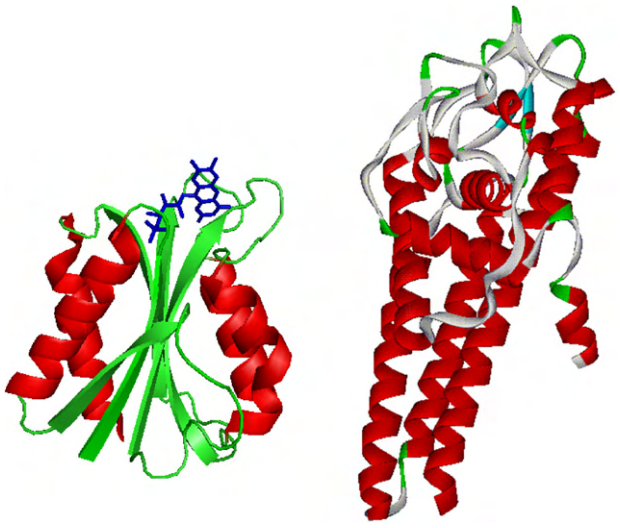

Fig. 1. Models of *Desulfovibrio vulgaris* flavodoxin (a. *D. desulfuricans* homolog, left) and *Borrelia burgdorferi* VlsE (right) based on the crystal structures 2fx2 and 1L8W. The FMN cofactor in flavodoxin is shown in stick; red corresponds to α-helices, green represents β-strands in flavodoxin and turns in VlsE.

used. Thermal unfolding experiments were probed by CD at 220 nm (20–95 °C; scan rate 1 deg/min) for samples of protein mixed with different fixed concentrations of Ficoll 70 or dextran 70 (in the range 0–400 mg/ml). Varying the scan rate between 0.5 and 2.5 deg/min did not change the profiles. The thermal unfolding reactions were not fully reversible: for both proteins, only 50–70% (depending on buffer conditions and amount of crowding agent) of the starting CD signal was recovered upon cooling. Thermal irreversibility has been noted earlier for flavodoxin [21].

3. Results

In Fig. 2A, we show the far-UV circular dichroism (CD) spectra of native flavodoxin in the presence of increasing amounts of Ficoll 70 (0–400 mg/ml; pH 7.0, 20 °C). It is clear that the negative far-UV CD signal grows larger, suggesting gain of secondary structure as a function of crowding. The negative signal at 220 nm increases by 24% in 200 mg/ml and by 33% at 400 mg/ml Ficoll 70. By contrast, in both 3 and 4 M GuHCl, denaturant conditions known to cause complete flavodoxin unfolding [20,21], there is no effect by the same Ficoll 70 additions (Fig. 2B). Thermally unfolded flavodoxin (at 95 °C, pH 7) displays minor changes in CD signal as a function of Ficoll 70 concentration albeit the spectral shape remains characteristic of that of unfolded polypeptides (Fig. 2C). We note that there was no contribution to the CD signal from the Ficoll 70 itself and no protein aggregation occurred in any of the solutions.

Similar effects on the folded (Table 1) and unfolded (not shown) states were obtained when dextran 70 was incubated with flavodoxin. Moreover, when the same Ficoll and dextran experiments were repeated with folded and unfolded forms of apoflavodoxin (*i.e.*, no FMN), again, the same trends were observed (not shown). Secondary structure estimations (using SOMCD neural network algorithm), based on the CD spectra

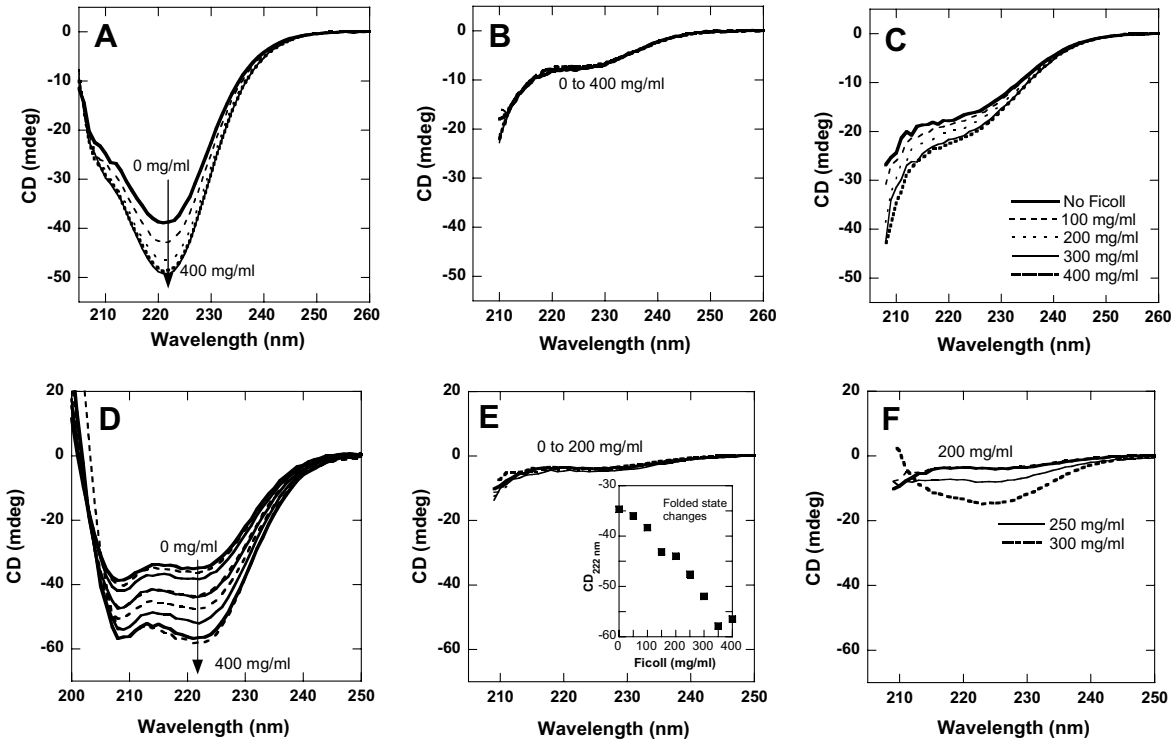

Fig. 2. Far-UV CD of (A) folded (pH 7, 20 °C), (B) chemically-unfolded (3 M GuHCl, 20 °C) and, (C) thermally-unfolded (95 °C) flavodoxin in the presence of various amounts of Ficoll 70 (0–400 mg/ml). Far-UV CD of (D) folded (pH 7, 20 °C) VlsE in the presence of various amounts of Ficoll 70 (0–400 mg/ml, 50 mg/ml increments) and, (E and F) chemically-unfolded (2.5 M urea, 20 °C) VlsE in the presence of various amounts of Ficoll 70 as indicated. Inset in E shows CD at 222 nm versus Ficoll 70 concentration for folded VlsE (*i.e.*, based on the spectra in D).

Table 1
Effects of different macromolecular crowding agents on the native-state structures of flavodoxin and VlsE (buffer, pH 7, 20 °C) as measured by far-UV CD

Protein	Agent	% change
Flavodoxin	Ficoll 70	24 ± 4
	Dextran 70	10 ± 3
	PEG 1,450	5 ± 2
	Glycerol	0 ± 3
VlsE	Ficoll 70	30 ± 3
	Dextran 70	33 ± 3
	PEG 1,450	20 ± 4
	Glycerol	0 ± 2

The percentages represent increases in negative CD signal at 220 nm (*i.e.*, 100% *CD(crowder)/CD(buffer) – 100%) when 200 mg/ml of crowding agent was added. The small osmolyte, glycerol, (known to stabilize proteins) was also tested as a control. Note that for Ficoll 70, the changes are found to be higher in 400 mg/ml (see text and Fig. 2A, D).

for folded flavodoxin at different conditions, revealed that the helical content increased while the random coil content decreased, with no change in β-sheet content, when going from 0 to 400 mg/ml Ficoll 70 (in buffer pH 7, 20 °C).

To test the generality of the observation, we performed the same experiments with another, structurally-different protein: the α-helical VlsE. Based on the increased negative far-UV CD signal, there is a dramatic build up of helical content in the native state of VlsE upon additions of Ficoll 70 (Fig. 2D). The negative CD signal at 220 nm increases approximately linearly with Ficoll concentration up to 400 mg/ml (Inset, Fig. 2E). Structural estimates using the SOMCD algorithm disclosed that the helix content rises from 52% to 80% when going from 0 to 400 mg/ml Ficoll 70 (in buffer pH 7, 20 °C). Again, at denaturant conditions causing complete VlsE unfolding (2.5 M urea, pH 7, 20 °C) [17], there is no effect on the CD spectra for Ficoll 70 additions up to 200 mg/ml (Fig. 2E). However, at 250 and 300 mg/ml Ficoll 70, a distinct non-native form of VlsE appears (Fig. 2F) exhibiting a negative far-UV CD peak centered at 220–225 nm, in agreement with β-sheet/turn content [24]. Interestingly, this species resembles a non-native state of VlsE detected in high concentrations of alcohols [25]. We previously proposed that this conformation may be biologically significant as alcohols mimic dielectric properties of the environment near membranes. Like in the case of flavodoxin, dextran 70 had similar effects on the native-state conformation of VlsE as Ficoll 70 (Table 1).

Since excluded-volume theory predicts that protein stability is enhanced by crowding, we tested if the structural effects observed on the native states correlated with increased thermal stability. In Fig. 3 we show thermal profiles, as monitored by far-UV CD, for flavodoxin as a function of increasing amounts of Ficoll 70 (A) and dextran 70 (B). As expected, both macromolecular crowding agents have stabilizing effects on flavodoxin. The thermal midpoint, T_m, increases gradually from 48 °C with no crowder (pH 7, HEPES buffer) to 64 °C in 400 mg/ml of Ficoll 70, and to 70 °C in 400 mg/ml of dextran 70 (pH 7). Analogously VlsE was found to gradually shift its thermal midpoint from 49 to 55 °C when the Ficoll 70 concentration was increased stepwise from 0 to 400 mg/ml (Fig. 3C). We note that the thermal transitions were only partially reversible (probed by the return of the native-like CD signal).

4. Discussion

This is the first assessment of protein native-state structural effects by macromolecular crowding in solution at physiological pH. Surprisingly, we discovered that for two unrelated single-domain proteins (Fig. 1), their folded states become more ordered, in terms of secondary-structure content, in the presence of crowding agents (*i.e.*, spherical Ficoll 70 and rod-shaped dextran 70) (Fig. 2; Table 1). These effects on the native-state conformations correlate with increased thermal stability in both proteins (Fig. 3). Our findings imply that the crowded cellular environment can have conformational effects on the *folded* states of proteins. Since the same results are obtained for two unrelated proteins with different folds, we propose that this may be a general phenomenon for small, single-domain proteins *in vivo*. In support of this idea, an increased structural content in the native state of a third, unrelated protein, *Pseudomonas aeruginosa* azurin was also detected (not shown). It is possible that observed differences between NMR-solution and crystallographic structures of proteins [26,27] are due to macromolecular crowding effects (due to the close packing of identical proteins) in the crystals. Clearly, there are parallels between high-volume occupancy

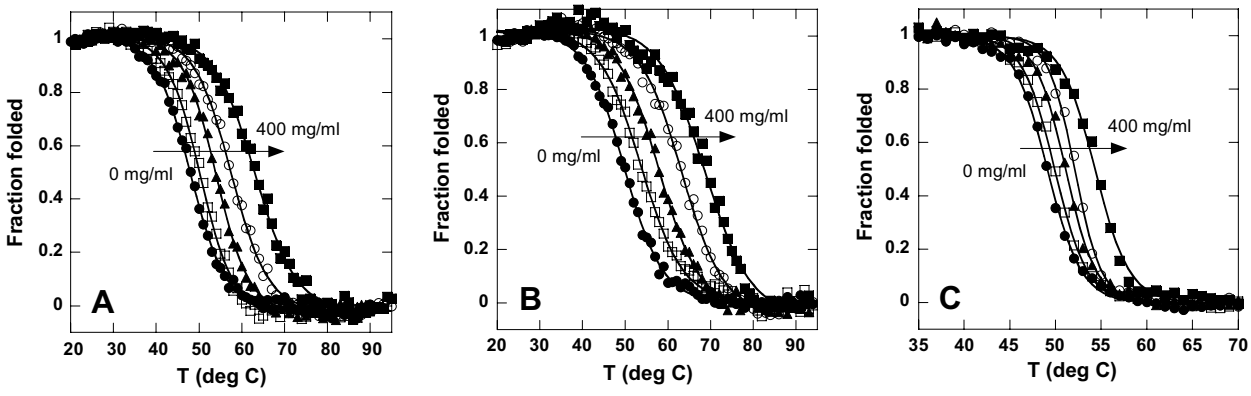

Fig. 3. Thermal profiles for flavodoxin (CD at 220 nm) as a function of Ficoll 70 (A) and dextran 70 (B) amounts (pH 7, 10 mM HEPES). (C) Thermal profiles for VlsE as a function of Ficoll 70 amounts (pH 7, 20 mM phosphate). Filled circles, no crowder; open squares, 100 mg/ml; filled triangles, 200 mg/ml; open circles, 400 mg/ml; filled squares, 400 mg/ml of crowder. Solid lines are two-state fits to the data points. In accord with a two-state mechanism for VlsE, CD-detected transitions match fluorescence-detected curves at each condition (fluorescence data shown).

of macromolecular-crowding agents in solution and close packing of proteins in crystalline states.

Since Ficoll 70 and dextran 70 are both sugar-based polymers, we also tested the effect of a chemically-different crowding agent, *i.e.*, polyethylene glycol (PEG 1,450). PEG is best modeled as a spherical particle. We found that the native-state structures of flavodoxin and VlsE were similarly perturbed in the presence of PEG, as in the presence of Ficoll and dextran (Table 1). However, the extent of the change (as measured by CD) was less with PEG. This may be due to the smaller size of the PEG variant we used as compared to the sugar-based polymers (MW of 1450 for PEG versus 70,000 for Ficoll and dextran). The excluded-volume theory implies that macromolecular crowding affects the unfolded states of proteins, thereby indirectly making the folded states more stable [4–7]. Although this theory states that changes in protein stability are due mostly to unfavorable effects on the unfolded-state ensemble, direct effects on the folded state is not excluded [28,29]. Thus, our findings are not in direct disparity with excluded-volume theory but they clearly emphasize that structural perturbations on the native state should be given deeper consideration in future experiments and theoretical models.

Analogously to our results presented here, upon encapsulation in a silica gel with hydrophobic modifications, apo-myoglobin acquired a higher helical content than that found for the folded state in solution [30]. In earlier studies of unfolded apo-myoglobin in different sol–gel systems, it was proposed that its ability to fold was influenced by the properties of confined water molecules in the silica pores [31,32]. The effect of water on hydrophobic and ionic interactions in small molecules confined in water droplets [33] as well as on protein-conformational changes in confined spaces [34,35] have recently been addressed. We speculate that interactions with confined water molecules, in combination with other factors, play a role in the formation of the non-native VlsE species observed in high amounts of Ficoll at denaturing conditions (Fig. 2F). We note that VlsE was found as a dimer in the crystal structure and at some solution conditions [18,36]; therefore, we probed the possibility of VlsE dimers at our crowded conditions *in vitro*. Based on cross-linking experiments, we conclude that a fraction (20–30%) of VlsE dimers may exist at high Ficoll 70 amounts (*i.e.*, 300–400 mg/ml) whereas only monomers (>95%) are detected in buffer and at low Ficoll amounts (*i.e.*, 100–200 mg/ml). Since the dimer and monomer forms of VlsE have about the same amount of α-helices [18,36], dimer formation does not explain the increased structural content in the presence of crowding agents.

We propose that crowded conditions cause enrichment of a subset of protein structures, within the folded ensemble of species, which are most ordered. Extension of α-helices may be the dominant consequence of macromolecular crowding as the random coil-to-helix process can be viewed as a simple one-dimensional phase transition [37]. This agrees with our observations of non-cooperative, gradual changes in protein structure as a function of Ficoll 70 concentration (*e.g.* inset, Fig. 2E). As β-sheets involve long-range interactions, their formation will require cooperativity and spatial precision. Notably, all proteins studied here, and previous ones found to fold in crowded conditions [15,16,30], contain some helical elements. In addition, for both VlsE and flavodoxin, the structural effects found in Ficoll/dextran correspond to increases in α-helix, and not β-sheet, content as based on CD spectra predictions.

In an attempt to correlate the native-state structural effects to thermodynamics, the thermal-unfolding data in Fig. 3 was analyzed. Since thermal unfolding of flavodoxin is non-two-state [21], two-state analysis of the curves is not valid. Instead, we measured the calorimetric enthalpy change for flavodoxin unfolding in buffer (using differential scanning calorimetry; $\Delta H_{cal} = 275 \pm 20$ kJ/mol) and, together with the ΔT_m values from the CD measurements at various crowded conditions, change in protein stability (ΔG_U) was derived as described in Eq. (20) in [38]. For the largest ΔT_m (*i.e.*, in 400 mg/ml dextran 70), the estimated increase in ΔG_U is ~16 kJ/mol. In contrast, VlsE unfolding is two-state and the enthalpy change was obtained using van't Hoff equation [38] and the thermal profile in buffer ($\Delta H_{vH} = 460 \pm 15$ kJ/mol). Using this value and the ΔT_m for VlsE in 400 mg/ml Ficoll 70, we estimated an increase in ΔG_U of ~9 kJ/mol. Thus, both proteins appear to be substantially stabilized in the presence of crowding agents. We note that further thermodynamic analysis is not reliable since the reactions in high Ficoll concentrations are not reversible and, for VlsE, the protein adopts a non-native state.

In conclusion, our findings propose that 'native' states of proteins (at least for small proteins with marginal stability) *in vivo* and *in vitro* may differ: there appears to be 'room for improvement', *e.g.* tightening of loops and helix extensions, depending on the surrounding solute environment. Future studies using other detection methods (*e.g.* NMR), to pinpoint the location of the structural changes in the sequence, as well as correlations with protein activity will be of high interest.

Acknowledgements: Support for this project was provided by the Robert A. Welch Foundation (C-1588) and the USAMRAA (W81XWH-06-1-0572). M.P. is supported by the NIH Training Grant Houston Area Molecular Biophysics Program (HAMBP) (T32 GM008280).

References

[1] Ellis, R.J. (2001) Macromolecular crowding: obvious but underappreciated. Trends Biochem. Sci. 26, 597–604.
[2] van den Berg, B., Ellis, R.J. and Dobson, C.M. (1999) Effects of macromolecular crowding on protein folding and aggregation. EMBO J. 18, 6927–6933.
[3] Rivas, G., Ferrone, F. and Herzfeld, J. (2004) Life in a crowded world. EMBO Rep. 5, 23–27.
[4] Zimmerman, S.B. and Minton, A.P. (1993) Macromolecular crowding: biochemical, biophysical, and physiological consequences. Annu. Rev. Biophys. Biomol. Struct. 22, 27–65.
[5] Minton, A.P. (2005) Models for excluded volume interaction between an unfolded protein and rigid macromolecular cosolutes: macromolecular crowding and protein stability revisited. Biophys. J. 88, 971–985.
[6] Minton, A.P. (2005) Influence of macromolecular crowding upon the stability and state of association of proteins: predictions and observations. J. Pharm. Sci. 94, 1668–1675.
[7] Zhou, H.X. (2004) Protein folding and binding in confined spaces and in crowded solutions. J. Mol. Recognit. 17, 368–375.
[8] van den Berg, B., Wain, R., Dobson, C.M. and Ellis, R.J. (2000) Macromolecular crowding perturbs protein refolding kinetics: implications for folding inside the cell. EMBO. J. 19, 3870–3875.
[9] Uversky, V.N.E.M.C., Bower, K.S., Li, J. and Fink, A.L. (2002) Accelerated alpha-synuclein fibrillation in crowded milieu. FEBS Lett. 515, 99–103.
[10] Cheung, M.S., Klimov, D. and Thirumalai, D. (2005) Molecular crowding enhances native state stability and refolding rates of globular proteins. Proc. Natl. Acad. Sci. USA 102, 4753–4758.

[11] Ai, X., Zhou, Z., Bai, Y. and Choy, W.Y. (2006) 15N NMR spin relaxation dispersion study of the molecular crowding effects on protein folding under native conditions. J. Am. Chem. Soc. 128, 3916–3917.
[12] Zhou, B.R., Liang, Y., Du, F., Zhou, Z. and Chen, J. (2004) Mixed macromolecular crowding accelerates the oxidative refolding of reduced, denatured lysozyme: implications for protein folding in intracellular environments. J. Biol. Chem. 279, 55109–55116.
[13] Galan, A., Sot, B., Llorca, O., Carrascosa, J.L., Valpuesta, J.M. and Muga, A. (2001) Excluded volume effects on the refolding and assembly of an oligomeric protein. GroEL, a case study. J. Biol. Chem. 276, 957–964.
[14] Sasahara, K., McPhie, P. and Minton, A.P. (2003) Effect of dextran on protein stability and conformation attributed to macromolecular crowding. J. Mol. Biol. 326, 1227–1237.
[15] Qu, Y. and Bolen, D.W. (2002) Efficacy of macromolecular crowding in forcing proteins to fold. Biophys. Chem. 101–102, 155–165.
[16] Dedmon, M.M., Patel, C.N., Young, G.B. and Pielak, G.J. (2002) FlgM gains structure in living cells. Proc. Natl. Acad. Sci. USA 99, 12681–12684.
[17] Jones, K. and Wittung-Stafshede, P. (2003) The largest protein observed to fold by two-state kinetic mechanism does not obey contact-order correlation. J. Am. Chem. Soc. 125, 9606–9607.
[18] Eicken, C., Sharma, V., Klabunde, T., Lawrenz, M.B., Hardham, J.M., Norris, S.J. and Sacchettini, J.C. (2002) Crystal structure of Lyme disease variable surface antigen VlsE of Borrelia burgdorferi. J. Biol. Chem. 28, 28.
[19] Steensma, E. and van Mierlo, C.P. (1998) Structural characterisation of apoflavodoxin shows that the location of the stable nucleus differs among proteins with a flavodoxin-like topology. J. Mol. Biol. 282, 653–666.
[20] Muralidhara, B.K., Chen, M., Ma, J. and Wittung-Stafshede, P. (2005) Effect of inorganic phosphate on FMN binding and loop flexibility in *Desulfovibrio desulfuricans* apo-flavodoxin. J. Mol. Biol. 349, 87–97.
[21] Muralidhara, B.K. and Wittung-Stafshede, P. (2004) Thermal unfolding of apo and holo *Desulfovibrio desulfuricans* flavodoxin: cofactor stabilizes folded and intermediate states. Biochemistry 43, 12855–12864.
[22] Luby-Phelps, K., Castle, P.E., Taylor, D.L. and Lanni, F. (1987) Hindered diffusion of inert tracer particles in the cytoplasm of mouse 3T3 cells. Proc. Natl. Acad. Sci. USA 84, 4910–4913.
[23] Venturoli, D. and Rippe, B. (2005) Ficoll and dextran vs. globular proteins as probes for testing glomerular permselectivity: effects of molecular size, shape, charge, and deformability. Am. J. Physiol. Renal. Physiol. 288, F605–F613.
[24] Manning, M.C., Illangasekare, M. and Woody, R.W. (1988) Circular dichroism studies of distorted alpha-helices, twisted beta-sheets, and beta turns. Biophys. Chem. 31, 77–86.
[25] Perham, M., Liao, J. and Wittung-Stafshede, P. (2006) Differential effects of alcohols on conformational switchovers in alpha-helical and beta-sheet protein models. Biochemistry 45, 7740–7749.
[26] Li, A. and Daggett, V. (1995) Investigation of the solution structure of chymotrypsin inhibitor 2 using molecular dynamics: comparison to x-ray crystallographic and NMR data. Protein Eng. 8, 1117–1128.
[27] Philippopoulos, M. and Lim, C. (1999) Exploring the dynamic information content of a protein NMR structure: comparison of a molecular dynamics simulation with the NMR and X-ray structures of *Escherichia coli* ribonuclease HI. Proteins 36, 87–110.
[28] Minton, A.P. (2000) Effect of a concentrated''inert'' macromolecular cosolute on the stability of a globular protein with respect to denaturation by heat and by chaotropes: a statistical-thermodynamic model. Biophys. J. 78, 101–109.
[29] Hall, D. and Minton, A.P. (2003) Macromolecular crowding: qualitative and semiquantitative successes, quantitative challenges. Biochim. Biophys. Acta 1649, 127–139.
[30] Rocha, V.A. and Eggers, D.K. (2007) Hydrophobic, organically-modified silica gels enhance the secondary structure of encapsulated apomyoglobin. Chem. Commun. (Camb.), 1266–1268.
[31] Eggers, D.K. and Valentine, J.S. (2001) Crowding and hydration effects on protein conformation: a study with sol–gel encapsulated proteins. J. Mol. Biol. 314, 911–922.
[32] Eggers, D.K. and Valentine, J.S. (2001) Molecular confinement influences protein structure and enhances thermal protein stability. Protein Sci. 10, 250–261.
[33] Vaitheeswaran, S. and Thirumalai, D. (2006) Hydrophobic and ionic interactions in nanosized water droplets. J. Am. Chem. Soc. 128, 13490–13496.
[34] Lucent, D., Vishal, V. and Pande, V.S. (2007) Protein folding under confinement: a role for solvent. Proc. Natl. Acad. Sci. USA.
[35] Cheung, J.K. and Truskett, T.M. (2005) Coarse-grained strategy for modeling protein stability in concentrated solutions. Biophys. J. 89, 2372–2384.
[36] Jones, K., Guidry, J. and Wittung-Stafshede, P. (2001) Characterization of surface antigen from Lyme disease spirochete *Borrelia burgdorferi*. Biochem. Biophys. Res. Commun. 289, 389–394.
[37] Finkelstein, A.V. and Ptitsyn, O.B. (2002) Protein Physics, Academic Press.
[38] Becktel, W.J. and Schellman, J.A. (1987) Protein stability curves. Biopolymers 26, 1859–1877.

Molecular crowding enhances native structure and stability of α/β protein flavodoxin

Loren Stagg*, Shao-Qing Zhang†, Margaret S. Cheung†, and Pernilla Wittung-Stafshede*‡§¶

Departments of *Biochemistry and Cell Biology and ‡Chemistry, §Keck Center for Structural Computational Biology, Rice University, Houston, TX 77251; and †Department of Physics, University of Houston, Houston, TX 77204

Edited by José N. Onuchic, University of California at San Diego, La Jolla, CA, and approved October 15, 2007 (received for review May 31, 2007)

To investigate the consequences of macromolecular crowding on the behavior of a globular protein, we performed a combined experimental and computational study on the 148-residue single-domain α/β protein, *Desulfovibrio desulfuricans* apoflavodoxin. *In vitro* thermal unfolding experiments, as well as assessment of native and denatured structures, were probed by using far-UV CD in the presence of various amounts of Ficoll 70, an inert spherical crowding agent. Ficoll 70 has a concentration-dependent effect on the thermal stability of apoflavodoxin (ΔT_m of 20°C at 400 mg/ml; pH 7). As judged by CD, addition of Ficoll 70 causes an increase in the amount of secondary structure in the native-state ensemble (pH 7, 20°C) but only minor effects on the denatured state. Theoretical calculations, based on an off-lattice model and hard-sphere particles, are in good agreement with the *in vitro* data. The simulations demonstrate that, in the presence of 25% volume occupancy of spheres, native flavodoxin is thermally stabilized, and the free energy landscape shifts to favor more compact structures in both native and denatured states. The difference contact map reveals that the native-state compaction originates in stronger interactions between the helices and the central β-sheet, as well as by less fraying in the terminal helices. This study demonstrates that macromolecular crowding has structural effects on the folded ensemble of polypeptides.

energy landscape theory | excluded volume effect | molecular simulations | protein folding

Protein folding *in vitro* has been extensively characterized in dilute conditions. However, the intracellular environment is highly crowded because of the presence of large amounts of soluble and insoluble macromolecules, including proteins, nucleic acids, ribosomes, and carbohydrates. This means that a significant fraction of the intracellular space is not available to other macromolecular species. It has been estimated that the concentration of macromolecules in the cytoplasm is in the range of 80–400 mg/ml (1, 2). All macromolecules in physiological fluids collectively occupy between 10% and 40% of the total fluid volume (3, 4). The term "macromolecular crowding" implies the nonspecific influence of steric repulsions on specific reactions that occur in highly volume-occupied media. Because of excluded volume effects, any reaction that amplifies the available volume will be stimulated by macromolecular crowding (5–8). It is proposed that crowding provides a stabilizing effect to the folded protein indirectly because of compaction of the denatured states. Crowding can be mimicked experimentally by adding high concentrations of inert synthetic or natural macromolecules, termed crowding agents, to the systems *in vitro*. Experimental and theoretical work has demonstrated large effects of crowding on the thermodynamics and kinetics of many biological processes, including protein binding, folding, and aggregation (1, 9–12).

Whereas theoretical simulations have focused on very small proteins or peptides (11), experimental crowding studies have mostly involved large complex proteins (i.e., multidomain and/or disulfide containing) and often extreme solvent conditions (such as acidic pH). For example, the effects of crowding agents on the refolding of reduced denatured lysozyme (1, 9), oligomerization of GroEL subunits (13), self-assembly of the cell division protein FtsZ (14) and the capsid protein of HIV (15), and amyloid formation of the human apolipoprotein C-II (16) have been reported. A few studies have focused on the ability of crowding agents to induce conformational changes in unfolded states of proteins (17, 18). For example, it was shown that unfolded cytochrome *c* adopts a molten globule state in the presence of crowding agents at low pH (19). Notably, there are no detailed studies of the effects of macromolecular crowding on the behavior of small single-domain proteins that fold with simple mechanisms in dilute solutions.

To fill this gap, we have combined experimental and theoretical approaches to carefully assess the native and denatured structural ensembles, as well as the thermal stability, of a well behaved α/β model protein (i.e., apoflavodoxin) as a function of concentration of an inert spherical macromolecular crowding agent (i.e., Ficoll 70). Our *in vitro* and *in silico* results are in excellent agreement and demonstrate that crowding increases protein-thermal stability via structural enhancement in both the folded and denatured ensembles of molecules.

Results

Choice of Protein and Crowding Agent. The model system, *Desulfovibrio desulfuricans* flavodoxin (Fig. 1*A*), was selected because it is a small α/β protein (148 residues) with a common fold (i.e., the flavodoxin-like fold) in which a central β-sheet is surrounded by four helices (20–22). This protein has been extensively characterized previously in our laboratory in terms of its chemical and thermal unfolding behaviors in dilute solutions (23–27). It unfolds in an apparent two-state reaction upon chemical and thermal perturbations when monitored by far-UV CD. To be able to match with simulations, flavodoxin devoid of the FMN cofactor, i.e., apoflavodoxin, is used in all work herein. Apoflavodoxin has the same folded structure as with the cofactor; it exhibits a rather modest stability (≈15 kJ/mol, pH 7) at room temperature, indicating there is span for possible improvement because of crowding effects. The crowding agent selected for this work is Ficoll 70. This agent has many advantages; it is a polysaccharide (i.e., sucrose epichlorohydrin copolymer; average molecular mass of 74 kDa) that is inert, polar, and does not interact with proteins. It behaves like a semirigid sphere (radius of ≈55 Å) (28, 29); thus it is an attractive mimic of globular macromolecules that may be present in the biological setting where proteins normally fold. In addition, it can readily be

Author contributions: M.S.C. and P.W.-S. designed research; L.S. and S.-Q.Z. performed research; L.S., S.-Q.Z., M.S.C., and P.W.-S. analyzed data; and M.S.C. and P.W.-S. wrote the paper.

The authors declare no conflict of interest.

This article is a PNAS Direct Submission.

¶To whom correspondence should be addressed. E-mail: pernilla@rice.edu.

This article contains supporting information online at www.pnas.org/cgi/content/full/0705127104/DC1.

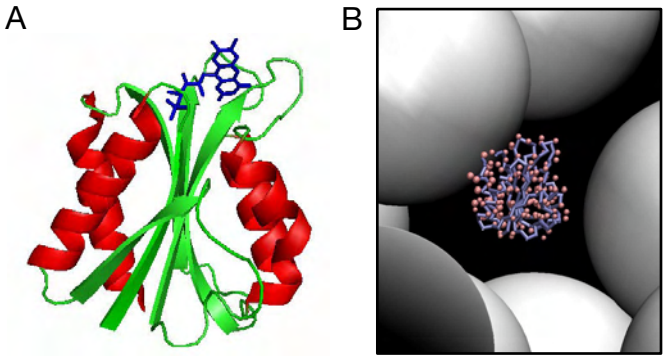

Fig. 1. Protein system used in this study. (*A*) Model of *D. vulgaris* flavodoxin (2fx2). The sequence of *D. desulfuricans* flavodoxin, used in our *in vitro* experiments, is 46% identical to that of *D. vulgaris*. Green, β-sheets and loops; red, α-helices; blue, FMN cofactor (removed in our experiments). (*B*) Snapshot of apoflavodoxin and hard spheres of the size of Ficoll 70 (volume fraction = 25%) as used in the simulations.

represented in computer simulations as repulsive hard spheres of the appropriate size (Fig. 1*B*; for volume occupancy, ϕ_c, of 25%).

Ficoll 70 Increases Protein Thermal Stability *in Vitro*. Far-UV CD at 222 nm was used to probe thermal unfolding of apoflavodoxin as a function of increasing Ficoll 70 concentrations (0–400 mg/ml, pH 7). All reactions appear as single cooperative transitions and are 70–80% reversible; in addition, there is no scan-rate dependence in accord with equilibrated reactions. As demonstrated in Fig. 2*A*, the presence of Ficoll 70 has a dramatic effect on apoflavodoxin thermal stability. The more Ficoll 70 is present in the samples, the higher the thermal midpoint (T_m) for apoflavodoxin. In fact, T_m increases from 45°C to 65°C, going from 0 to 400 mg/ml Ficoll 70 in Hepes buffer, pH 7 (Table 1).

Apoflavodoxin is sensitive to buffer composition. For example, the protein is thermodynamically more stable in phosphate than in Hepes buffer (23). We found that by changing only the buffer conditions, the T_m value for apoflavodoxin can shift as much as 25°C (i.e., comparing phosphate plus salt vs. Hepes buffers at pH 7). This implies that population shifts within the native-state ensemble are possible and, moreover, that this ensemble contains a distribution of molecules with slightly different thermodynamic properties (30, 31). Nonetheless, the addition of Ficoll 70 always has a stabilizing effect on apoflavodoxin thermal stability, albeit the magnitude depends on the buffer choice (Table 1). The lower the protein stability without crowding agent in a particular buffer, the larger the stabilizing effect due to Ficoll 70 (Fig. 2*B*).

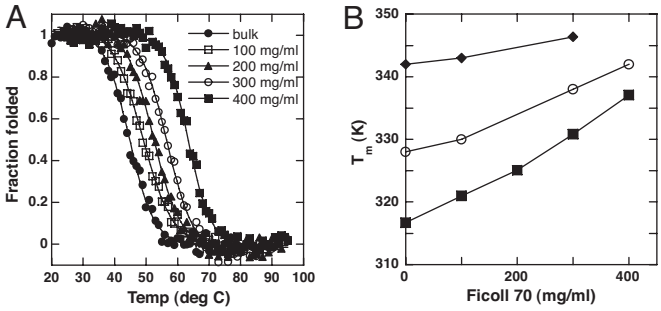

Fig. 2. *In vitro* thermal stability as a function of crowding agent. (*A*) Thermal unfolding curves for apoflavodoxin probed by far-UV CD in the presence of various amounts of Ficoll 70. (*B*) T_m vs. Ficoll 70 concentrations for apoflavodoxin in three different buffer conditions (squares, 10 mM Hepes; circles, 20 mM phosphate; diamonds, 40 mM phosphate plus 250 mM NaCl, all at pH 7).

Table 1. T_m values (in kelvin) for apo-flavodoxin unfolding in different buffers (pH 7) combined with different amounts of Ficoll 70, as indicated

Buffer	Bulk	100 mg/ml	200 mg/ml	300 mg/ml	400 mg/ml
Hepes	317 ± 1	321 ± 1	325 ± 1	331 ± 1	337 ± 1
Phosphate	328 ± 1	330 ± 1	—	338 ± 1	341 ± 1
Phosphate + NaCl	342 ± 1	343 ± 1	—	346 ± 1	—
Simulation	365	372 (volume occupancy of 25%)			

The experimental midpoints were derived from CD-detected unfolding curves. All transitions were >80% reversible.

Structural Effects on Native State by Ficoll 70. In Fig. 3*A*, we show the far-UV CD spectra of native apoflavodoxin in the presence of increasing amounts of Ficoll 70 (0–400 mg/ml; pH 7.0, 20°C). Unexpectedly, we find that the negative far-UV CD signal grows larger, suggesting gain of secondary structure, as a function of added crowding agent. The negative signal at 222 nm is raised by ≈10% in 200 mg/ml and by ≈15% at 400 mg/ml Ficoll 70. Thermally denatured apoflavodoxin (at 95°C, pH 7) also displays changes in the CD signal as a function of Ficoll 70 concentration, but the spectral shape remains characteristic of that of unfolded polypeptides (Fig. 2*B*). For comparison, we also collected CD spectra of apoflavodoxin unfolded in 3 M guanidine hydrochloride (GuHCl) as a function of Ficoll 70 additions (at pH 7, 20°C). As seen in Fig. 3*C*, the addition of Ficoll (up to 250 mg/ml tested) to the chemically denatured protein has no major effect on secondary structure content.

Secondary structure estimations based on the far-UV CD spectra of folded flavodoxin (using the SOMCD neural network algorithm, http://geneura.ugr.es/cgi-bin/somcd/index.cgi) reveal that the helical content rises up to 20%, whereas the random coil contribution shrinks >10% when going from 0 to 400 mg/ml Ficoll 70 conditions (in buffer pH 7, 20°C). In the crystal structure of *Desulfovibrio vulgaris* flavodoxin (i.e., 2fx2, the closest structural homolog to *D. desulfuricans* flavodoxin in the Protein Data Bank), the protein has ≈37% helix, ≈29% β-sheet, and ≈34% random coil; interestingly, this composition is very similar to that estimated for our apoflavodoxin in 400 mg/ml Ficoll 70. Thus, with Ficoll 70, the mean of the native-state ensemble distribution in solution shifts toward a structure that is similar to that in the crystals. We note that when the same Ficoll 70 titrations were repeated with folded and unfolded forms of holoflavodoxin (i.e., with FMN bound), similar trends as for the apoform were observed (data not shown). In addition, we found that another crowding agent, Dextran 70 (a glucose polymer that adopts a rod-shape structure), also induces additional structure in folded flavodoxin (data not shown).

Simulated Effects of Crowding Matches *in Vitro* Data. To assess the effects of macromolecular crowding on apoflavodoxin from a theoretical view, we computed thermodynamic properties and simulated the free-energy landscape for apoflavodoxin at different temperatures, with and without hard-sphere Ficoll 70 particles at a volume occupancy of ϕ_c = 25% (scenario depicted in Fig. 1*B*). The folding transition temperature was calculated from the temperature dependence of the Q parameter to be 365 K without crowder. As in the *in vitro* experiments, apoflavodoxin unfolds in a single thermal transition *in silico* that is shifted to higher temperatures (i.e., T_m of 372 K) at ϕ_c = 25% (data not shown). The stabilizing effect and the relative change in T_m value

BIOPHYSICS

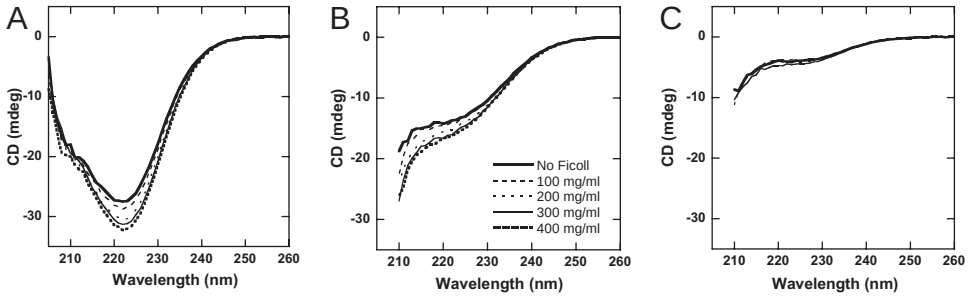

Fig. 3. *In vitro* structural effects due to macromolecular crowding. Far-UV CD of (*A*) folded (pH 7, 20°C), (*B*) thermally unfolded (pH 7, 95°C), and (*C*) chemically unfolded (3 M GuHCl, pH 7, 20°C) flavodoxin in the presence of various amounts of Ficoll 70 (key for all in *B*).

due to the presence of crowders agree well between *in silico* and *in vitro* data (Table 1).

The trend of enhanced native-like structure in the presence of crowders is seen from 1D energy profiles, F as a function of Q, at a temperature close to the folding transition [supporting information (SI) Fig. 7]. The shifts in the minimum of the folded state, from $Q = 0.76$ (for bulk) to $Q = 0.80$ ($\phi_c = 25\%$) and $Q = 0.82$ ($\phi_c = 40\%$), indicate augmentation of native-like structures in the folded ensemble in the presence of crowders. This type of native-state change was not observed in the previous investigation of the WW domain (11). This difference may be due to the fact that flavodoxin is longer (148 residues) and contains more complex secondary and tertiary structures than the WW domain (34 residues).

In Fig. 4, we show the resulting 2D energy landscapes for apoflavodoxin as a function of radius of gyration, R_g, and fraction of native contacts, Q, at $T = 360$ K for bulk (Fig. 4*A*) and $\phi_c = 25\%$ (Fig. 4*B*) crowding conditions. Comparing Fig. 4 *A* with *B*, it is clear that the shape of the energy landscape shifts toward the low R_g region in the presence of crowder. The ensemble structures of apoflavodoxin become more compact (i.e., R_g decreases) when crowders are added. Notably, this is apparent for both the unfolded and the native-state ensembles. For the native-state ensemble, the average R_g is $4.052 \pm 0.001\sigma$ ($\sigma = 3.8$ Å) for bulk conditions and $4.039 \pm 0.001\sigma$ for $\phi_c = 25\%$ conditions. Interestingly, despite the reduction in size of the native-state ensemble in the presence of crowders, the shape parameters remain the same in both cases (for bulk, $\Delta = 0.035 \pm 0.001$ and $S = -0.011 \pm 0.001$; for $\phi_c = 25\%$, $\Delta = 0.036 \pm 0.001$ and $S = -0.011 \pm 0.001$). This observation demonstrates that the effects on protein compaction due to crowding are isotropic.

To reveal the molecular origin of the crowding-induced protein compaction and increased structural content, we derived difference contact maps of the folded states of apoflavodoxin between the $\phi_c = 25\%$ and the bulk conditions (Fig. 5*A*). The same difference contact map was created between the two denatured states (Fig. 5*B*). Inspection of these maps reveal that the compaction of folded flavodoxin stems from improved interactions between the surrounding helices and the core β-sheet, as well as from less helix fraying in the terminal helices. Because helical contacts are stable in both bulk and crowded cases, these contacts do not show much of a color change in the difference map, although it is possible that the helices become more rigid in the presence of crowding agents. The extension of helices agrees well with the far-UV CD data that implied more α-helical content in folded apoflavodoxin at crowded conditions. In contrast, in the denatured state, crowding appears only to promote some native contacts between residue regions 70–90 (helix 2/loop region in folded protein) and 40–60 (loop/β-strand region in folded protein) (Fig. 5*B*). From an overall perspective, structural fluctuations in the native state, as measured by the rmsd for each residue, are diminished by a factor of 2 in the presence of crowders at $\phi_c = 25\%$ (SI Fig. 8).

Discussion

This is a combined experimental/computational study elucidating the effects of molecular crowding on thermal and structural properties of a small single-domain globular α/β protein (i.e., 148-residue apoflavodoxin). Earlier experimental work has focused on the effects of crowding on kinetic refolding of complex proteins and on protein nonnative states at extreme conditions, whereas theoretical approaches have instead involved simple lattice models or small peptide systems (1, 9–12).

An equilibrium statistical-thermodynamic model, developed primarily by A. P. Minton (32), predicts that macromolecular crowding should increase protein thermal stability (T_m) by a magnitude of ≈5–20°C at physiological solute conditions. However, there have been few experimental verifications of this prediction. The reason is likely that many proteins unfold irreversibly and aggregate in the presence of high concentrations of crowding agents. The (irreversible) thermal midpoint for G-actin was found to increase by 5°C in the presence of 100 mg/ml PEG (33); the presence of 300 mg/ml dextran had a 3°C favorable effect on lysozyme thermal stability at pH 2 (19), and the presence of 370 mg/ml dextran raised T_m by 3.5°C for cytochrome *c* (34). In contrast to these modest effects, but in agreement with the prediction, we discovered that Ficoll 70 dramatically enhances apoflavodoxin (reversible) thermal stability: stabilizing effects of up to 20°C were observed *in vitro*. Notably, the stabilizing effect on apoflavodoxin due to crowding is similar to that observed for α-lactalbumin when placed in pores of silica glass (35, 36).

The excluded-volume theory implies that macromolecular crowding acts on unfolded-state conformations. By making the

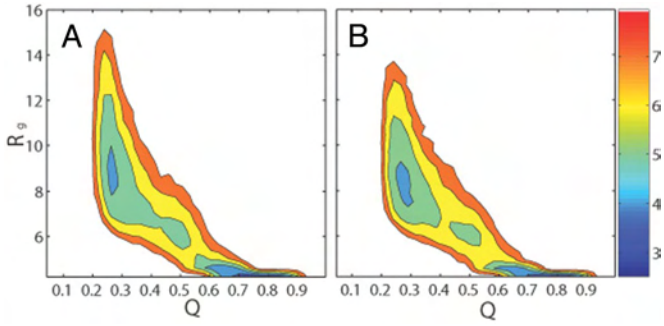

Fig. 4. *In silico* energy landscapes for apoflavodoxin with and without crowding. The 2D free-energy landscape as a function of R_g and Q at $T = 360$ K at volume fractions of crowder of zero (i.e., bulk) (*A*) and 25% (*B*). R_g is the radius of gyration in unit of σ ($\sigma = 3.8$ Å). Q is the fraction of native contacts. The color is scaled by k_BT.

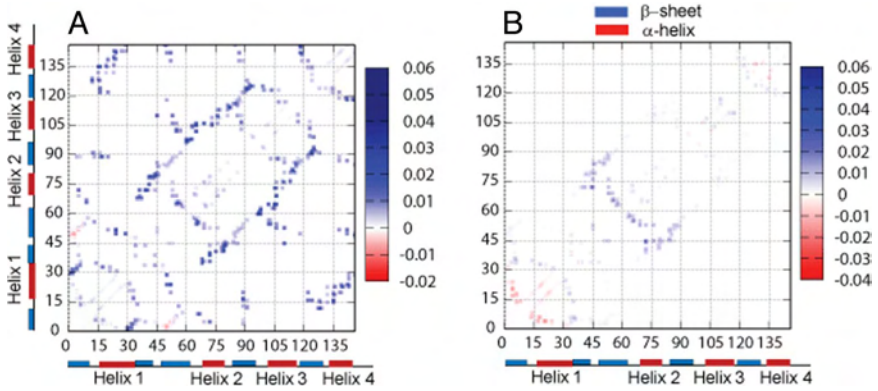

Fig. 5. Mapping of *in silico* structural changes due to crowding against residue numbers. Difference contact map of the folded (*A*) and unfolded states (*B*) between 25% and 0% volume occupancy of crowders at $T = 360$ K. Secondary structure elements are indicated.

denatured state more compact and thereby less energetically favorable, the native state is indirectly stabilized (5–8). However, our experimental and computational observations of structural changes in both the native and denatured states of apoflavodoxin indicate that direct crowding effects on the native protein molecules are feasible (Fig. 6). We have observed both a compaction of the overall size of the native protein (i.e., effects on R_g) and a more native-like structure (i.e., more negative far-UV CD signal and Q value closer to 1) for apoflavodoxin in the presence of crowder. The structural effect appears larger in the folded than in the denatured ensemble although the compaction effect is more pronounced in the denatured ensemble.

We also analyzed the changes in the folded and unfolded states due to crowding from a thermodynamic point of view. For this, the simulation data were used to compute the energy (which roughly corresponds to enthalpy), E, and the entropy, S (37), for folded and unfolded states in buffer and in 40% of crowders at 350, 360, and 370 K (SI Fig. 9 *A* and *B*). From this analysis, it emerges that there are energetic and entropic effects due to crowding in both unfolded (i.e., $Q_U = 0.25$) and folded states (i.e., $Q_F = 0.8$) of apoflavodoxin: for the $\varphi_c = 40\%$ condition, $\Delta E_{FU} \approx -19$ kcal/mol, $\Delta S_{FU}/k_B \approx -24$ (S/k_B is unitless) (k_B, Boltzmann constant), and $\Delta G_{FU} \approx -1.72$ kcal/mol at 360 K. For apoflavodoxin in buffer (i.e., bulk), $\Delta E_{FU} \approx -47.4$ kcal/mol, $\Delta S_{FU}/k_B \approx -66$, and $\Delta G_{FU} \approx 0.12$ kcal/mol at 360 K (SI Fig. 10). Interestingly, the crowding effects on folded- and unfolded-state entropy values are favorable. This may be explained by the existence of a large number of substates within the folded and unfolded ensembles as a result of crowder–protein interactions at high volume fraction of crowders. In contrast, the effect on the enthalpy/energy change due to crowding appears unfavorable, which may be explained by crowding-induced compaction having a negative effect on internal bonds (compression of structural bonds; these are modeled as harmonic springs).

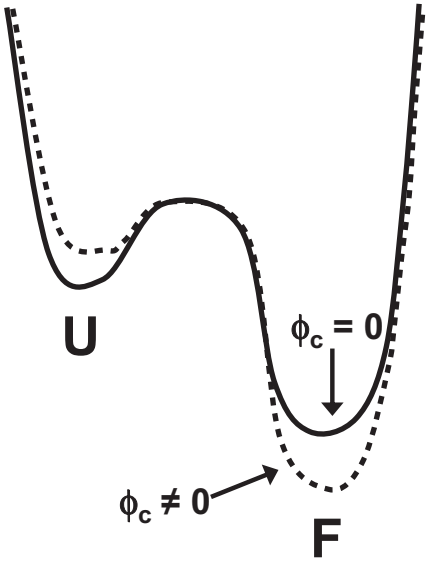

Fig. 6. Crowding affects both folded and unfolded ensembles. Schematic free-energy profile for flavodoxin folding. The enhanced stability at $\phi_c \neq 0$ (dashed curve) is due to a combination of unfolded-state destabilization and stabilizing of the folded state.

Crowded conditions may cause enrichment of a large number of slightly different protein structures that are all within the native ensemble of molecules but have the highest degree of order. This can be achieved by a shift (and broadening in terms of number of substates) of the average distribution of species within the native-state ensemble toward $Q = 1$. In agreement, the difference contact map reveals that the secondary and tertiary structures are not altered *per se*, but that they become better packed and exhibit less breathing/terminal fraying in the presence of crowders. Thus, crowding forces the native ensemble of the protein molecules in solution to be on average more like they are in the crystalline state. We propose that native-state structural effects caused by macromolecular crowding may be common *in vivo* for globular proteins that exhibit marginal stability. The volume fraction of macromolecules may be as high as 40% in living cells. For proteins with inherent plasticity in their native states, protein–crowder interactions may play a role in the modulation of local conformations at active sites. In addition, macromolecular-crowding effects may be of high significance for intrinsically unstructured proteins (for example, FlgM), which may be unfolded in dilute solutions *in vitro* but adopt folded structures in the crowded *in vivo* environment (38).

Materials and Methods

Protein Preparation. Flavodoxin from *D. desulfuricans* (American Type Culture Collection strain 29577) was expressed in *Escherichia coli* and purified as described (39, 40). In short, the apo-form of wild-type flavodoxin was isolated on a Q-Sepharose column and further purified by gel permeation on a Superdex-75 by using an FPLC system (Amersham–Amersham Pharmacia) (25).

***In Vitro* Measurements.** Apoflavodoxin native- and unfolded-state far-UV CD spectra (1-mm cell, 200–300 nm) were monitored at 20°C and 95°C, respectively, on a Jasco-810 spectrometer. Thermal unfolding experiments were carried out by following CD at 222 nm as a function of temperature. All experiments were

performed in different buffers and in the presence and absence of various amounts of Ficoll 70 (Sigma). Three solvent conditions (10 mM Hepes, 20 mM phosphate, and 40 mM phosphate plus 250 mM NaCl, all at pH 7) were tested in separate experiments. Ficoll 70 was included in 100 mg/ml steps, from 0 to 400 mg/ml; higher concentrations of Ficoll 70 were not accessible due to limited solubility. Care was taken to let all buffer/Ficoll/protein mixtures equilibrate before measurements. Both unfolding (from 20°C to 95°C) and refolding (from 95°C to 20°C data points were collected every degree with a scan rate of 2.5°C per minute scan rate. Scan rates were varied between 0.1°C per minute to 2.5°C per minute; there was no scan-rate dependence observed in the process. All unfolding transitions were >80% reversible; aggregation was never observed. Differential scanning calorimetry tests were performed on Ficoll 70 solutions to assure that Ficoll itself did not exhibit any phase transitions within the temperature range of flavodoxin unfolding. These experiments revealed no detectable transitions for Ficoll (not shown). Assuming a spherical shape (28, 29), 50 mg/ml Ficoll 70 corresponds to a volume occupancy, ϕ_c, of ≈25%; 100 mg/ml to $\phi_c \approx 50\%$; at Ficoll 70 concentrations >200 mg/ml; however, the spherical shape may be distorted (28, 29).

Model of Flavodoxin and Crowders. We used a coarse-grained C_α side-chain model (C_α-SCM) (11, 41, 42) to represent apoflavodoxin [Protein Data Bank (PDB) ID no. 2FX2; this structure is for *D. vulgaris* flavodoxin, which is the closest structural analog to *D. desulfuricans* flavodoxin for which there is a PDB structure). Each amino acid (excluding glycine) is represented by using two interaction sites, one corresponding to the C_α atom and the other the center of mass of the side chain. A modified Go-like (43) interaction is used for mimicking protein-like behavior in which the principle of minimal frustration is implemented to construct a funnel-like folding energy landscape (44–46). The structural Hamiltonian that includes bond-length potential, side-chain backbone connectivity potential, bond-angle potential, and dihedral potential follows Go-like behavior in which equilibrium values are justified from the native structure.

The interaction energy for nonbonded native side-chain interactions is:

$$E_{ij}^{\mathrm{NB}} = \varepsilon_{ij}\left\{\left(\frac{\sigma_{ij}}{r}\right)^{12} - 2\left(\frac{\sigma_{ij}}{r}\right)^{6}\right\}, \qquad [1]$$

where a native contact between side chain i and side chain j, $i-j>1$, is determined from the native structure by using the CSU program (47). Moreover, $\sigma_{ij} = 0.9(\sigma_i + \sigma_j)$. We take σ_i to be the distance between the center of mass of side-chain atoms and the C_α atom, which is the effective van der Waals radius of a side chain. For the native contact energies ε_{ij}, we use the Betancourt–Thirumalai (48) statistical potential. For backbone hydrogen-bond interactions, we consider an angular-dependent function to capture directional property of hydrogen bonds.

$$E_{ij}^{\mathrm{HB}} = A(\rho)E_{ij}^{\mathrm{NB}}, \qquad [2]$$

where $A(\rho)$ is

$$A(\rho) = \frac{1}{1 + \left[(1+\cos\rho)(1-\cos\rho)\left(1 - \frac{\cos\rho}{\cos\rho_a}\right)\right]^2}. \qquad [3]$$

In this equation, ρ is the angular alignment between two interacting strands of backbones and defined in ref. 41. ρ_a is the pseudo dihedral angle of a canonical helical turn, 0.466 (rad). A native pair of hydrogen bonding between C_α^i and C_α^j is determined by using the DSSP program (49). ε_{ij} for backbone hydrogen bonding between C_α^i and C_α^j is 2.5 kJ/mol. σ_{ij} is the hydrogen bond length, 4.6 Å. The crowding particle, Ficoll 70, is modeled as an inert sphere with a radius of 55.0 Å, which is 3.8 times the radius of gyration (R_g) of flavodoxin in the native state (14.6 Å). Interactions between Ficoll 70 spheres and flavodoxin are repulsive. We choose to study volume occupancy of crowders, ϕ_c, of 25% and 40%. In most simulations, $\phi_c = 25\%$ was used because of the limitation of computing resources.

Simulation Details and Calculations. Thermodynamics properties are simulated in a periodic cubic box in which each length (L) is 300σ, and σ is 3.8 Å, the average distance between two adjacent C_αs in the C_α-side-chain model. L is chosen to be at least twice as long as the extended flavodoxin polypeptide. In addition, pair correlation functions between the Ficoll 70 particles in the box are computed, and L is large enough to ensure that the finite size effects are avoided in the calculation. Simulation procedures follow those in the previous study by Cheung *et al.* (11). The Replica Exchange Method (REM) (50) is used to enhance the sampling efficiency in the molecular simulations (51). Thermodynamic properties such as the radius of gyration (R_g), shape parameters[‖] (Δ and S) (11), and the fraction of native contacts (Q) with respect to the crystal structure are computed to characterize the free-energy landscape of flavodoxin folding. The use of REM and Langevin equations of motion in the low friction limit (52) ensures that these thermodynamic properties, calculated with the weighted histogram analysis method (WHAM) (53) are converged.

[‖]For a sphere, Δ is 0; $S > 0$ (< 0) corresponds to prolate (oblate) ellipsoid.

Support for this project was provided by the Robert A. Welch Foundation (Grant C-1588, to P.W.-S.) and the USAMRAA (Grant W81XWH-06-1-0572, to P.W.-S.). M.S.C. is supported by the University of Houston. Computations were performed on the National Science Foundation Terascale Computing System (Teragrid, TG-MCB060051T) and at the Texas Learning Computation Center at the University of Houston.

1. van den Berg B, Ellis RJ, Dobson CM (1999) *EMBO J* 18:6927–6933.
2. Rivas G, Ferrone F, Herzfeld J (2004) *EMBO Rep* 5:23–27.
3. Record MT, Jr, Courtenay ES, Cayley S, Guttman HJ (1998) *Trends Biochem Sci* 23:190–194.
4. Ellis RJ, Minton AP (2003) *Nature* 425:27–28.
5. Zimmerman SB, Minton AP (1993) *Annu Rev Biophys Biomol Struct* 22:27–65.
6. Minton AP (2005) *Biophys J* 88:971–985.
7. Minton AP (2005) *J Pharmacol Sci* 94:1668–1675.
8. Zhou HX (2004) *J Mol Recognit* 17:368–375.
9. van den Berg B, Wain R, Dobson CM, Ellis RJ (2000) *EMBO J* 19:3870–3875.
10. Uversky VN, EMC, Bower KS, Li J, Fink AL (2002) *FEBS Lett* 515:99–103.
11. Cheung MS, Klimov D, Thirumalai D (2005) *Proc Natl Acad Sci USA* 102:4753–4758.
12. Ai X, Zhou Z, Bai Y, Choy WY (2006) *J Am Chem Soc* 128:3916–3917.
13. Galan A, Sot B, Llorca O, Carrascosa JL, Valpuesta JM, Muga A (2001) *J Biol Chem* 276:957–964.
14. Rivas G, Fernandez JA, Minton AP (2001) *Proc Natl Acad Sci USA* 98:3150–3155.
15. del Alamo M, Rivas G, Mateu MG (2005) *J Virol* 79:14271–14281.
16. Hatters DM, Minton AP, Howlett GJ (2002) *J Biol Chem* 277:7824–7830.
17. Tokuriki N, Kinjo M, Negi S, Hoshino M, Goto Y, Urabe I, Yomo T (2004) *Protein Sci* 13:125–133.
18. Qu Y, Bolen DW (2002) *Biophys Chem* 101–102:155–165.
19. Sasahara K, McPhie P, Minton AP (2003) *J Mol Biol* 326:1227–1237.
20. Muller F (1992) *Chemistry and Biochemistry of Flavoenzymes* (CRC Press, Boca Raton, FL).
21. Steensma E, van Mierlo CP (1998) *J Mol Biol* 282:653–666.
22. Genzor CG, Perales-Alcon A, Sancho J, Romero A (1996) *Nat Struct Biol* 3:329–332.

23. Muralidhara BK, Chen M, Ma J, Wittung-Stafshede P (2005) *J Mol Biol* 349:87–97.
24. Muralidhara BK, Rathinakumar R, Wittung-Stafshede P (2006) *Arch Biochem Biophys* 451:51–58.
25. Muralidhara BK, Wittung-Stafshede P (2003) *Biochemistry* 42:13074–13080.
26. Muralidhara BK, Wittung-Stafshede P (2005) *Biochim Biophys Acta* 1747:239–250.
27. Muralidhara BK, Wittung-Stafshede P (2004) *Biochemistry* 43:12855–12864.
28. Luby-Phelps K, Castle PE, Taylor DL, Lanni F (1987) *Proc Natl Acad Sci USA* 84:4910–4913.
29. Venturoli D, Rippe B (2005) *Am J Physiol* 288:F605–F613.
30. Vertrees J, Barritt P, Whitten S, Hilser VJ (2005) *Bioinformatics* 21:3318–3319.
31. Wrabl JO, Larson SA, Hilser VJ (2001) *Protein Sci* 10:1032–1045.
32. Minton AP (2000) *Biophys J* 78:101–109.
33. Tellam RL, Sculley MJ, Nichol LW, Wills PR (1983) *Biochem J* 213:651–659.
34. Hall D, Dobson CM (2006) *FEBS Lett* 580:2584–2590.
35. Eggers DK, Valentine JS (2001) *J Mol Biol* 314:911–922.
36. Eggers DK, Valentine JS (2001) *Protein Sci* 10:250–261.
37. Nymeyer H, Garcia AE, Onuchic JN (1998) *Proc Natl Acad Sci USA* 95:5921–5928.
38. Dedmon MM, Patel CN, Young GB, Pielak GJ (2002) *Proc Natl Acad Sci USA* 99:12681–12684.
39. Helms LR, Swenson RP (1991) *Biochim Biophys Acta* 1089:417–419.
40. Apiyo D, Wittung-Stafshede P (2002) *Protein Sci* 11:1129–1135.
41. Cheung MS, Finke JM, Callahan B, Onuchic JN (2003) *J Phys Chem B* 107:11193–11200.
42. Klimov DK, Thirumalai D (2000) *Proc Natl Acad Sci USA* 97:2544–2549.
43. Udea Y, Taketomi H, Go N (1975) *Int J Peptide Res* 7:445–459.
44. Onuchic JN, Luthey-Schulten Z, Wolynes PG (1997) *Annu Rev Phys Chem* 48:545–600.
45. Shea JE, Brooks CL, 3rd (2001) *Annu Rev Phys Chem* 52:499–535.
46. Clementi C, Nymeyer H, Onuchic JN (2000) *J Mol Biol* 298:937–953.
47. Sololev V, Wade R, Vriend G, Edelman M (1996) *Proteins* 25:120–129.
48. Betancourt MR, Thirumalai D (1999) *J Mol Biol* 287:627–644.
49. Kabsch W, Sander C (1983) *Biopolymers* 22:2577–2637.
50. Sugita Y, Okamoto Y (1999) *Chem Phys Lett* 314:141–151.
51. Sanbonmatsu KY, Garcia AE (2002) *Proteins* 46:225–234.
52. Veitshans T, Klimov D, Thirumalai D (1997) *Fold Des* 2:1–22.
53. Chodera JD, Swope WC, Pitera JW, Seok C, Dill KA (2007) *J Chem Theor Comput* 3:26–41.

Novel Breast Cancer Therapeutics Based on Bacterial Cupredoxin

Background and Objectives:
Reports of regression of cancer in humans infected with microbial pathogens date back more than 100 years. However, live bacteria produce significant toxicity, limiting their use. The unprecedented observation that the small bacterial protein *Pseudomonas aeruginosa* azurin forms a complex with the well-known tumor suppressor protein p53 and triggers cell death provides *a new avenue for cancer research*. Despite being a novel concept to target cancer, there are no thermodynamic details known for the proposed azurin-p53 complex. This project aims to fill this gap as outlined in four specific aims.
Aims and Methodologies:
We will reveal (1.) which p53 domain interacts with azurin and probe affinity and stoichiometry, (2.) the molecular mechanism by which azurin increases cellular levels of p53, (3.) the region on azurin that interacts with p53 and (4.) use the acquired information to propose smaller molecules that retain properties of azurin. For this, we use a battery of biophysical, spectroscopic and biochemical techniques in conjunction with purified proteins and strategic variants for *in vitro* experiments.
Results to date:
To this date, several discoveries have been made: most importantly, azurin is found to bind to the unstructured N-terminal domain of p53 and a small 13-residue peptide is able to reproduce part of the azurin interaction. Also, properties of two human copper-metabolism proteins have been identified; these proteins are important as they may cross-react with azurin-based drugs
Conclusions and Impact:
Our biophysical project provides key physical, chemical and structural understanding of azurin's interaction with p53 *in vitro*. We propose that the results of our studies may be used to develop small peptide constructs that bind and stabilize p53 like full-length azurin. If these molecules turn out to work *in vivo*, it may be the gateway to an innovative class of new cancer therapeutics.